THE OXIDATION OF DIAMOND

BY

JANE YUAN HOWE

A THESIS

SUBMITTED TO THE FACULTY OF

ALFRED UNIVERSITY

IN PARTIAL FULFILLMENT OF THE REQUIREMENTS

FOR THE DEGREE OF

DOCTOR OF PHILOSOPHY

IN CERAMICS

ALFRED, NEW YORK

FEBRUARY, 2001

THE OXIDATION OF DIAMOND

BY

JANE YUAN HOWE

B.S. CHANGSHA INSTITUTE OF TECHNOLOGY, CHINA (1992)

M.S. ALFRED UNIVERSITY (1997)

SIGNATURE OF AUTHOR (SIGNATURE ON FILE)

APPROVED BY (SIGNATURE ON FILE)
LINDA JONES, ADVISOR

(SIGNATURE ON FILE)
SCOTT MISTURE, ADVISORY COMMITTEE

(SIGNATURE ON FILE)
ALASTAIR N. CORMACK, ADVISORY COMMITTEE

(SIGNATURE ON FILE)
ROBERT A. CONDRATE, ADVISORY COMMITTEE

ACCEPTED BY (SIGNATURE ON FILE)
RONALD S. GORDON, DEAN, SCHOOL OF CERAMIC ENGINEERING AND MATERIALS SCIENCE

ACCEPTED BY (SIGNATURE O FILE)
SUSAN STRONG, DIRECTOR OF GRADUATE STUDIES, ALFRED UNIVERSITY

ACKNOWLEDGEMENTS

At age seven, I embarked on my journey as a schoolgirl. I left my home in a small town in southern China, and braved the elementary school in the big city of Shanghai. After the first few days of school, I sadly sighed, "Gosh, elementary school will take five years? That's too long!" But luckily it didn't take that long before I discovered the exhilaration of learning. I would not have guessed then that those long years of preparation were to help me become a scientist, in America, farther from Shanghai, which usually only exists in movies or appears on TV screens.

I would like to extend my deepest gratitude to the following people and institutions that have helped to get me this far:

First, I would like to thank my advisor, Dr. Linda Jones, whom I have been studying with for five years and three months. I respect her as both a mentor and a wonderful friend who occasionally appreciates my strange sense of humor.

I acknowledge the School of Ceramic Engineering and Materials Science, which has provided a Teaching Assistantship throughout my entire graduate study. Also, numerous travel and research expenses were covered through Dr. Jones' research funds. Part of this research project was conducted through the High Temperature Materials Laboratory User Program at Oak Ridge National Laboratory, sponsored by the U.S. Department of Energy under contract DE-AC05-00OR22725.

To my advisory committee members: Dr. Alastair Cormack, who showed me the beauty of theoretical work and was a role model for me as a goofy scientist. To Dr. Scott Misture, who got me hooked to X-ray diffraction and initiated me into the painful Rietveld method. And to Dr. Robert Condrate, Sr., who shared his knowledge in spectroscopy as well as his good taste in Mozart and Telemann.

To my colleagues at Oak Ridge National Laboratory: Mr. David Braski and Dr. Claudia Rawn for assisting in the experimental work. And Dr. Karl Sohlberg, for your stimulating discussions, which brought insight into my simulation work.

To the Composites Gang at Alfred, with whom I have been merrily working and playing for more than five years. Please keep the plants alive, so that the fame of the most interesting grads in McMahon will live on for generations to come.

To the people who make Alfred a hometown: Carla and Bill Coch, and little Jannie, the crimson birch.

My parents and grandparents (especially my paternal grandmother, as I am so sure that I inherited all the weirdo genes from her.)

Last, but not least, my gratitude to Chloe, who helped me to endure the pain of writing this dissertation.

Puufph, I am finally out of school now! Thank goodness.

TABLE OF CONTENTS

LIST OF FIGURES

LIST OF TABLES

ABSTRACT

The objective of this project is to develop a fundamental understanding of the oxidation behavior of diamond. Research efforts on oxidation and phase transition of diamond have been undertaken through a combination of experimental and computational approaches. Heat treatments are carried out on CVD diamond film ET100, manufactured by Norton Diamond Film, in a wide temperature (420 to 1500 ^{o}C) and oxygen partial pressure range (from $6x10^{-10}$ to 95 kPa). Theoretically, surface chemisorption and reconstruction of diamond surfaces are investigated using density functional theory.

Taking both oxidation and phase transition into consideration, we propose that diamond can take either one of the two different paths during the heat treatment of diamond in oxygen at elevated temperatures: 1) direct gasification of sp^3-bonded carbon; and 2) sp^3 to sp^2 phase transition (surface reconstruction) first, then gasification of sp^2-bonded carbon. Diamond oxidation and phase transition are results of these two competing mechanisms. We further suggest that surface oxygen coverage and temperature are the two most influential factors that govern the surface reaction of diamond. The reaction between oxygen and diamond (111) surface at ambient pressure is summarized as:

- Room temperature and 0 % coverage:
  The (111) surface reconstructs to (2x2) or (2x1) reconstruction. This occurs without any change of the bond character.
- Elevated temperature (~ 700 ^{o}C to 1500 ^{o}C), zero coverage:
  The bond character of diamond (111) surface changes from sp^3 to sp^2. Thus, diamond goes through a phase transition and forms amorphous, sp^2-bonded carbon. If the temperature reaches 1600 ^{o}C or higher, the amorphous carbon graphitizes and becomes crystalline.
- Elevated temperature (~ 700 ^{o}C and higher), low coverage (up to 20%):
  Diamond converts to amorphous, sp^2-bonded carbon first. Then the oxidation of carbon proceeds, yielding gaseous products CO and/or CO_2.
- Elevated temperature (~ 500 ^{o}C and higher), high coverage (more than 50%):
  Diamond converts to amorphous, sp3-bonded carbon first. Then the oxidation proceeds, yielding gaseous products CO and/or CO_2.

1 INTRODUCTION

"Our description of nature has become increasingly simple. More and more is being explained by fewer and fewer fundamental principles."

— Steven Weinberg, 2000

Simple is beautiful.

The ultimate goal for the author is to make this description of nature simple. The objective of this project is to develop a fundamental understanding of the oxidation behavior of diamond. There are two questions to be answered:

- Where are the active sites on the diamond surfaces?
- Is the surface reconstruction from sp^3 to sp^2 bond character during oxidation the governing phenomenon?

There is a renewed interest in the oxidation of diamond because of the development and application of diamond-based electronic devices. Diamond oxidation and phase transition are connected phenomena, yet they are not well understood. Identifying surface active sites, activity of specific crystallographic facets, and the extent to which surface conversion is involved in the oxidation process is key to the fabrication and design of diamond materials.

The carbon atom in its ground state has a $2s^2\ 2p^2$ electronic configuration. In diamond, the four electrons hybridize and adopt an sp^3 configuration in which all four valence electrons have the same energy. Carbon and graphite materials have an sp^2 hybridization. A phase transition in diamond may occur when the electronic configuration changes from sp^3 to sp^2 and vice versa. Both sp^3 and sp^2 bonded carbons are subject to oxidation at elevated temperatures in an oxygen containing atmosphere. Carbon reacts with oxygen and yields the gaseous products CO and/or CO_2. Under debate since the early 1960's, how oxidation and phase transition of diamond are related still remains controversial and unclear. A common inadequacy of diamond oxidation research is caused by ignoring the phenomena of diamond phase transition. In many ways, phase transition is an inseparable issue from the oxidation of diamond.

It is the author's ambition to provide a simple explanation of diamond oxidation behavior based upon our extensive investigations.

In this study, the investigation of oxidation and phase transition of diamond is undertaken through a combination of experimental and theoretical approaches. CVD diamond film ET100, manufactured by Norton Diamond Film, is the material of interest. Heat treatments are carried out in wide temperatures (from 420 to 1500 ^oC) and oxygen partial pressures (from 6×10^{-10} to 95 kPa) ranges. The conditions are chosen so that the influence of temperature and oxygen partial pressure can be identified easily. Whether there is a phase transition or not is determined by the hybridization state of carbon using Auger spectroscopy. The impact of oxidation and phase transition of diamond on the

microstructure is evaluated using scanning and transmission electron microscopic techniques. The kinetics of diamond oxidation is investigated using thermal gravimetric analysis (TGA) under the above mentioned conditions.

Theoretically, a quantum mechanical simulation on surface chemisorption and reconstruction of diamond is undertaken using the density functional theory method. Surface reconstruction and oxygen-chemisorption on low index diamond surfaces are investigated. The surface energy, the energy of chemisorption and surface reconstruction are calculated as well. These computational findings are substantiated by our experimental results. They also serve as supplements to experimental work, which makes our findings more convincing.

Taking both oxidation and phase transition into consideration, we propose that diamond can take either one of the two different paths during the heat treatment of diamond in oxygen at elevated temperatures: 1) direct gasification of sp^3-bonded carbon; and 2) sp^3 to sp^2 phase transition (surface reconstruction) first, then gasification of sp^2-bonded carbon. Diamond oxidation and phase transition are results of these two competing mechanisms. We hereby suggest that surface oxygen coverage and temperature are the two most influential factors on the surface reaction of diamond. A discussion of oxidation of diamond (111) is given here based upon the surface oxygen coverage and temperature conditions.

2 THE OXIDATION OF DIAMOND: A LITERATURE REVIEW

2.1 History of Diamond

"Diamond" is derived from the Greek word, "adamo", translated as "I tame" or "I subdue". Diamond has long been known as a gem stone. It was first mined in India and traded to the Mediterranean and China. Indians recognized the qualities of a fine diamond octahedron and valued them. "Vajra", the word most generally used for diamond in Sanskrit, means "thunderbolt". The earliest known reference of diamond is a Sanskrit manuscript, the Arthasastra ("The Lesson of Profit") by Kautiliya, a minister of the Mauryan dynasty in northern India, dated 320-296 BC.[1] Kautiliya states that a diamond is considered excellent if it is big, heavy, capable of bearing blows, having symmetrical points, capable of scratching a glass vessel, revolving like a spindle and brilliantly shining. The hardness of diamond is also realized by archaeological evidence: the use of twin-diamond drills on hard gem stones is found in Sri Lanka, India, Thailand, Yemen, and Egypt prior to 700 AD and as early as the 4th century BC in Yemen.[1] Diamond was so rare that its possession was once the prerogative of royalty and those at the very top of society. Abundant supplies from South Africa from the 1870's made diamonds available to all who could afford them. Simultaneously, after the fall of Napoleon III in 1871, the bulk of the crown jewels were auctioned off. Tiffany & Co. of New York bought the major share: 22 lots for $480,000, a sum greater than the combined purchases of the 9 next-largest buyers. The newly rich, fashionably displaying jewelry and diamonds, gave the Metropolitan Opera House seating section its name, "Diamond Circle".[1] The sensation and exclusivity of diamond have been continuously promoted by

De Beers Consolidated Mines, Ltd. for well over a century. The company has monopolized the natural diamond resources and sales worldwide through a "single channel marketing" system, which has proved an effective cartel.[1]

Mankind has long been dedicated to synthesizing diamond and the earliest patents date back to the nineteenth century.[2] The British Museum still possesses the diamonds "synthesized" by J.B. Hannay in 1880. According to Bundy,[3] Hannay claimed that he had made diamonds by heating a mixture of hydrocarbons, bone oil, and lithium at "red heat" (the temperature was not reported) in sealed wrought-iron tubes. Londsdale analyzed these "synthesized diamonds" in1942 and 1962 and reported that they were actually pieces of natural diamonds.[4] Although diamond was first synthesized by a group lead by Baltazar von Platen, at the AllmSnna Svenska Elektriska Aktiebolaget (ASEA) Laboratory in Stockholm, Sweden, in 1953, the initial success was not publicized or published.[5] The first report of manmade diamond from graphite was published in Nature on July 9th, 1955, by Bundy, Hall, Strong, and Wentorf. They were the scientists in General Electric, who made diamonds under ultra-high pressure (> 10 GPa) and high temperature (above 2300 K) (HPHT).[3] HPHT diamond is widely used nowadays as cutting tools and as polishing and grinding compounds.

Along with being a precious gem, diamond has many extraordinary properties which makes it a useful industrial material. The successful synthesis of diamond via vapor deposition methods since the 1980's marks a new era for diamond materials.

2.2 The Carbon Family – From sp to sp^3

Carbon is the 6^{th} element on the periodic table. The elemental carbon may be found in many different pure forms in nature. The carbon atom in its ground state has $1s^2 2s^2 2p^2$ electronic configuration. The four valence electrons can hybridize to sp, sp^2, sp^3, and even to a valence state in fractional numbers, sp^m, ($1<m<3$, $m\neq2$). For example, carbyne, a rare form of chain-like allotrope, has the valence state of sp^1.[6] Graphite is the layer-structured 2-D carbon with sp^2 hybridization. Diamond is the 3-D networked carbon with sp^3 hybridization. C_{60} , a form of buckminsterfullerene, has a hybridization state of $sp^{2.28}$.[7] A fractional hybridization state with a value of 2.28 implies that the material is not a 2-D structure. C_{60} molecule is spherical with a soccer ball like structure. Graphite and diamond are by far the most common allotropes of carbon. In diamond, the four electrons hybridize and adopt an sp^3 configuration in which all four valence electrons have the same energy. Diamond may have a cubic structure if the stacking sequence is ABCABC. There is also a hexagonal form of diamond, lonsdaleite, with a stacking sequence of ABABAB. Diamond is thermodynamically metastable at room temperature and room pressure. Graphite is the thermodynamically stable phase at room temperature and room pressure. Figure 2-1 represents the phase diagram of carbon over a wide range of pressures and temperatures.[8] The boundary between the diamond and graphite stable regions runs from 1.7 GPa at 0 K to the graphite/diamond/liquid triple point at 12 GPa in 5000 K.

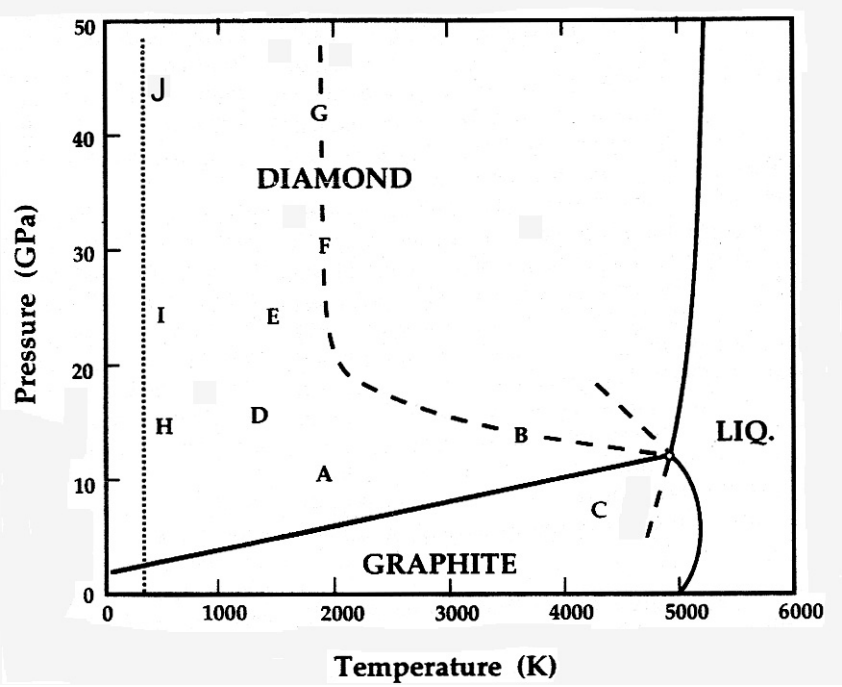

Figure 2-1. Phase diagram by Bundy, Bassett, Weathers, Hemley, Mao, and Goncharov for carbon as understood from experimental observations through 1994.[8] The solid lines in the figure represent equilibrium phase boundaries. A: commercial synthesis of diamond from graphite by catalysis (HPHT); B: P/T threshold of very fast (less than 1 ms) solid-solid transformation of graphite to diamond; C: P/T threshold of very fast transformation from diamond to graphite; D: single crystal hexagonal graphite transformation to retrievable hexagonal-type diamond; E: upper limit of shock compression/quench cycles that convert hex-type graphite to lonsdaleite; F: upper limit of shock compression/quench cycles that convert hex-type graphite to cubic-type diamond; Line B-F-G: threshold of fast P/T cycles that convert graphite or lonsdaleite into cubic-type diamond; Line H-I-J: route along which a single crystal hex-type graphite compressed in the c-direction at room temperature loses some graphite characteristics and obtains properties consistent with a diamond like polytype, but reserves to graphite upon release of pressure.

2.2.1 The Crystal Structure of Diamond and Graphite

The space group of cubic diamond is Fd3m with a lattice parameter of 3.567Å. The unit cell of diamond is given in Figure 2-2. The covalent bonding in diamond is isodesmic and arranged in a tetrahedral configuration. The carbon-carbon bond length in diamond is 1.54Å, and the bond angle is 109.5^{o}.

The unit cell of hexagonal graphite is given in Figure 2-3. The space group is $P6_3mmc$, and the lattice parameters are $a = 2.46$ Å and $c = 6.71$ Å. The electrons in graphite have an sp^2 bond character. Each carbon is linked to three other carbons in a trigonal bond arrangement. The bond length is 1.42 Å, and the bond angle is 120^{o}. Thus, these carbon atoms bond together and form the so-called graphene layer.[9] The interlayer spacing is 3.354 Å. If the stacking sequence is *ABABAB*, hexagonal graphite is formed. If the stacking is *ABCABC*, graphite adopts a rhombohedral structure. The interlayer distance is an indication of the degree of graphitization of carbon materials. The interlayer spacing of amorphous carbon runs between 3.40 to even more than 4.0 Å. The term turbostratic is often used to describe this class of sp^2 carbons. Amorphous carbon can be used as a term to describe any sp^2 and sp^3 carbon. Lacking long range order, sp^2 and sp^3 carbons exist in amorphous forms. For instance, diamond-like carbon (DLC) is a material with mostly sp^3 -bonded carbon which lacks long range order. As mentioned, turbostratic carbon and also glassy carbon are amorphous forms of sp^2-bonded carbons. The term phase transition of diamond is frequently used in this document; it refers to the change in the hybridization state from sp^3 to sp^2.

There are two distinctive types of bonds existing in graphite. The in-plane bonding is clearly covalent by nature, but there is still some disagreement in terms of the character of the interlayer bonding. IUPAC (International Union of Pure and Applied Chemistry) defines the weak interlayer bonding as "metallic with a strength comparable to van der Waals bonding only".[9] Nonetheless, Kingery calls on van der Waals forces to explain the bonding of these neutral planar layers in graphite.[10] Van der Waals forces originate from dispersion or fluctuating dipoles on separated atoms or molecules. However, the importance of van der Waals forces in solids is still unclear. Cohen argues that the interlayer bonding more likely results from the local many-body exchange and correlation interactions among electrons, not the van der Waals forces.[11]

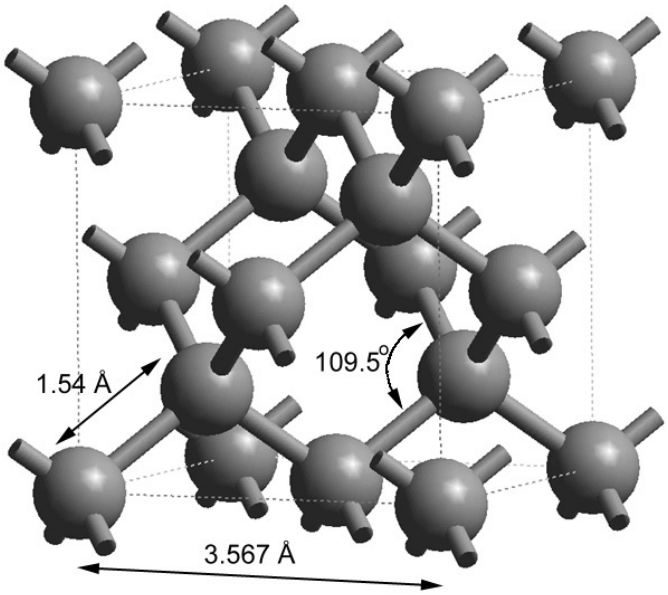

Figure 2-2. The unit cell of diamond Fd3m (produced using Cerius2® Visualizer). [®]

[®] Cerius2 is a software developed by Molecular Simulations Inc., San Diego, California.

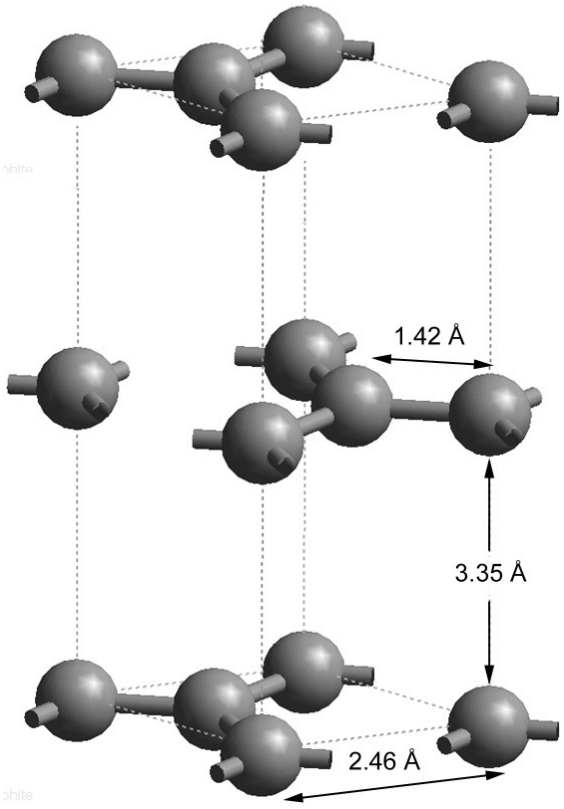

Figure 2-3. The unit cell of graphite $P6_3mmc$ (generated using Cerius2® Visualizer).

2.2.2 The Surface of Diamond

{111} is the cleavage plane in diamond. {111}, {110}, and {100} are the low index planes that receive much research interest. The binding energy between carbon atoms is great in diamond. For instance, the cohesive energy is 717 kJ/mol.[12] Harkins calculates the surface energy of diamond based upon the estimated bond energy of 377 kJ/mol.[12] He reports that the surface energy of (111) is 5.65 kJ/mol and 9.82 kJ/mol for (100) surface. The high surface energy implies that once the bonds are broken and the new surfaces are generated, the unsaturated bonds, i.e., the dangling bonds, are unstable and ready for reconstruction and/or chemisorption. Fluorine, chlorine, oxygen, and hydrogen are the species that readily chemisorb on diamond surfaces. Chemisorbed hydrogen or oxygen stabilizes sp^3 bonding and prevents the (111) surface from reconstruction.[13-15] Oxygen terminated diamond surfaces can accommodate stable potassium adsorption layer.[16] Without adsorbents, a (2x1) surface reconstruction occurs on diamond (111), but there is no such reconstruction on (100) or (110).[13] On the contrary, graphite (0001) has very low surface energy of 0.07 J/m^2.[17]

Surface Reconstruction on Diamond

Before the discussion of the surface reconstruction, it is worth the space to introduce the *short-hand notation*, which is widely used in surface science.[18] A crystalline surface is a 2-D lattice which can be described using two Miller indices. The short-hand notation is designated with respect to the bulk unit cell. A surface is designated (1x1) if the arrangement of the surface atoms that is identical to that in the bulk unit cell. For instance, a diamond (110)-(1x1) means the (110) surface is identical to that in the bulk.

The surface structure is denoted as (1x1)-S, where S is the chemical symbol or formula for the adsorbed species. For example, a diamond (111)-(1x1)-O represents a diamond (111) surface with adsorbed oxygen that holds the same periodicity as the bulk cell. If the surface unit cell indices are twice as large as the underlying bulk cell, it is designated as (2x2).

Marsh and Farnsworth investigate the (100) and (111) surfaces of semiconducting type IIB natural diamonds using low-energy electron diffraction (LEED).[19] A (2x1) surface reconstruction is observed on some of the (100) and all the (111) surfaces. Ion-bombardment makes the surface amorphous. They observe the decrease of diffraction intensity after heating the diamonds in a vacuum of $2x10^{-10}$ Torr ($2.7x10^{-8}$ Pa) at 450 ^{o}C for 1 h. The diffraction pattern extinguishes completely after heating at temperatures between 800 and 1100 ^{o}C in vacuum. The decrease of diffraction intensity and loss of diffraction pattern are attributed to the formation of carbon on diamond surfaces. However, heating the (100) diamonds in O_2, H_2, or CO_2 results in partial or complete recovery of a diffraction pattern that is destroyed by either ion-bombarding or carbonizing the surface. Lander and Morrison study clean (111) surface of natural diamonds using LEED.[20] A "benzene-ring" type of reconstruction is considered to fit the diffraction data the best. Heating diamond at high temperature in low hydrogen pressure produces a (111) surface without reconstruction. It is reported that no surface "graphitization" in high vacuum is observed after heating the specimens as high as 1300 ^{o}C for many hours.

Lurie and Wilson observe surface reconstruction on natural diamond (111) and (100) but no reconstruction on (110).[21] Pate argues that the natural diamond surfaces that are mechanically polished in olive oil (a routine in the jewelry industry) are hydrogen terminated, simply because olive oil is a source of hydrogen for surfaces during polishing.[13] He claims that both energy electron loss spectra (EELS) and photon stimulated ion desorption (PSID) verify that the mechanically polished (1x1) (111) surface is hydrogen terminated, and the reconstructed 2x2/2x1 surface is hydrogen free.

Küttel and his group extensively research the surface of diamond using scanning tunneling microscopy (STM), atomic force microscopy (AFM), LEED, and X-ray photoelectron diffraction (XPD). Küttel, Diederich, Schaller, Carnal, and Schlapbach report that diamond surfaces can be polished in hydrogen plasma at 870 ^{o}C and 0.4 Pa.[22] The surface roughness of (111) natural diamond decreases from 7 nm to 1 nm (RMS). The surface after the hydrogen plasma treatment is hydrogenated. The chemisorbed hydrogen is very stable even after two months of exposure in ambient air. Nonetheless, all the chemisorbed species leave the surface while annealing in a high vacuum at 1000^{o}C. A sharp 2x1 pattern is then observed on clean (111) surfaces. Nützenadel, Küttel, Diederich, Maillard-Schaller, Groning, and Schlapbach argue that clean (100) surface has a (2x1) reconstruction. Hydrogenated (100) can be either (1x1) or (2x1).[23]

Summarizing surface reconstruction on diamond, it is generally agreed that (2x1) reconstruction may occur on clean (111) and (100). According to the limited research efforts to date, there is no reconstruction observed on (110).

Surface Chemisorption on Diamond

Several research groups calculate or measure the number of dangling bonds on diamond surfaces, especially the low index facets (111), (110), and (100). Attempts are made to link the dangling bond density to the surface chemisorption and oxidation. The data of bond density and surface atomic density, calculated according to a defect-free bulk crystal structure, are tabulated in Table 2-1. In a defect free structure without any reconstruction, the {100} has the highest dangling bond density followed by {110} and {111}. There is a temptation to simply argue that {111} has the lowest reactivity because it has the lowest dangling bond density. However, this prediction contradicts the experimental findings of many researchers. Experimentally, only Nimmagadda, Joshi, and Hsu observe that {111} are more oxidation-resistant than {100}.[24] Evans and Phaal,[25] Miyata and Kobashi,[26] Bansal, Vastola and Walker,[27] Zhou, Kanda, Ohsawa and Yomaoka,[28] and Howe, Jones, and Coffey[29] report that (111) surface has the highest reactivity. For instance, kinetic studies of oxidation in O_2 from 10^{-2} to 0.5 Torr (1.33 to 66.5 Pa) by Evans and Phaal on bulk natural diamond indicate that, between 650 and 1000 °C, {111} are the most active with the highest oxidation rate followed by {110} and {100}.[25] They also observe that transparent diamonds are covered with black carbon after heat treatment. According to Marsh and Farnsworth, oxygen is found to be more readily adsorbed on (111) than (100) surface.[19] The study of Bansal, Vastola, and Walker on natural diamond powder reveals that chemisorption of oxygen occurs predominantly on {111} from 28 to 141 °C at 100 mTorr (13.3 Pa) O_2.[27] Howe, Jones and Coffey's oxidation study on CVD diamond film is consistent with these findings, concluding that {111} are the most active facets.[29]

Table II-1. The Low Index Facets that Make up the Diamond Surfaces[29]

	surface bonds per surface atom	area per face atom ($Å^2$)	relative dangling bond density	surface atoms $x10^{21}/m^2$
100	2	6.36	1.0	1.57
110	1	4.50	0.71	2.22
111	1	5.51	0.58	1.81

Sappok and Boehm study the chemisorption of H, F, Cl, Br, and O on the surface of diamond powder with a surface area of 20 m^2/g.[30] Surface coverage is studied under treatment with H_2 at 800°C, F_2 at 25 °C, and Cl_2 at 100 –400 °C. About a third of surface bonds can be saturated by H, F, or Cl under these conditions. Full oxygen coverage is achieved at 420 °C. Oxygen desorbs in the form of CO and CO_2, but never as O_2. Sappok et al. reports that diamond with chemisorbed halogens or hydrogen is hydrophobic, whereas it is hydrophilic if the surface is covered by chemisorbed oxygen. IR investigation indicates that oxygen-terminated surfaces have strong C=O bonds and ether typed C-O-C complexes.

Matsumoto, Kanda, Sato, and Setaka report that full oxygen coverage can be reached at 420 °C.[31] They observe that natural diamond powder is oxidized at temperatures of 505 and 554 °C in flowing 1.33 Pa O_2. The surface is fully covered by oxygen at 505 °C. However, oxidation at 554 °C occurs at a surface of 62 % coverage. It is of great importance that oxidation may occur with either full or partial oxygen coverage. The surface is more likely to be only partially covered by chemisorbed oxygen at higher temperatures.

Ando, Yamamoto, Ishii, Kamo, and Sato report a slightly higher temperature of full oxygen coverage, at 480 to 500 °C.[32] It is confirmed by Matsumoto and Setaka,[33] and Ando, et al.,[32] that chemisorbed hydrogen is easily desorbed as H_2 and less likely to be desorbed as hydrocarbon molecules such as CH_4. The work of Marsh and Farnsworth indicates that the thin carbon layer on diamond can be removed by heating in H_2 or O_2 at

proper temperature and pressure.[19] The gaseous products released from hydrogen etching are primarily CH_4 and CO and CO_2 if etched by O_2. Küttel, Diederich, Schaller, et al. report that diamond surfaces become hydrogenated after treatment in a hydrogen plasma at 870 ^oC and 0.4 Pa.[22] The chemisorbed hydrogen is very stable even after two months of exposure in ambient air. Nonetheless, all the chemisorbed species leave the surface while annealing in high vacuum at 1000 ^oC.

Regarding surface chemisorption influences on diamond surface reactions, it is of great importance to determine the role that oxygen and hydrogen play on the surface chemisorption of diamond. Oxygen preferentially chemisorbs on diamond (111). And (111) is the most reactive surface for the oxidation of diamond. The fact that hydrogen stabilizes sp^3 bond character and etches sp^2 carbon away makes hydrogen a critical species in diamond growth by chemical vapor deposition of hydrocarbon gas in the presence of H_2.

2.3 Synthesis of CVD Diamond Films

Figure 2-1 is a pressure-temperature phase diagram of elemental carbon as understood from experimental studies through 1994.[8] Region A is where commercial synthesis of diamond from graphite by catalysis (HPHT methods) is possible. HPHT diamonds are individual particles sized from microns to millimeters. Many potential applications of diamond require thin films or coatings which cannot be made of HPHT or natural diamond. The effort to vapor deposit diamond started in the 1950's in the Soviet Union led by Deryangin and in the United States by Angus.[34] The Japanese started their attempt

in the 1970's. Chemical vapor deposition (CVD) process can produce diamond films from a region under which graphite is a stable phase of carbon in Region C as shown in Figure 2-1. The favorable kinetic factors allow crystalline diamond to grow by the following chemical reaction:

$$CH_4\ (g) \rightarrow C\ (\text{diamond}) + 2\ H_2\ (g) \qquad (2\text{-}1)$$

Other than methane, a wide variety of carbon-containing reactant gases can be used. A typical CVD process consists of a mixture of reactant gas and hydrogen (>95 vol %) at less than atmospheric pressure, passing through a hot filament (> 2000 ^{o}C) or a plasma, then depositing on a substrate at 800 to 1000 ^{o}C.[35] After the reactant gas is activated, acetylene and methyl radicals are the most abundant vapor species near the growth surface. It is generally agreed that atomic hydrogen stabilizes sp^3 bonding of CH_3· (methyl) carbon , which contributes to the etching of deposited sp^2-carbon. Many report that at temperatures 900 ^{o}C and lower, {111} are the predominant vapor deposited faces; but become {100} dominant if the temperature is 1000 ^{o}C or higher. The fastest growth direction is <110>. CVD diamond films can grow on substrate materials, such as silicon, molybdenum, even diamond. The substrate may subsequently be removed by chemical etching.

2.4 Oxidation of Diamond

2.4.1 Kinetics

Similar to the gas reaction of carbon, the diamond-oxygen reaction is also a heterogeneous solid-gas reaction, which involves three major steps:[36]

1. Mass transport of reacting gas and product or products across a relatively stagnant gas film between the exterior surface of the solid and the main gas stream.
2. Mass transport of the reacting gas from the exterior surface to an active site beneath the surface and mass transport of the products in the opposite direction.
3. Chemisorption of reactant, wholly or in part; a rearrangement of chemisorbed species on the surface to a desorbable product(s); and desorption of product or products from the surface.

Since mass transport plays a role in the kinetics of the oxidation of diamond, special care is taken when trying to discuss the kinetic experimental results and to compare these results with other workers' findings.

It is generally agreed that oxidation of diamond is a function of the exposed crystallographic surfaces and defect concentrations. The low index facets {111}, {110}, and {100}, draw much attention as they are the ones that make up the surface of diamond.[25, 26, 29] The oxidation rates of natural diamond-oxygen reaction vary with the crystalline facets.[25] At low and moderate temperatures, {111} has the highest reaction rate, followed by {110}, with {100} the slowest. In addition, sp^2 carbon could appear on {111} and {110}. Table II-2 tabulates the activation energy data of diamond oxidation. The data are gained from oxidation of natural and synthetic diamonds in various gas and temperature conditions. The apparent activation energy varies from 96 to 230 kJ/mol. The temperature-dependence of the reaction rates and of the apparent activation energy disappears at high temperature. This indicates that the kinetics are moving away from

pure chemically controlled mechanisms to mass transport controlled ones. It is agreed that the true activation energy is 230 kJ/mol.

2.4.2 Oxidation of Natural Diamond

The major concerns of the oxidation of diamond are as follows: 1) whether graphite or sp^2-bonded carbon is a reacting intermediate; and 2) where the active site of oxidation is located. Sappok and Boehm report that oxidation of natural diamond powder initiates at 360 ^{o}C.[37] Ando, et al. suggest that oxidation starts at 480 ^{o}C.[32]

Lambert was the earliest to report an activation energy of 184 kJ/mol for the oxidation of natural diamond powder (see Table II-2).[38] It is determined that diamond-oxygen is a first order reaction without mass transport limitations. Lambert argues that direct formation of carbon dioxide is caused by impact of oxygen molecules on a clean diamond surface.

3 MATERIALS AND EXPERIMENTAL PROCEDURES

The oxidation and phase transition of CVD diamond films are studied through both experimental and theoretical approaches. The description of the theoretical (computational) approach is given in Section 7.5.2.

3.1. Materials of Interest

CVD diamond film ET100 manufactured by Norton Diamond Film, and type 2A natural diamonds with specific cuts, i.e., {111}, {110}, and {100}, from Drukker International, The Netherlands, are the subjects of the research effort. Detailed technical specifications of CVD diamond ET100 can be found on Norton Diamond Film's web site.[1] Although ET100 is of high quality approaching that of bulk diamond in crystallite size (60 μm) and well-defined crystallite orientation (growth orientation is <110> while {111} and {100} are the surface facets), impurities such as Si, Al, and hydrogen are found enriched at the grain boundaries. Therefore, investigation on high purity natural diamonds with specific cuts leads to an understanding of how impurity and heterogeneity influence the surface chemistry, a fundamental aspect of oxidation behavior. The type 2A natural diamond is the type with the highest purity. The dimension of the diamond discs used in the current study is 2 mm in diameter and 0.5 mm thick. The two surfaces of the discs are precisely cut and polished along the crystal directions [111], [110], and [100] with 2^{o} of misalignment, as determined using Laue X-ray diffraction. Thus, the exposed surfaces are {111}, {110}, and {100}. Highly oriented pyrolytic graphite (HOPG), grade ZYH, manufactured by Union Carbide, and glassy carbon, manufactured by SGL, are the

reference materials. HOPG and glassy carbon are chosen simply because they are the crystalline and amorphous carbon materials with sp^2 bond character.

3.2. Experimental Procedures

3.2.1 Kinetic Study of Diamond Oxidation

CVD diamond are treated isothermally at high, low, and very low oxygen partial pressures at elevated temperatures. Details of all the runs are tabulated in Appendix I. Oxidation at high oxygen partial pressure is carried out at Alfred University using an isothermal gravimetric analysis on a Setaram TAG24 Thermoanalyzer, in 95 kPa ultrahigh purity O_2 at 420, 500, 550, 575, 600, and 625 °C for 30 to 400 min with a flow rate of 70 to 95 sccm. Prior to the oxidation, samples are heated in UHP Ar. The reactant gas, O_2, is introduced 10 min after the oxidation temperature is first reached. Small pieces of diamond film, weighing ~ 8 to 15 mg each, are loaded in a fused silica crucible. The average total specimen size is 30 mg. The crucible is made in-house and a hole made at the bottom in order to let the gas flow through the crucible. Oxygen treatment at low partial pressure is carried out on the Setaram, at 750, 850, 1000, 1300, 1400, and 1500 °C. The low oxygen pressures of 0.4 to 18 Pa pO_2 is maintained using a rotary pump. Heat treatments at very low oxygen partial pressure are conducted at Oak Ridge using a Stanton-Redcroft (now Rheometric Scientific Inc.) Simultaneous Thermal Analyzer (STA 1500S) at 1003, 1303, and 1478 ^{o}C for 170 to 600 min. The experimental runs are conducted using flowing titanium-gettered helium. A flow rate of 50 sccm is used for all exposures. Prior to heating, the instrument is purged until the oxygen partial pressure in the exhaust stream lowered to 6 $x10^{-10}$ Pa, as indicated by a Centorr oxygen

analyzer. The pressure of 6 x10^{-10} Pa is sometimes referred to as "10^{-9} Pa", or "less than 10^{-9} Pa" throughout the context of the thesis. The temperature is calibrated against the melting point of gold and nickel at 1064 and 1455 ^{o}C, respectively. An alumina crucible is used with specimen size approximately 50 mg in all cases.

Oxidation rates are given as min^{-1}, which is the weight-loss normalized to the remaining weight per minute. All the rates and weight-loss data are corrected for the buoyancy effect. The buoyancy effect is a phenomenon associated with lifting or pulling of the sample crucible as a result of gas flow in the heat zone of the furnace. For instance, heating at atmospheric pressure causes an increase of apparent mass of 0.1 to 0.3 mg; heating under 2 to 90 Pa of total pressure decreases the mass between 0.5 and 1.0 mg, depending upon the pressure and the temperature. Buoyancy effect is also observed in experiments with flowing helium gas (the oxygen partial pressures were less than 10^{-9} Pa).

3.2.2 Auger Electron and X-Ray Photoelectron Spectroscopy

The Auger and XPS work is undertaken at Oak Ridge National Laboratory as two related HTML User Projects # 99-032 and 00-018. Auger and XPS spectra of CVD diamond are collected from the diamond surfaces after the treatments described previously. The natural diamond and glassy carbon are examined as-received (A.R.) after an ultrasonicate-rinse in methanol or ethanol. Auger and XPS of HOPG are obtained from the freshly cleaved {0002} using the conventional "Scotch Tape" method. Auger spectra are obtained using PHI 680 Auger Nanoprobe. The accelerating potential is 2 kV and the

beam current is 1 nA. Auger spectra of clean CVD diamond surface is obtained from surface fractured in vacuo. XPS study is carried out using a PHI 5600 X-Ray Photoelectron Spectrometer with Al kα at 15 keV. XP spectra are collected with the neutralizer on. Ion sputtering is conducted using Ar gas at 3.5 kV rastered an area of 2x2 mm^2 which produces a sputtering rate of 200 Å/min.

3.2.3. Hydrogen-Plasma Treatment of Diamond Film ET 100

The hydrogen treatment is carried out at Institute of Physical Chemistry, University of Hamburg, Germany, courtesy of Mr. Sven Hadenfeldt. The as-grown side of the ET100 is exposed in hydrogen plasma in Prof. C. Benndorf's PCVD apparatus at the Institute of Physical Chemistry for four hours at a substrate temperature ranging from 720 to 750 ^oC. The base pressure is better than 0.05 mbar (5 Pa). The hydrogen flow is 200 sccm at hydrogen pressure of 20 mbar (2 kPa) for plasma conditions. The plasma is ignited at 2 kV and maintained at 2.25 kV at 0.23 Amps, which results in a plasma power of ~ 520 Watts.

3.2.4. Scanning Electron Microscopy (SEM) and Energy-Dispersive Spectroscopy (EDS)

SEM images are taken using three different microscopes, ie, Amray 1810 at Alfred University, Hitachi S-800 FE-SEM and Hitachi S4700 SEM at Oak Ridge National Laboratory as two related HTML User Projects # 99-032 and 00-018. All the images are taken under secondary electron mode. The observations on the Amray 1810 are made at accelerating voltages of 20 to 25 kV. The observations on Hitachi S-800 FE-SEM and Hitachi S4700 are carried out at 5 and 10 kV, respectively. In order to identify the

chemical composition of certain features shown in the SEM images, EDS (energy dispersive spectroscopy) attachment on the Hitachi S4700 is used to collect the spectra.

3.2.5. Transmission Electron Microscopy (TEM) and Electron Diffraction

TEM observation is carried out using a JOEL 2000 FX under 120 kV. The ET100 film after heat treatment (in $6x10^{-10}$ Pa O_2 at 1478 ^oC for 600 min) is crushed down to small pieces. Only the pieces of the black carbon layer are carefully picked out and collected on a copper grid for TEM observation.

3.2.6. X-Ray Diffraction of Diamond

XRD is undertaken on the as-received film using a Siemens 500 X-ray Diffractometer with Cu K_α X-ray source at 30 mA and 40 kV. The XRD is scanned from 42 to 143° 2-theta with a step size of 0.02° and a count time of 10 sec. The specimens are examined on both as-grown and substrate sides. The film is pressed onto a specimen holder using vacuum putty. The diffractometer bears a Bragg-Brentano geometry. JCPDS card 6-675 of cubic diamond is referred to as the powder diffraction standard.[2]

3.2.7. Raman Spectroscopy

The Raman spectrum of the sample is obtained in bulk form using an ISA U-1000 MOLE double-grating Raman spectrometer. The spectra are collected using a 180^o scattering geometry, with the 514.532 nm Ar^+ ion laser, calibrated by the 142 cm^{-1} Raman band of anatase prior to sampling.

References

1. "ET100 CVD Diamond Substrates" (2000) In Norton Diamond Film. [World Wide Web]. Accessed on: October 19, 2000. Available at <http://www.nortondiamfilm.thomasregister.com/olc/nortondiamfilm/page8.htm>

2. Powder Diffraction File (PDF-2), Database Sets 147; Diamond, ICDD# 6-675. International Center for Diffraction Data, Newtown Square, Pennsylvania, 1997.

4 EVOLUTION OF DIAMOND MICROSTRUCTURE BY OXIDATION AND PHASE TRANSITION

Oxidation of diamond is a heterogeneous gas-solid reaction. Identifying surface active sites, the activity of specific crystallographic facets, and the extent to which surface conversion is involved in the oxidation process is key to the fabrication and design of diamond materials. This chapter documents the study of the evolution of CVD diamond (ET100) microstructure as influenced by oxygen partial pressure and heat treatment temperature. Sections 4.3, 4.4, and 4.5 detail the microstructure of diamond heat treatment (oxidation) in high (95 kPa), low (0.4 to 18 Pa), and very low oxygen partial pressures ($6x10^{-10}$ Pa), respectively. The investigation of microstructure is carried out using SEM and TEM. In order to characterize the as-received films, Raman and XRD investigations are undertaken.

4.1 Microstructure of As-Received ET100

The as-received Norton CVD diamond ET100 is polycrystalline with a thickness of 380 μm. The film is grown on a silicon substrate which is then removed. The microstructure of substrate and as-grown sides are different. The substrate side is the side on which nucleation occurs, and as a result, there is a void space between the small crystallites found on this side, Figure 4-1. The crystallite size is less than 1 μm. As revealed using EDS, small patches of silicon still remain on the substrate side. The microstructure of the as-grown side of the diamond film is given in Figure 4-2. On the as-grown side, crystallites are fully developed, and the crystallite size ranges from 40 to 100 μm.

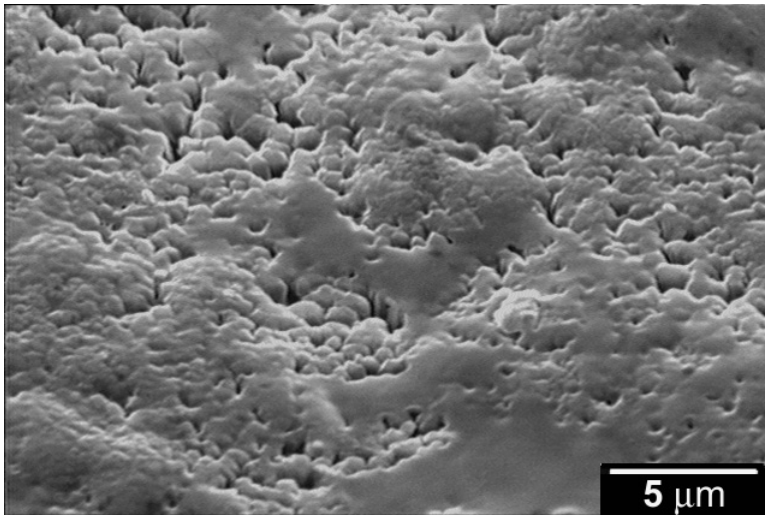

Figure 4-1. Substrate side of the as-received CVD diamond ET 100 (3800 x). The film is porous and crystallite size is less than 1 μm.

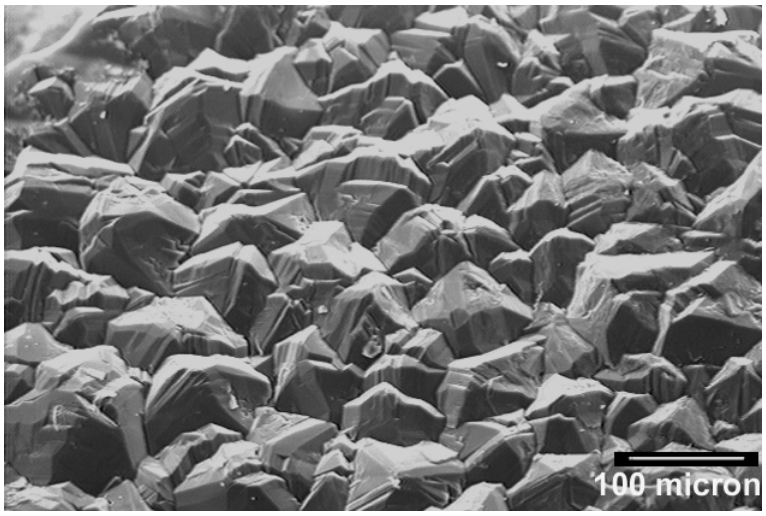

Figure 4-2. The as-grown side of as-received CVD diamond (150 x). Crystallite size ranges between 40 and 100 μm.

Figure 4-3 contains a micrograph of the as-grown side of the diamond film at magnification of 2 kx. {100} and {111} are the preferentially exposed facets on the as-grown surface where growth is terminated. These are the cubo-octahedral surfaces, as determined by knowing the preferred orientation of the film [110] and the angles of adjacent facets. In this case, {111} and {100} are adjacent facets, {111} facets are defined by 60 and 120 ^{o} angles, whereas, {100} are defined by 90 ^{o} angles. Two adjacent {111} are connected by a 109.5 ^{o} angle. Figure 4-4 contains a micrograph of a cross-section of the film. Preferred growth leads to a strongly oriented columnar film. As determined using X-ray diffraction, [110] is normal to the substrate surface and is the fast growth direction. XRD patterns of the diamond film in bulk form, from both substrate and as-grown sides, are given in Figure 4-5. The standard powder diffraction pattern, PDF 6-675,[1] is also included as Figure 4-5. The standard provides intensity ratio of a phase with random orientation. Therefore, a disagreement of the intensity ratio between a pattern and the standard implies preferred orientation. The (111) peak possesses the highest intensity of diamond standard, whereas (220) peak is the strongest peak of the film patterns. Significant difference between the relative intensities of standard and film indicates that <110> is the preferred growth orientation. The preference is enhanced along the film growth because the relative intensity of (220) peak is higher on the as-grown side than the substrate side. The numerical values of the relative intensity of ET100 at the substrate side and d-spacings are given in Table IV-1. The d-spacing values of the film and the standard are very close, but the relative intensity difference is significant.

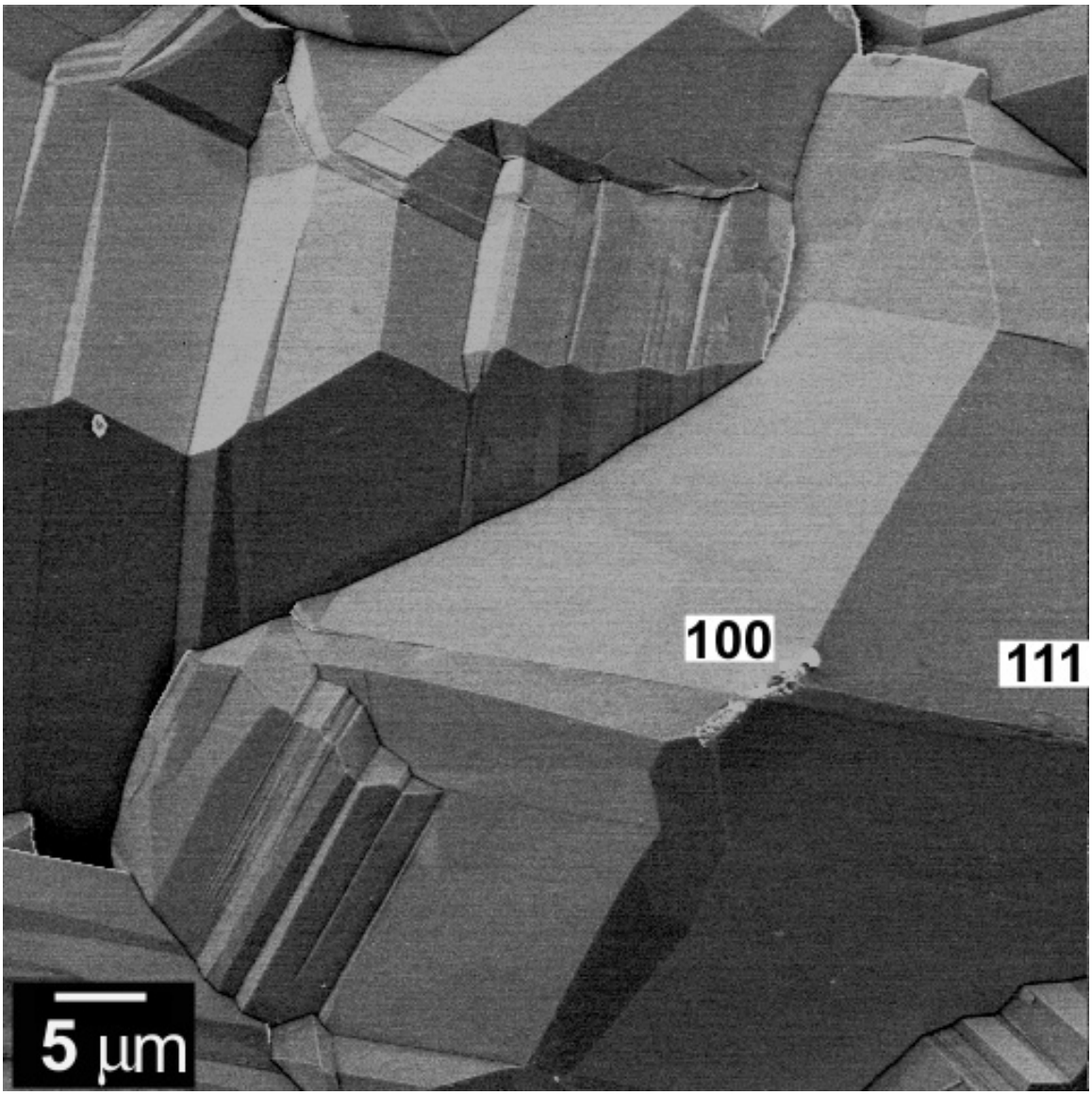

Figure 4-3. As-received CVD diamond ET100 (2 kx). It has the cubo-octahedral surface which is terminated by {111} and {100}.

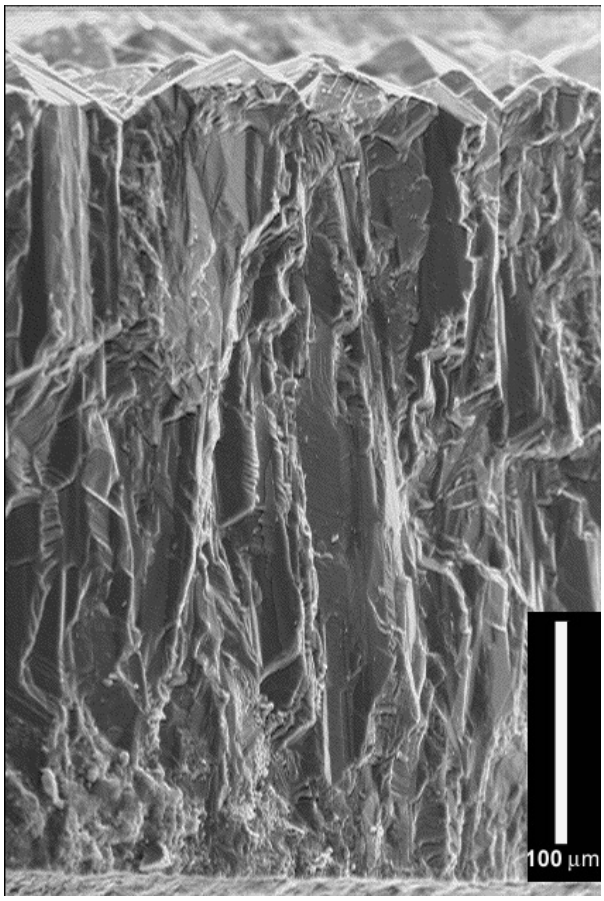

Figure 4-4. Cross section of as-received CVD diamond (300 x). The columnar grains are [110]-oriented and the growth direction is from bottom to top.

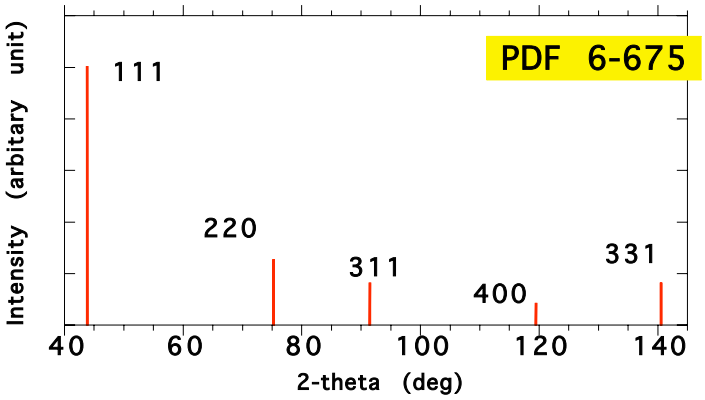

(a) PDF 6-675

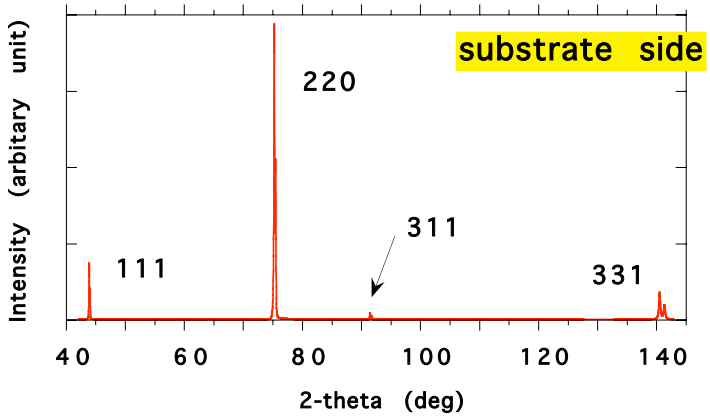

(b) substrate side

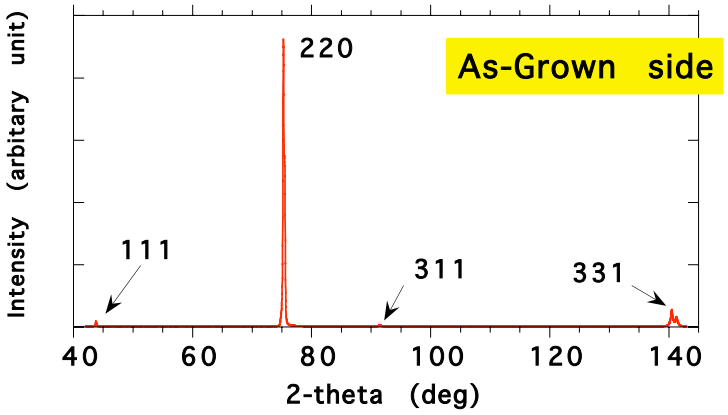

(c) as grown side

Figure 4-5. XRD patterns of diamond. (a) A powder standard PDF 6-675;[1] (b) the from the substrate side; and (c) the as-grown side of CVD diamond ET100.

Table IV-1. Peak Positions and Relative XRD Intensities of CVD Diamond Film and Diamond Powder

	PDF 6-675 [1]		ET 100 (the substrate side)	
hkl	d-spacing (Å)	Relative Int. (%)	d-spacing (Å)	Relative Int. (%)
111	2.0600	100	2.0585	15
220	1.2610	25	1.2614	100
311	1.0754	16	1.0756	2
400	0.8916	8	—	0
331	0.8182	16	0.8184	16

4.2 Raman Spectroscopy of As-Received Diamond

Raman spectroscopy is used to characterize the hybridization state of the diamond film. The Raman peak at 1332 ± 1 cm^{-1} indicates the characteristic sp^3 bonding, whereas, amorphous sp^2 carbon would introduce a broad band centered at ~ 1500 cm^{-1}.[2] Figure 4-6 contains the Raman spectra of the as-received film. The CVD diamond ET100 features a sharp narrow peak at 1331 cm^{-1} with a FWHM of 5.5 cm^{-1} and a flat background at ~ 1500 cm^{-1}. The film is crystalline and sp^3 is the dominant hybridization state.

4.3 Microstructure Influenced by Oxidation under 95 kPa O_2

4.3.1 Microstructure as a Function of Burn-Off Levels

The location of preferred oxidation sites on the surfaces of CVD diamond are of interest in this study. To determine this location, an investigation of microstructure as a function of weight-loss levels is undertaken at 625 ºC in 95 kPa UHP O_2, with a gas flow rate of 70 to 95 sccm. Oxidation is interrupted at weight-loss levels of 0.6, 3, 15, 50 and 90 wt. % (remaining weight normalized to initial weight) and the films are then examined using SEM. Images of Figure 4-7 are taken from the as-grown side as-received, at 3, 9, and 15 % weight-loss. At 3 % weight-loss, clear evidence of surface oxidation appears. The oxidation is localized and concentrated at the boundaries between individual crystallites where cracks formed along the grain boundaries. By 9 % weight-loss, each facet is strongly attacked. At 15 % weight-loss, little of the original surface remains. Attacks on the facet at grain boundaries and surfaces leave only the crystallite core regions. The specimen at 15 % weight-loss, Figure 4-7(d), does not resemble the as-received film given in Figure 4-7(a).

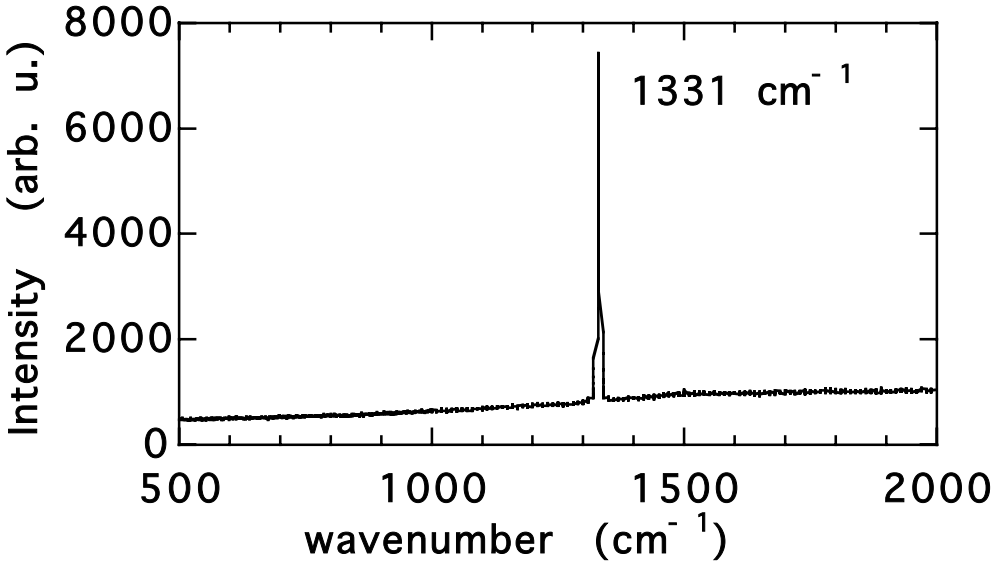

Figure 4-6. Raman spectra of as-received CVD diamond ET100.

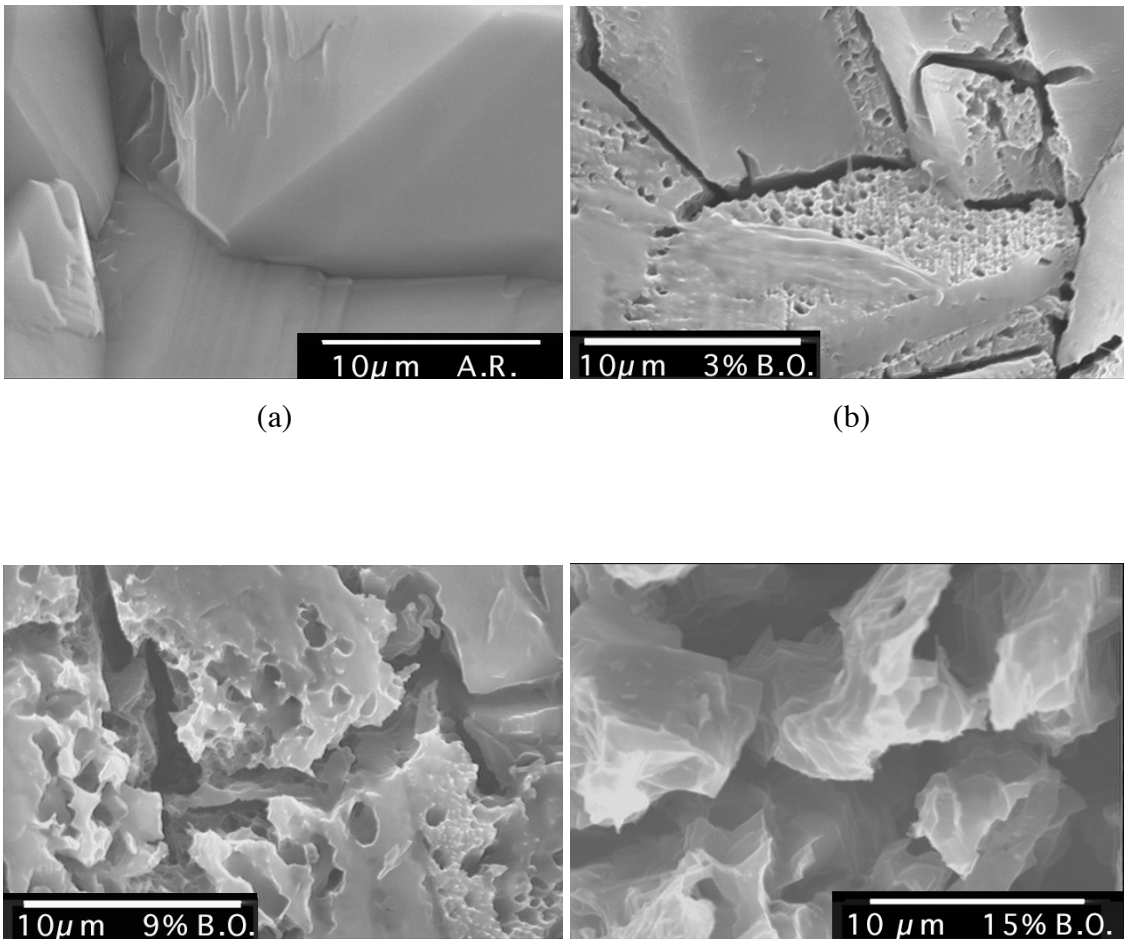

Figure 4-7. Change of microstructure on the as-grown side of the CVD diamond film ET100 in 95 kPa O_2 flowing at 80 sccm. (a) As-received, zero % weight-loss; (b) 3 % weight-loss; (c) 9 % weight-loss; and (d) 15 % weight-loss. Images have the same magnification at 2.85 kx.

Images in Figure 4-8 are taken from the substrate-side, as received, at 0.6, 3, and 9 % weight-loss. Oxidation continues to preferentially occur at crystallite boundaries. Because the crystallites on the substrate side are so small, the degree of oxidation is accentuated. Also, the residual silicon may play a role in oxidation at the substrate side. Overall, the oxidation is more pronounced. Secondary SEM images in Figure 4-9 are taken along the film thickness (380 μm thick) after 3 to 50 % weight-loss in 95 kPa O_2. Oxidation initially occurs at both top and bottom surfaces. The cracks shown in the 3, 9, and 15 % weight-loss images are also observed under high resolution SEM. They are not stress-induced, but rather the result of oxidation. Images of these cracks at magnification of 100 kx are given in Figures 4-17 and 4-21.

The kinetics of oxidation of diamond films at 625 ºC in 95 kPa O_2 are detailed in Section 6.1. Oxidation at this temperature is a two-stage process. During the first stage of up to approximately 10 % weight-loss, the oxidation rate is rather slow. Whereas during the second stage, which starts from approximately 10 % weight-loss and levels off at ~ 90 % weight-loss, the oxidation rate is 30 times faster than that of the first stage. The kinetic study of the two stage oxidation is given in Section 6.1. along with Figure 6-4. Figure 4-10 contains a set of two micrographs of the remaining materials after oxidation has proceeded through a steady state and leveled off. The remaining material is small, faceted pieces of diamond particles.

At any weight-loss level during the oxidation in 95 kPa O_2 (considered as high partial pressure of O_2), there is no black carbon observed. The as-received film is grayish

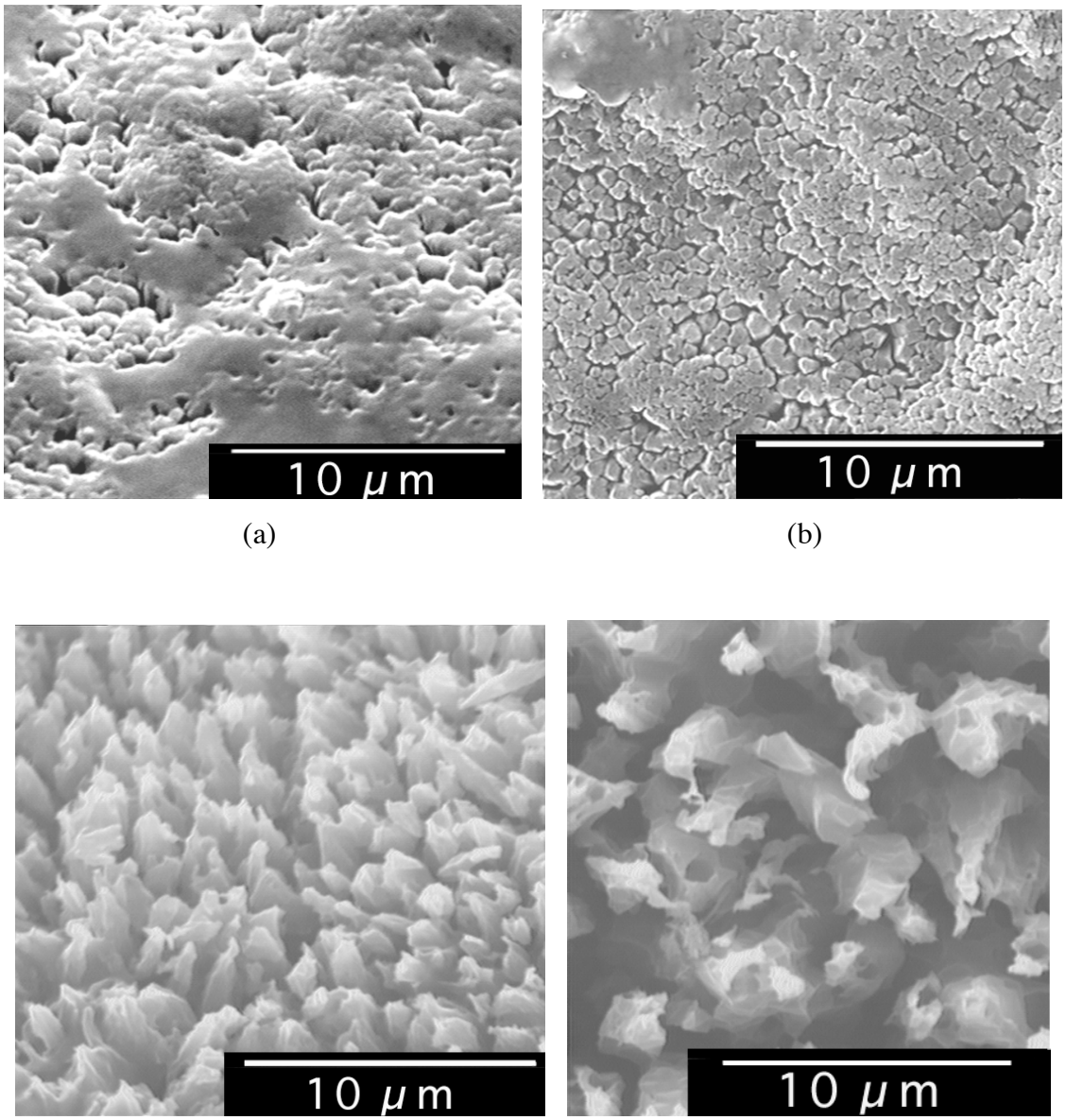

Figure 4-8. Change of microstructure on the substrate side of the CVD diamond film ET100 in 95 kPa O_2 flowing at 80 sccm. (a) As-received, zero % weight-loss; (b) 0.6 % weight-loss; (c) 3 % weight-loss; and (d) 9 % weight-loss. Images have the same magnification at 4 kx.

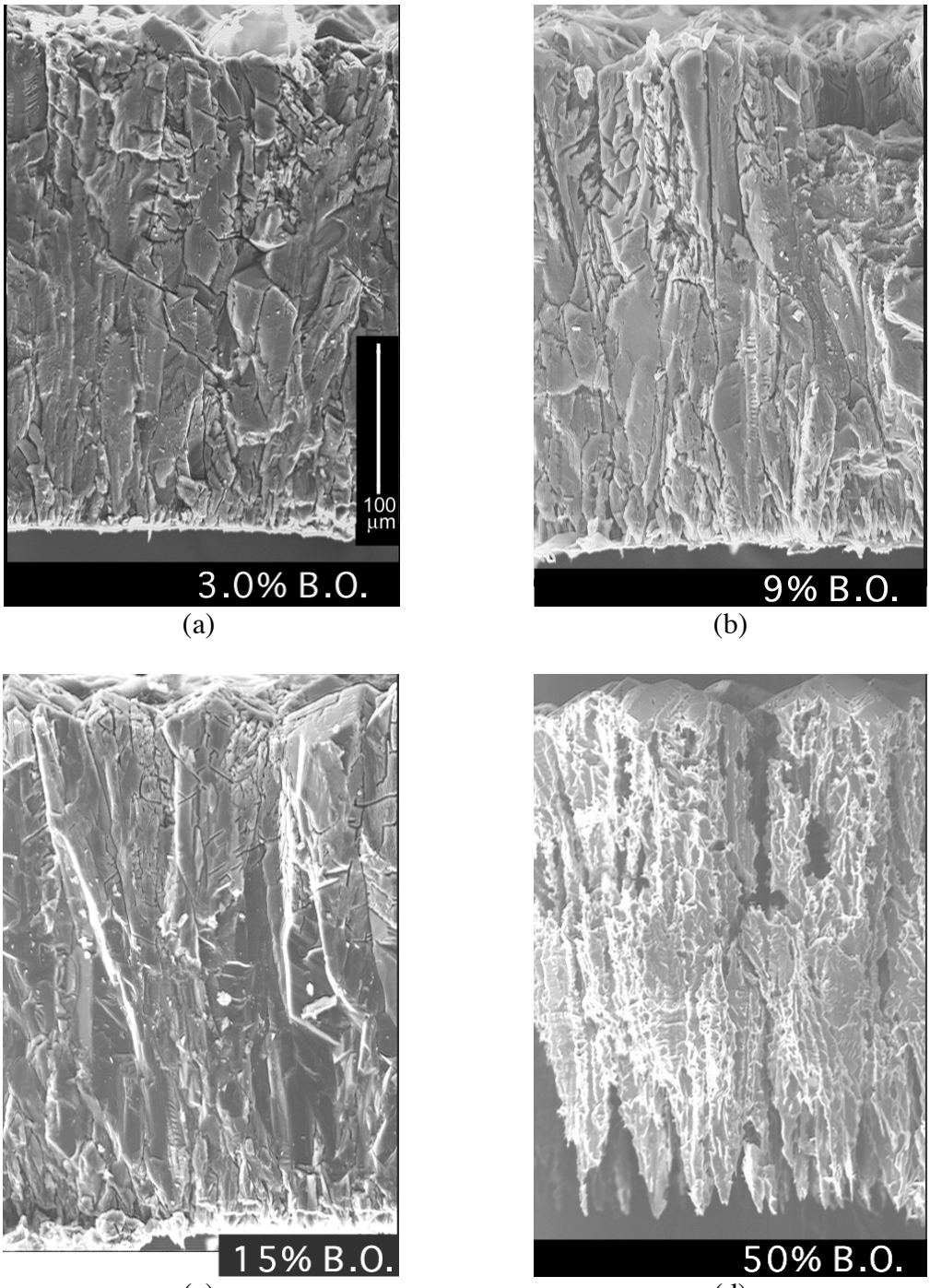

Figure 4-9. Change of microstructure on the cross-section of the CVD diamond film ET100 in 95 kPa O_2 flowing at 80 sccm. (a) 3 % weight-loss; (b) 9 % weight-loss; (c) 15% weight-loss; and (d) 50 % weight-loss. Images have the same magnification at 300 x. Oxidation begins on both exposed surfaces (as-grown and substrate sides).

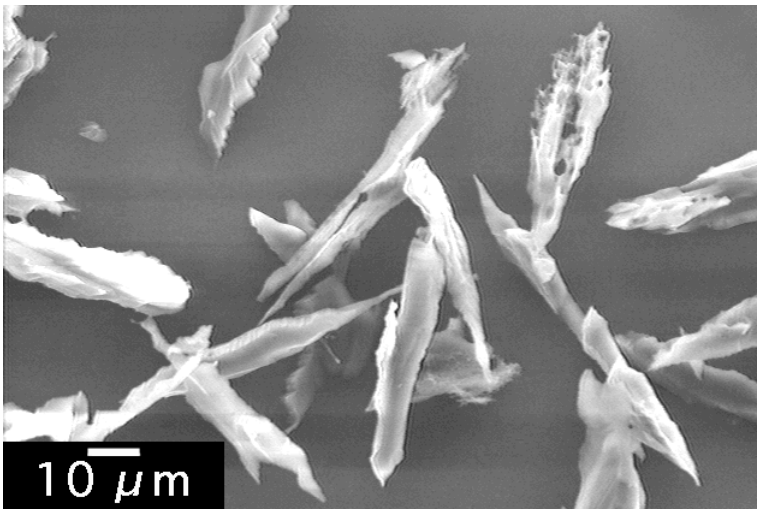

(a)

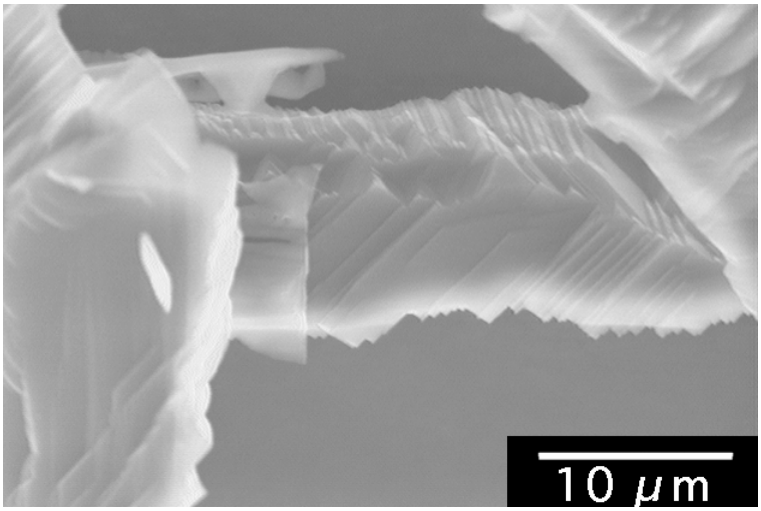

(b)

Figure 4-10. Remaining pieces of CVD diamond ET100 after oxidation at 625 ºC in 95 kPa O_2 flowing at 80 sccm and leveled-out at ~ 90 % weight-loss. The pieces are faceted. (a) The image at 800 x; and (b) the image taken at 2600 x.

and translucent due to the small amount of sp^2 carbon existing at the grain boundary.[3] These diamonds are actually whitened after oxidation due to the removal of sp^2 carbon at the grain boundaries and to the scattering effect of the smaller particle size.

4.3.2 Oxidation of CVD Diamond Films in 95 kPa O_2 at Low Weight-Loss Levels

The microstructure at low weight-loss level (less than 10 wt %) has generated great interest because the initiation stage is the most important part of the oxidation study. The kinetics of oxidation at low weight-loss levels is documented in Section 6.1. An oxidation study of ET100 films is carried out from 420 to 625 ºC in 95 kPa O_2 flowing at 80 sccm. Oxidation begins at 515 ºC. Oxidation preferentially occurs on {111} between 515 ºC and the highest tested temperature, 625 ºC. Figure 4-11 is a micrograph of oxidized diamond film at 550 °C. The weight-loss was 2.4 % after 170 min of oxidation. Compare to the micrograph of the film prior to oxidation (Figure 4-3), the entire {111} becomes rough; whereas, only a few etch pits appear on the {100}. Figure 4-12 contains a micrograph of the surface oxidized at 575 °C at a magnification of 17 kx. The weight-loss after 170 min of oxidation is 5.4 % at 575 °C, which is twice the mass loss observed at 550 °C. The arrow points to an oxidation wave front in Figure 4-12. Behind this line, oxidation converts the {100} to {111}. However, this newly created {111} have finer features compared to the original {111}, indicating that oxidation has progressed further on these surfaces. Again, there is no color change of the diamond films after oxidation at both temperatures in 95 kPa O_2.

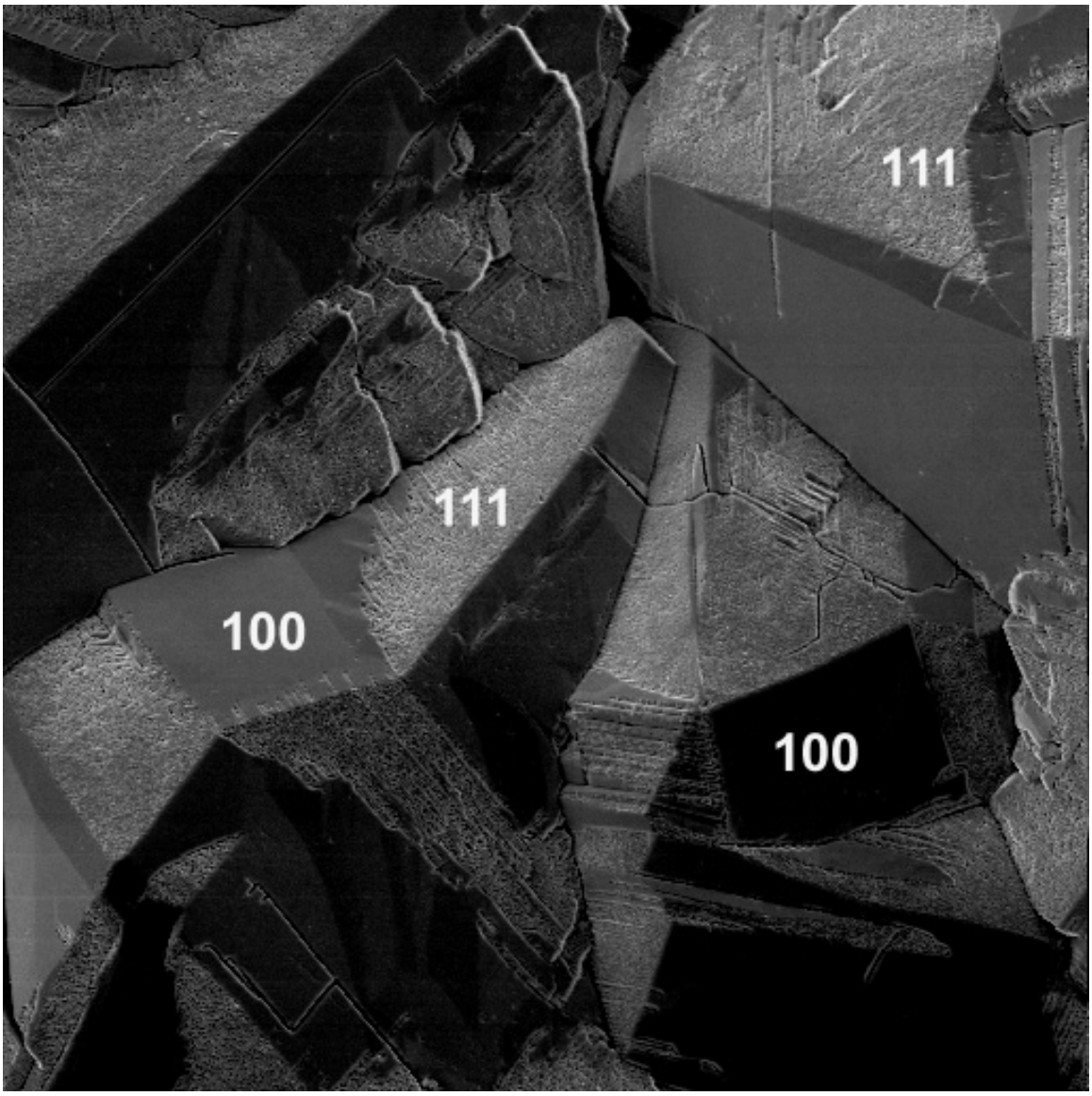

Figure 4-11. CVD diamond ET 100 oxidized at 550 °C in 95 kPa O_2 flowing at 80 sccm to a weight-loss of 2.4 wt %. Oxidation occurs preferentially on {111}.

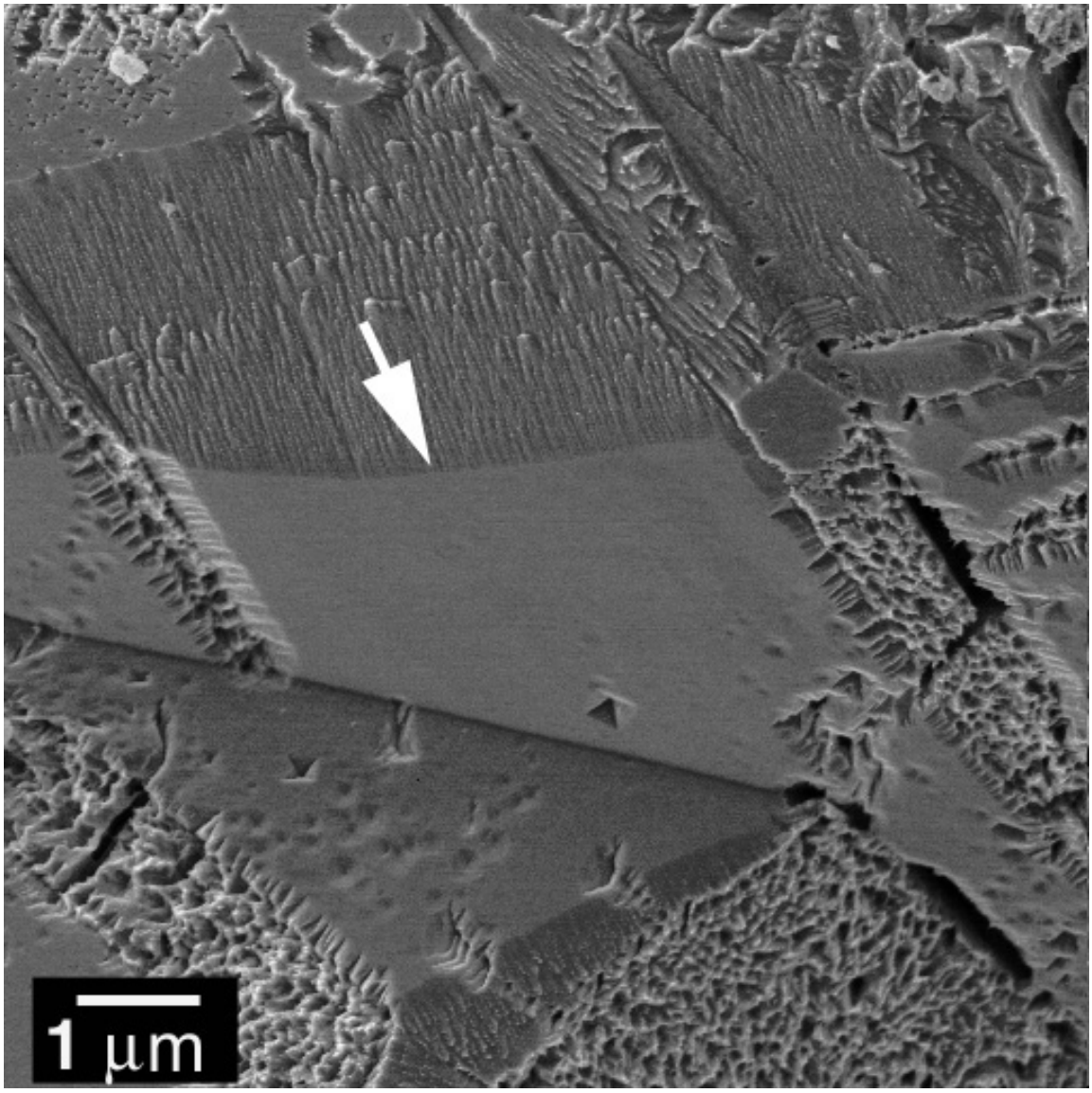

Figure 4-12. CVD diamond ET 100 oxidized at 575 ºC in 95 kPa O_2 flowing at 80 sccm (17 kx) to a weight-loss of 5.4 wt %. The {111} surfaces are severely degraded while the {100} remain relatively untouched. This image reveals an oxidation wave front moving along the edge of {100} converting this surface directly to {111}.

As Figures 4-11and 4-12 contain the images of large oxidized diamond surfaces. The fine features resulting from oxygen attack are highlighted in Figures 4-13 through 4-18 as these micrographs are taken at higher magnification between 30 and 200 kx. The oxidation process on (100) at an early stage can be traced from these micrographs. Prior to oxidation, all facets of the diamond film are smooth and pristine, Figure 4-3. There are no distinguishable features larger than 10 nm on these surfaces. The first step in oxidation is that these surfaces become "rough", as distinctive features appear on these once "smooth" facets. In the next step, the {111}-faceted pits form on roughened {100}. Finally, at the location of a pit, the pit extends laterally to form a groove during oxidation. Figure 4-13 contains a micrograph of pitted {100} with a groove just starting to form.

Figure 4-14 contains a micrograph showing a newly formed surface with rows of nodules (5.4% weight-loss). These nodules are 30 to 60 nm in diameter, residing on the tips of the crystalline facets, Figures 4-15 and 4-16. The nodule feature has not been observed on surfaces oxidized at 530ºC or lower. EDS analysis on these nodules indicates that they have the same chemical composition as the rest of the material, carbon. It is proposed that these nodules are sp^3-bonded amorphous carbon, as a product of partial oxygen coverage at elevated temperatures in high oxygen partial pressure conditions. This postulate is supported by our simulation findings described in Section 7.6.1.

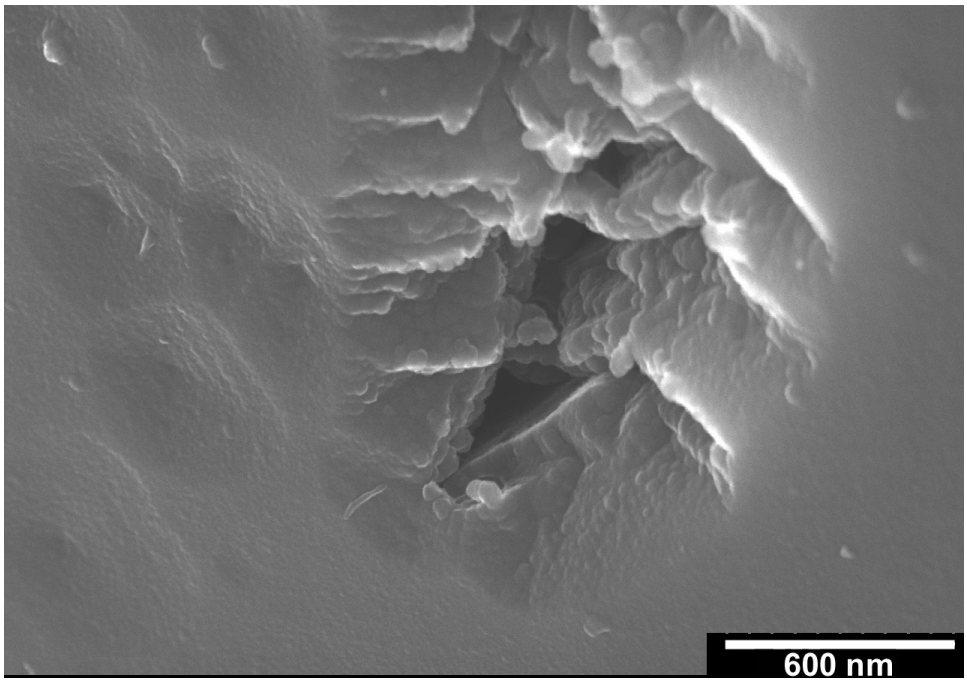

Figure 4-13. CVD diamond ET100 after exposure to 95 kPa O_2 flowing at 80 sccm at 575 ºC for 170 min to a 5.4 % weight-loss (50 kx). Pits and oxidation grooves on {100}.

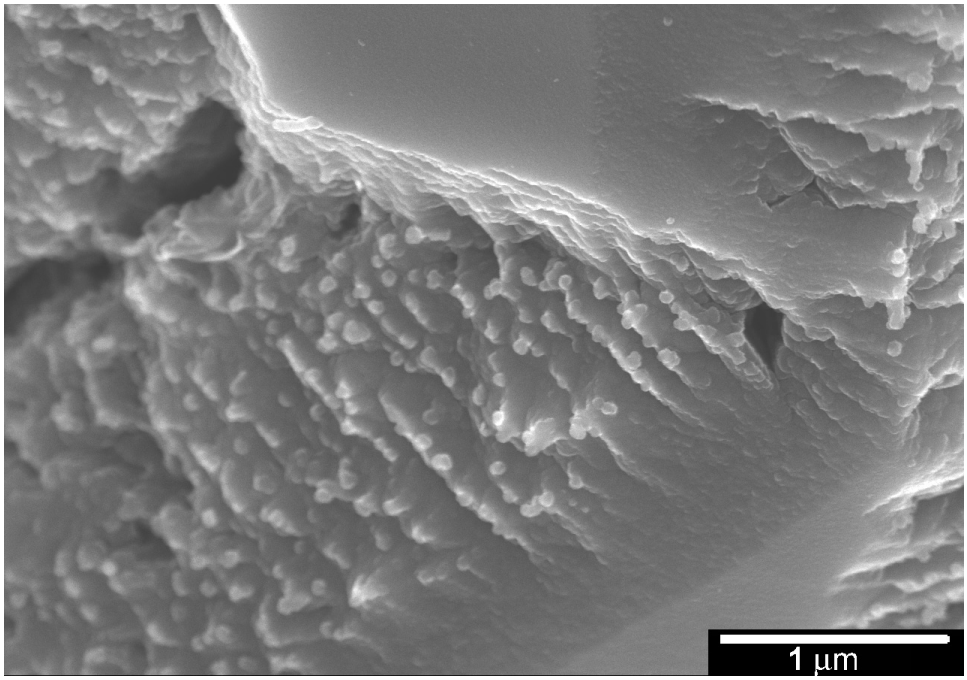

Figure 4-14. CVD diamond ET100 after exposure to 95 kPa O_2 flowing at 80 sccm at 575ºC for 170 min to a 5.4 % weight-loss (30 kx). Extensively oxidized {111} with nodules and the relatively smooth {100} elsewhere.

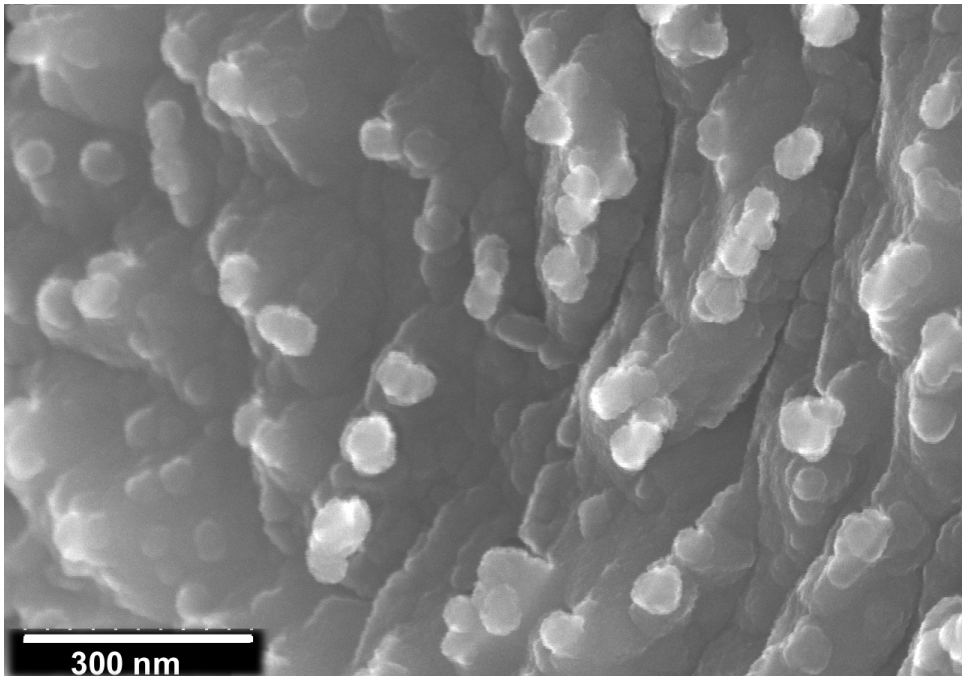

Figure 4-15. CVD diamond ET100 after exposure to 95 kPa O_2 flowing at 80 sccm at 575ºC for 170 min to a 5.4 % weight-loss (100 kx). The extensively oxidized {111} with arrays of nodules. The composition of the nodules is solely carbon, as identified by EDS.

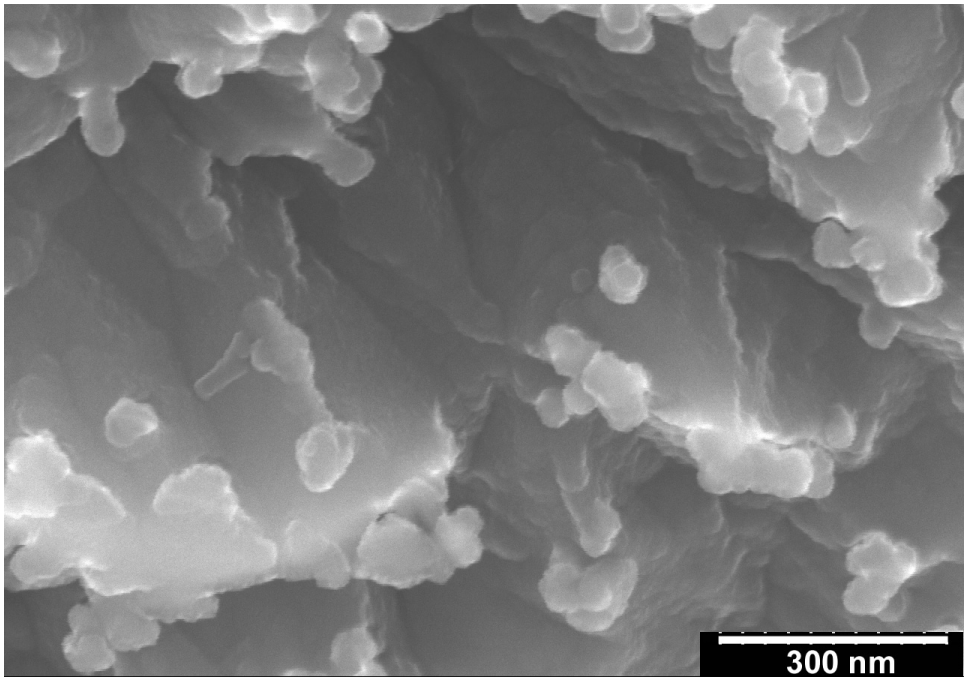

Figure 4-16. CVD diamond ET100 after exposure to 95 kPa O_2 at 575 ºC for 170 min to a 5.4 % weight-loss (100 kx). Nodules on the tips of the well-defined crystalline sheets.

There are many cracks also visible on the surface of diamond, Figure 4-11. Figure 4-17 contains a micrograph of the cracks taken at 100 kx. The cracks are the result of oxygen etching the surface deep into the bulk, rather than of the thermal mismatch at elevated temperatures. The nodules are also found along the edges of these cracks. The micrograph given in Figure 4-18 is taken at 300 kx. It reveals that the {100} become rough and converts to {111}. Although heat treating of ET100 at 500 °C in 95 kPa O_2 does not cause any degradation, oxidation of the diamond film initiates at 515 °C in 95 kPa O_2. Evidence of oxidation can be found at the roughened {111}, Figure 4-19. The roughing of {111} becomes more obvious in Figures 4-20 and 4-21.

Based upon the information provided by these images, a scenario of oxidation in 95 kPa O_2 can be plotted. Oxidation roughens the surfaces of both {111} and {100}. The rate of oxidation on {111} is faster and therefore initially visible. {111}-faceted pits are the preferential form on {100}. Once {111} surfaces are exposed, then these surfaces continue to react and open up more {111}-terminated surfaces.

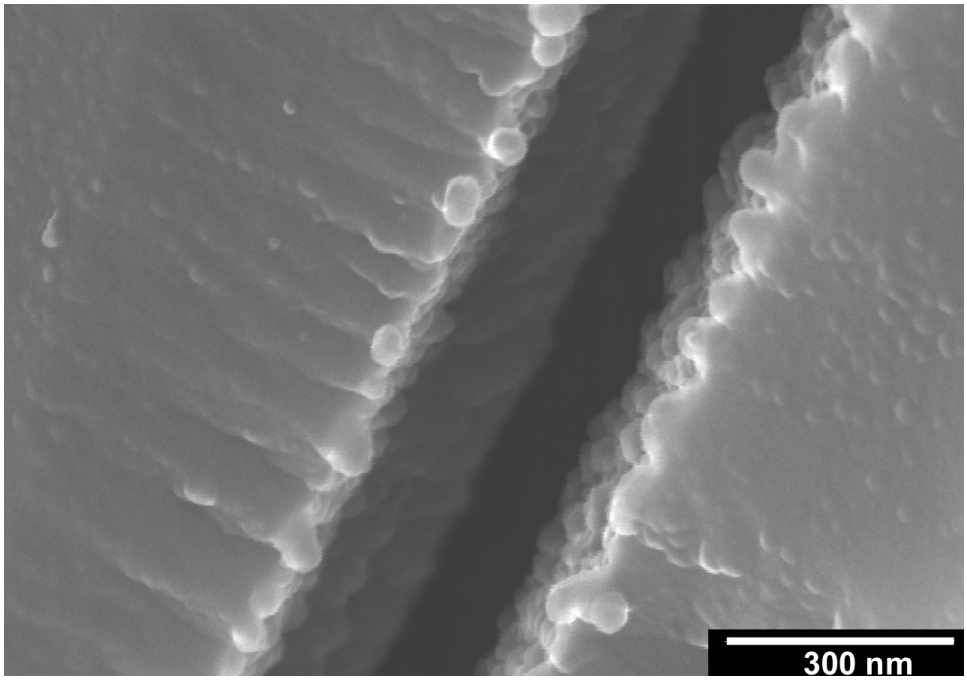

Figure 4-17. CVD diamond ET 100 after exposure to 95 kPa O_2 at 550 ºC to 2.4% weight-loss (100 kx). The nodules along the sides of the crack result from oxidation.

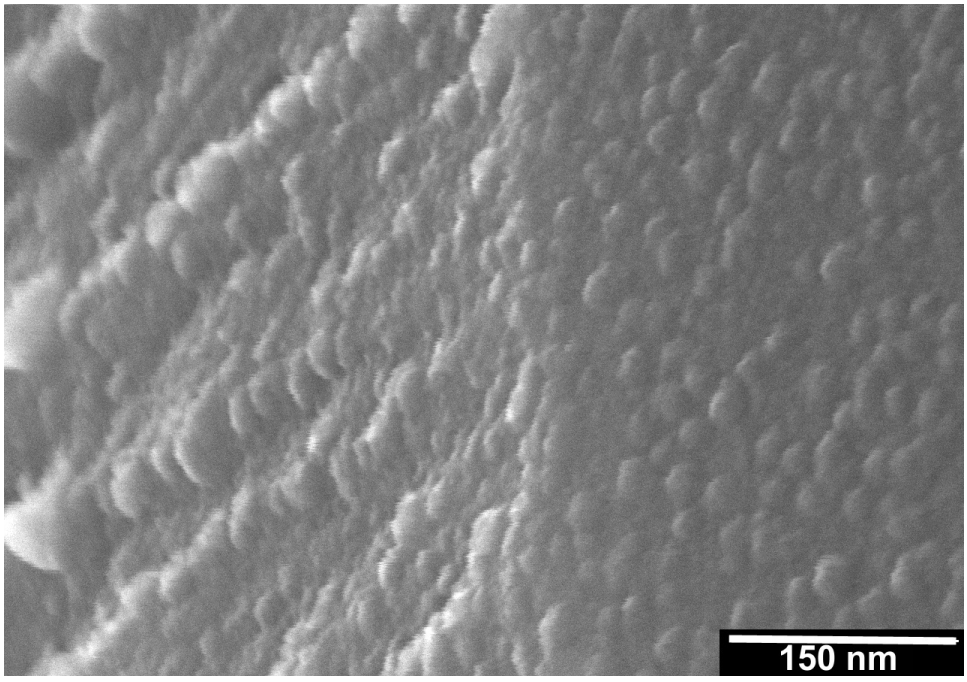

Figure 4-18. CVD diamond ET 100 after exposure to 95 kPa O_2 at 550 ºC to a 2.4% weight-loss (200 kx). Oxidation front moves from left to right on a roughened (100).

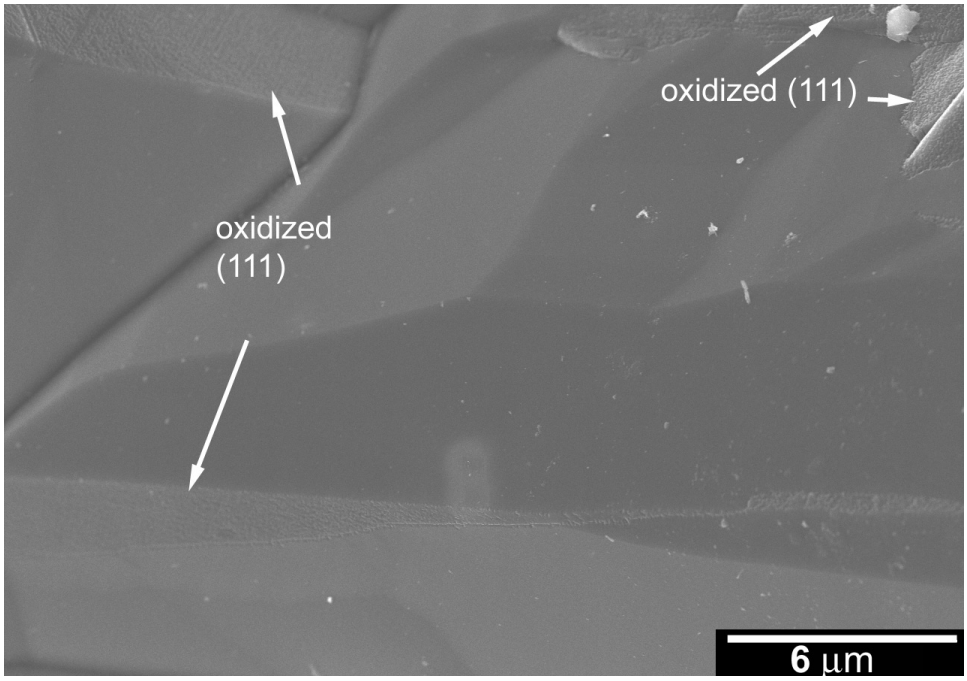

Figure 4-19. CVD diamond ET 100 treated at 515 ºC in 95 kPa O_2 for 170 min (5 kx). The film is oxidized as {111} becomes rough, but the{100} are still smooth.

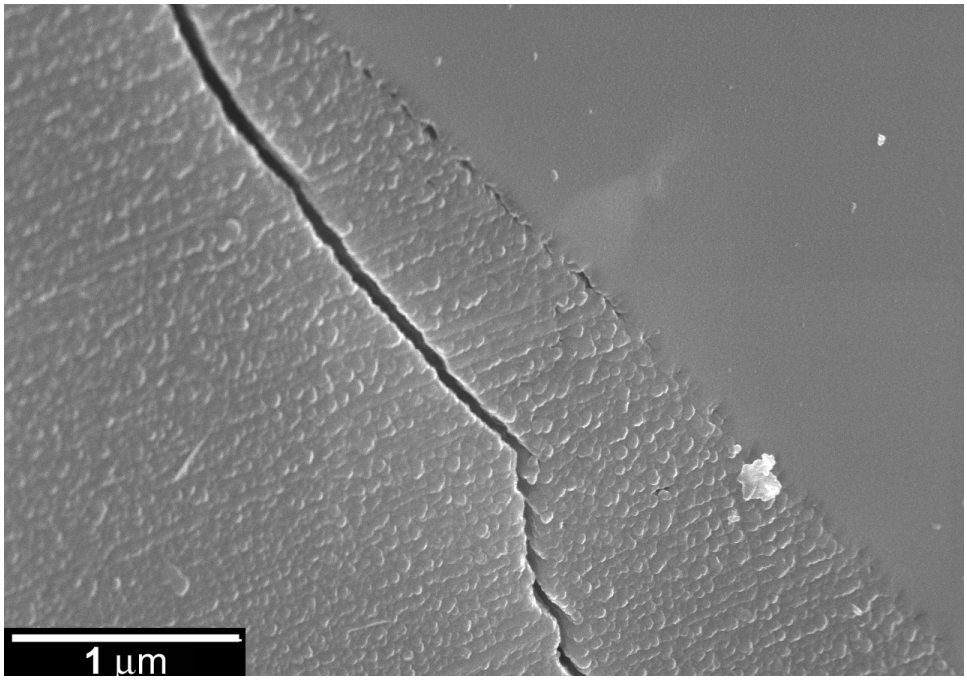

Figure 4-20. CVD diamond ET 100 after exposure to 95 kPa O_2 at 515 ºC (30 kx). The roughening of the surface is obvious at higher magnification.

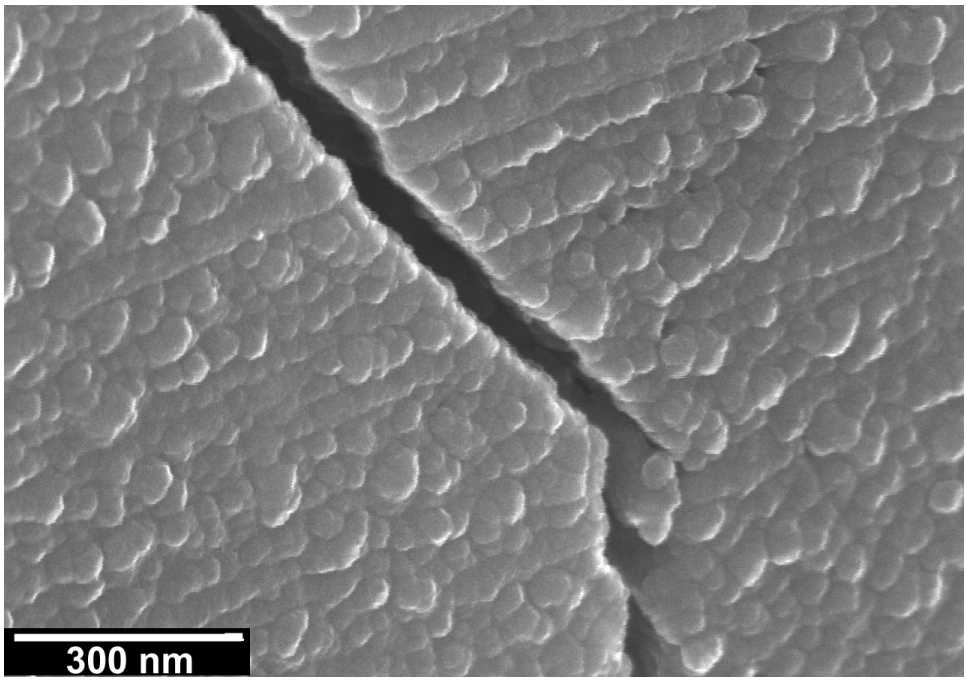

Figure 4-21. CVD diamond ET 100 after exposure to 95 kPa O_2 at 515 ºC. The round features and cracks on the roughened {111} result from oxygen attack.

4.4. Oxidation of CVD Diamond Film under 0.5 to 18 Pa O_2

Heat treatments of CVD diamond film ET100 are undertaken at temperatures between 750 and 1500 ^oC in oxygen with partial pressures ranging from 0.5 to 18 Pa. This pressure range is considered to be low oxygen partial pressure in the current study. There is neither a noticeable change of color nor microstructure after heat treatment in 0.6 Pa O_2 at 750 ^oC for 115 min. There is no weight-loss either. There is no evidence of oxidation or phase transition after examining the micrographs in Figures 4-22 and 4-23.

Oxidation and phase transition do occur simultaneously at low oxygen partial pressures when heat treatment temperature reaches 850 ^oC and higher. Figure 4-24 contains a micrograph taken from the film exposed to 18 Pa O_2 at 850 ^oC for 180 min. The film becomes dark and opaque, although the color does not turn dark uniformly throughout the entire surface. Oxygen preferentially attacks {111} and leaves {111}-faceted etch pits on {100}, Figure 4-24. This behavior is similar to that at high oxygen pressure (95 kPa O_2). However, the etched {111} have a different morphology (Figures 4-25 and 4-26) as compared to those oxidized in 95 kPa O_2 (Figures 4-13 to 4-16). In the low oxygen partial pressure case, there are no rows of nodules. The layer of black carbon is assumed to be very thin (positively less than 500 nm), and the layer is not distinguishable from the diamond film.

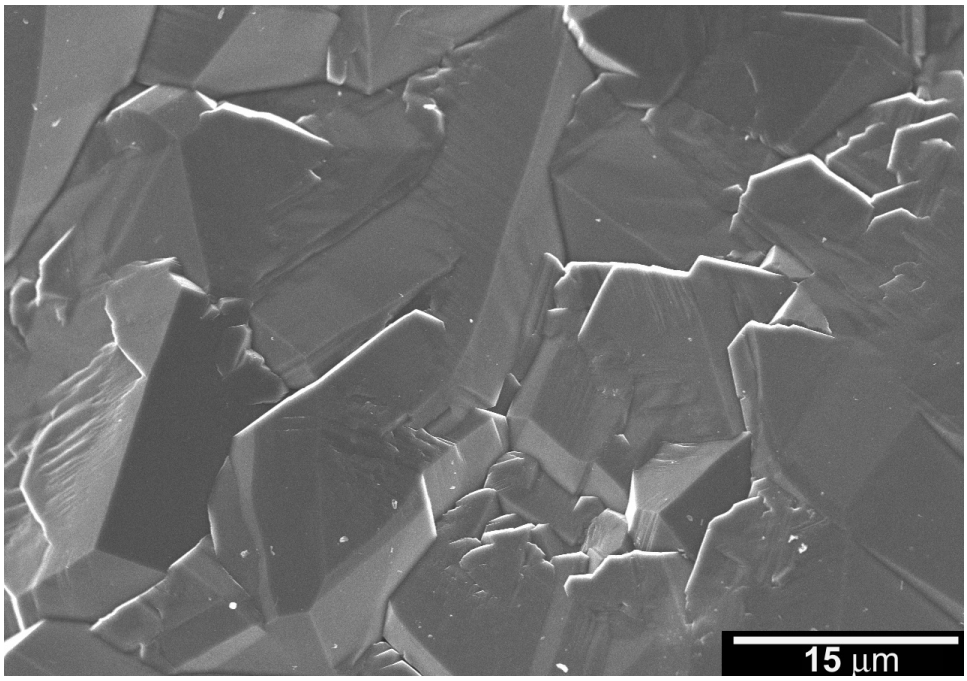

Figure 4-22. CVD diamond ET 100 exposed to 750 ^{o}C in 0.6 Pa O_2 for 110 min (2 kx). No evidence of oxidation or phase transition.

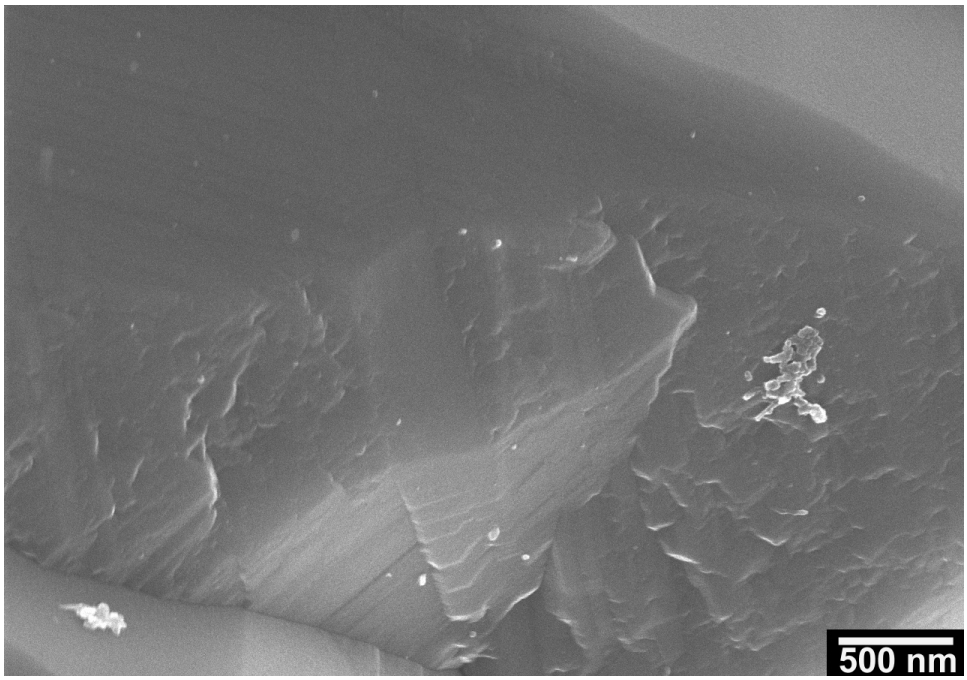

Figure 4-23. CVD diamond ET 100 exposed to 750 ^{o}C in 0.6 Pa O_2 for 110 min (30 kx). The bright spots on the surface are foreign debris.

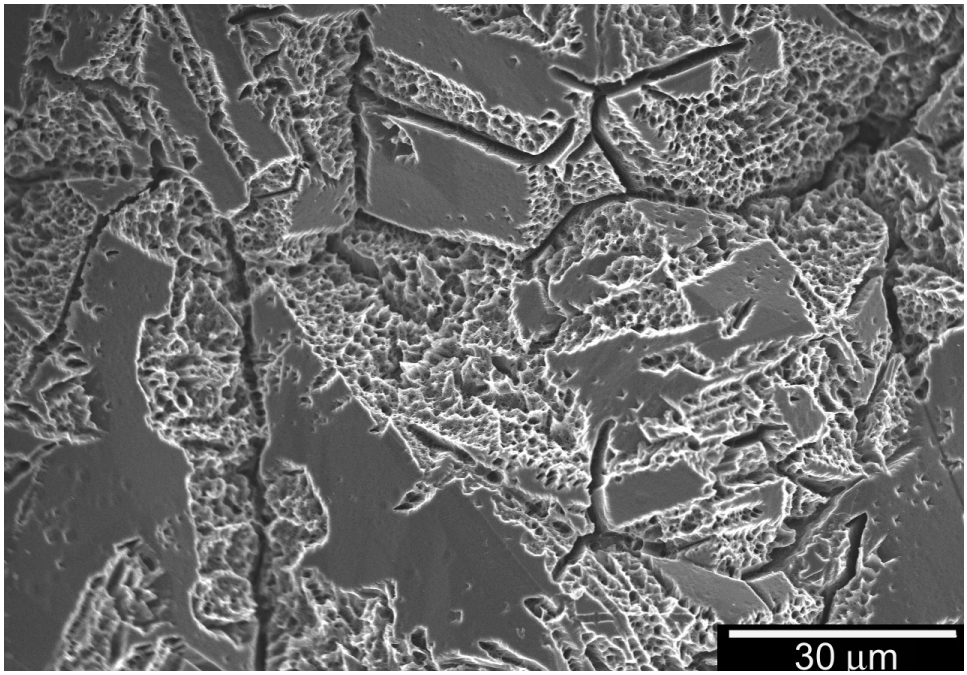

Figure 4-24. CVD diamond ET 100 exposed to 850 ^{o}C in 18 Pa O_2 for 180 min (1 kx).

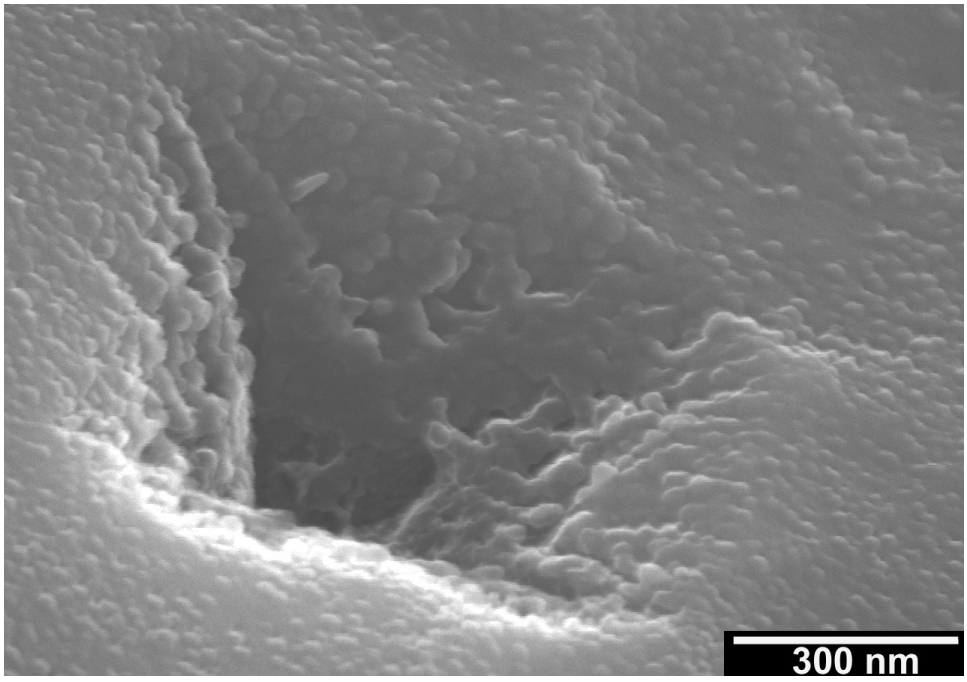

Figure 4-25. CVD diamond ET 100 exposed to 850 ^{o}C in 18 Pa O_2 for 180 min (100 kx). The {111}-faceted pit on the relatively smooth (100).

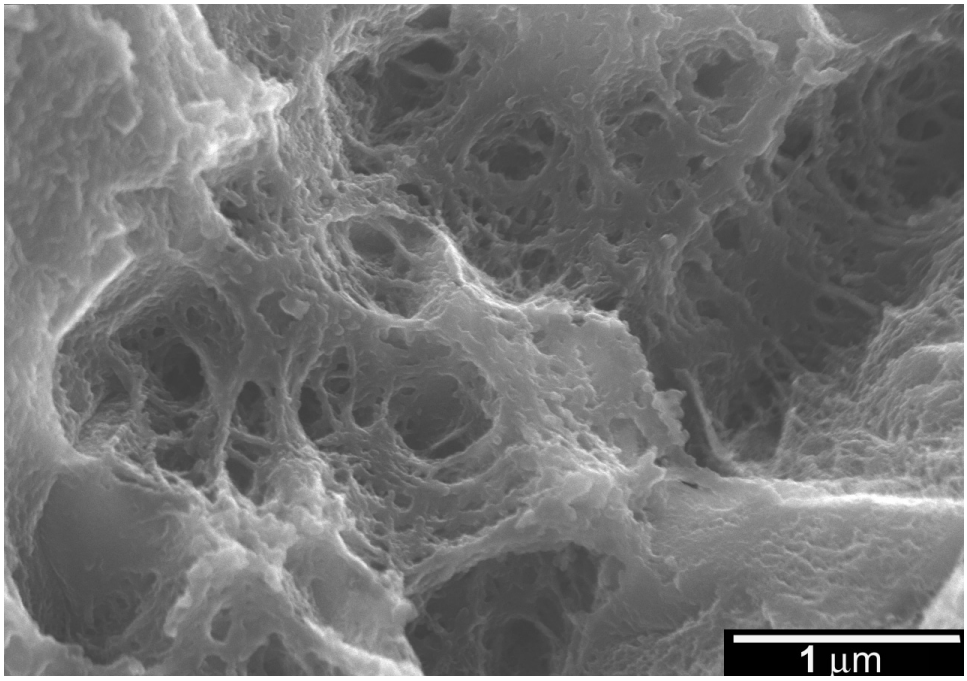

Figure 4-26. CVD diamond ET 100 exposed to 850 ^{o}C in 18 Pa O_2 for 180 min. The heavily oxidized {111} at 30 kx.

Figures 4-27 to 4-29 include the micrographs taken from films exposed to 0.6 Pa O_2 at 1000^{o}C for 170 min to a 1.6 % weight-loss. At 1000^{o}C, the carbon layer grows thicker than at 850^{o}C and separates from the diamond surfaces at some regions. If the diamond film treated at 850^{o}C in 18 Pa O_2 can be considered similar to those treated at 575^{o}C in 95 kPa O_2, the microstructure of these treated in 0.6 Pa O_2 at 1000^{o}C is less similar to the ones treated in 95 kPa O_2. Nonetheless, the {111} are still preferentially oxidized, as shown in Figure 4-27. The carbon layers are rolling and spalling out, Figure 4-28. The thickness of the layer is approximately 0.6 μm, Figure 4-29.

Figures 4-30 to 4-34 contain the micrographs taken from ET100 films treated at 1500 ^{o}C in 0.5 Pa O_2 for 120 min to a 12% weight-loss. Heat treating diamond films at these conditions give the surfaces a drastically different look as compared to those treated at lower temperatures and high oxygen pressures, Figure 4-30. There are no faceted etch pits, but rather round dents and cracks, Figures 4-31 and 4-32. The cracks here are different from those found on the surfaces oxidized in 95 kPa O_2 (Figures 4-17 and 4-21). It is hard to tell if the cracks follow certain crystalline directions which is the case at high pressure. A micrograph of a crack running through the carbon layer is given in Figure 4–33. Dents are formed along the cracks, Figure 4-34.

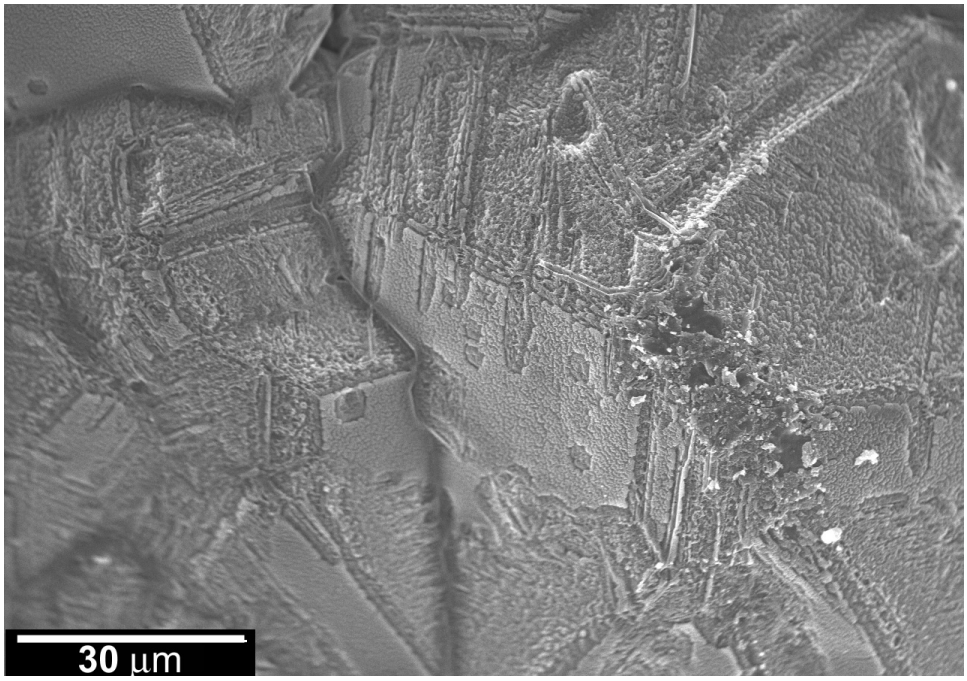

Figure 4-27. CVD diamond ET100 exposed to 0.6 Pa O_2 at 1000 ^oC for 170 min to a 1.6% weight-loss. The microstructure indicates a combination of oxidation and phase transition (1 kx).

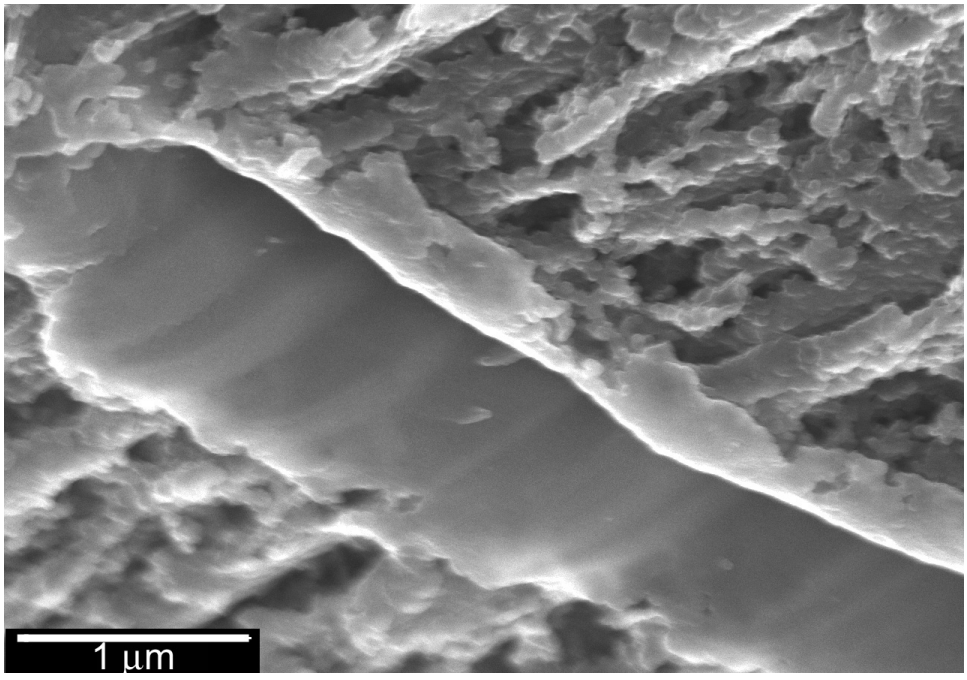

Figure 4-28. CVD diamond ET 100 exposed to 0.6 Pa O_2 at 1000 ^oC for 170 min to a 1.6% weight-loss (30 kx). The peeling carbon layer results from phase transition.

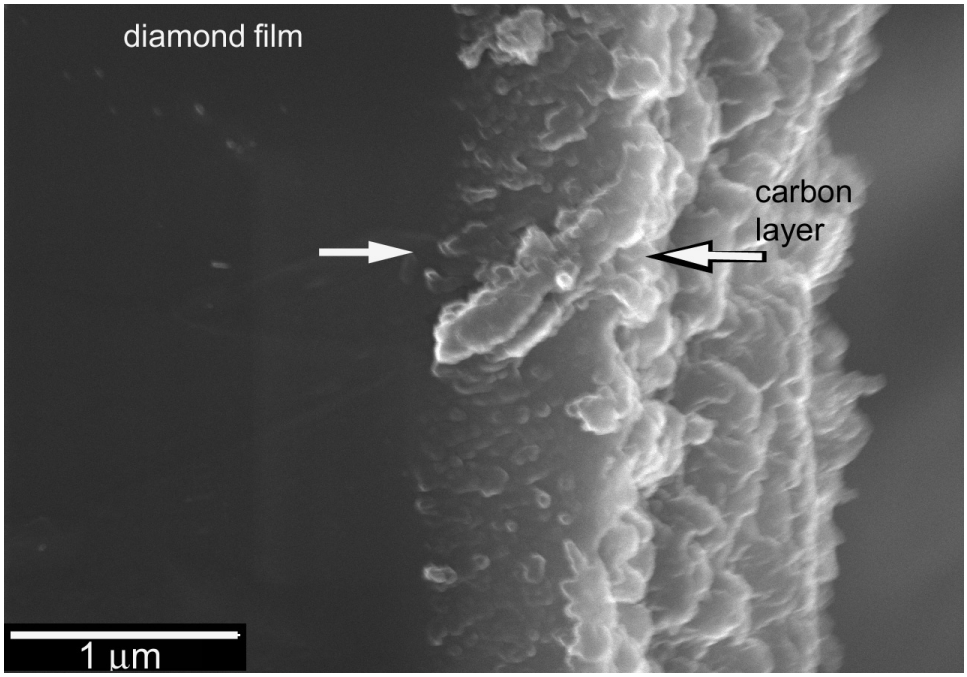

Figure 4-29. CVD diamond ET 100 exposed to 0.6 Pa O_2 at 1000 ^{o}C for 170 min to a 1.6% weight-loss. The surface is fully covered by the black-colored carbon layer (30 kx).

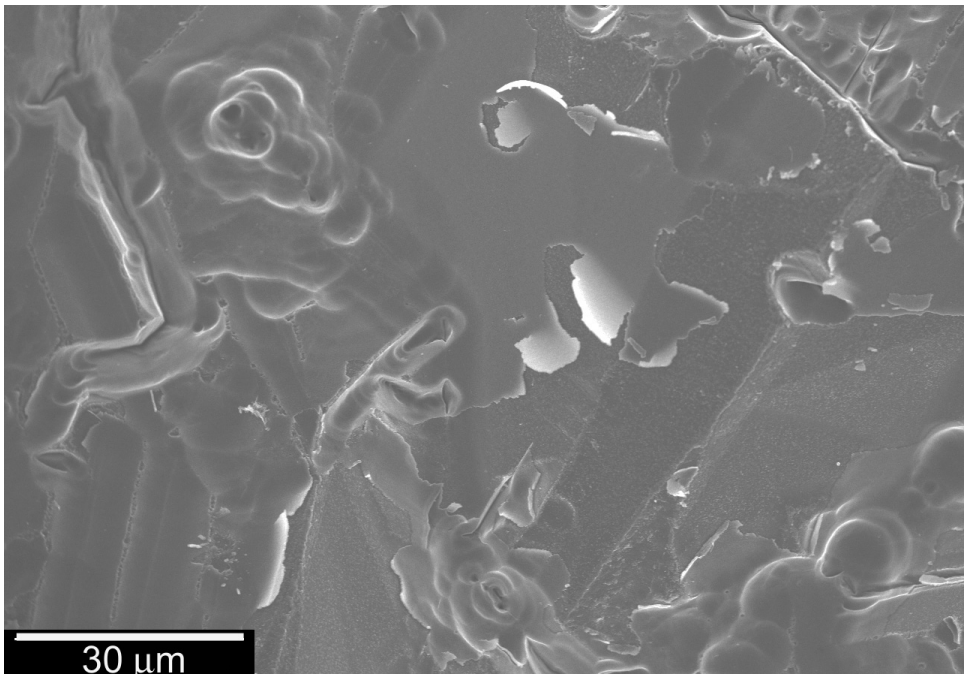

Figure 4-30. CVD diamond ET100 treated at 1500 ^{o}C in 0.5 Pa O_2 for 120 min to a 12% weight-loss (1 kx). The peeling layers of carbon and the round craters on the surface are ubiquitous.

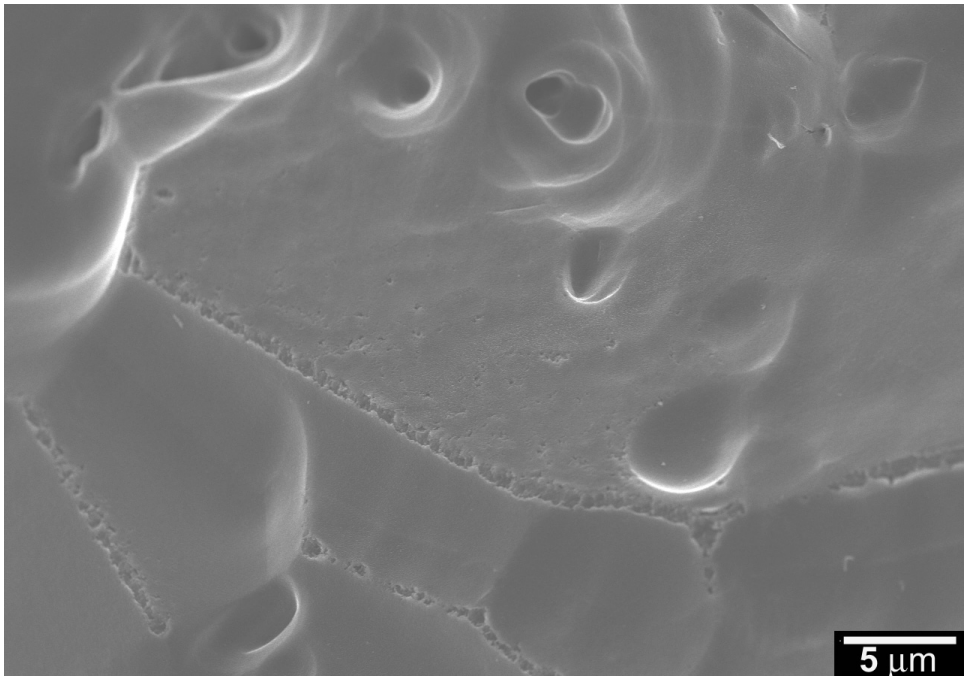

Figure 4-31. CVD diamond ET 100 treated at 1500 ^{o}C in 0.5 Pa O_2 for 120 min to a 12% weight-loss (3 kx). The rounded dents and cracks are the common features.

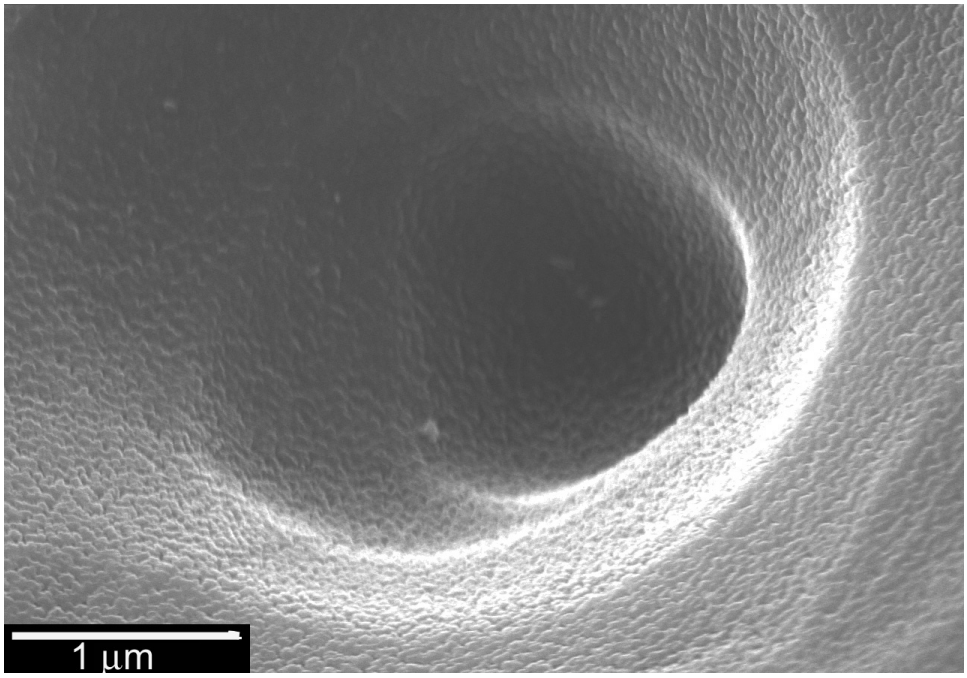

Figure 4-32. CVD diamond ET 100 treated at 1500 ^{o}C in 0.5 Pa O_2 for 120 min to a 12% weight-loss (30 kx).

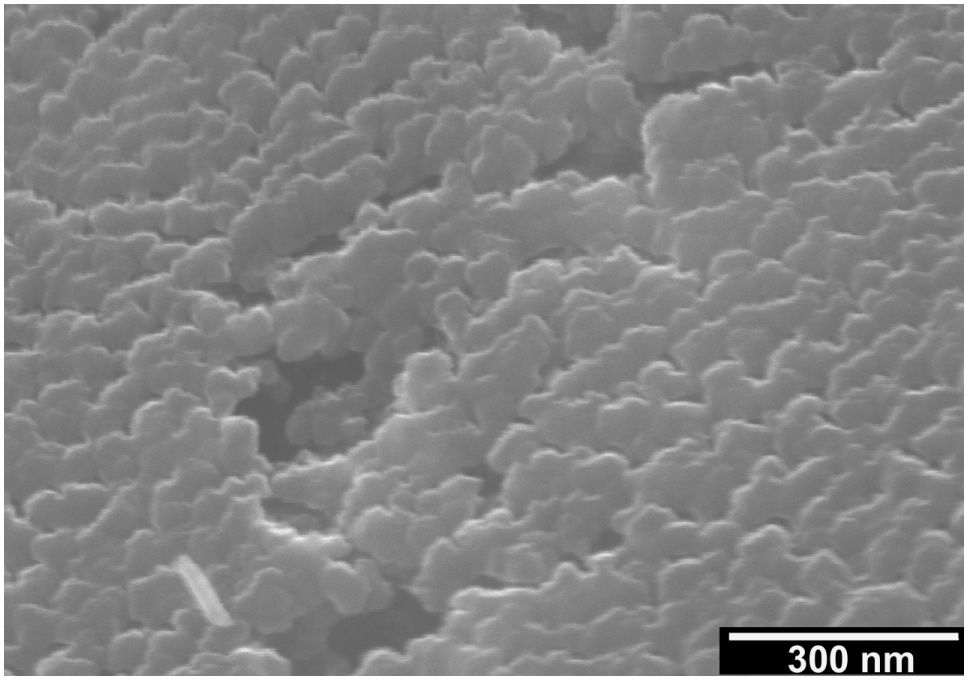

Figure 4-33. CVD diamond ET 100 treated at 1500 ^{o}C in 0.5 Pa O_2 for 120 min to a 12% weight-loss. The fine details of the carbon layer with cracking running through (100 kx).

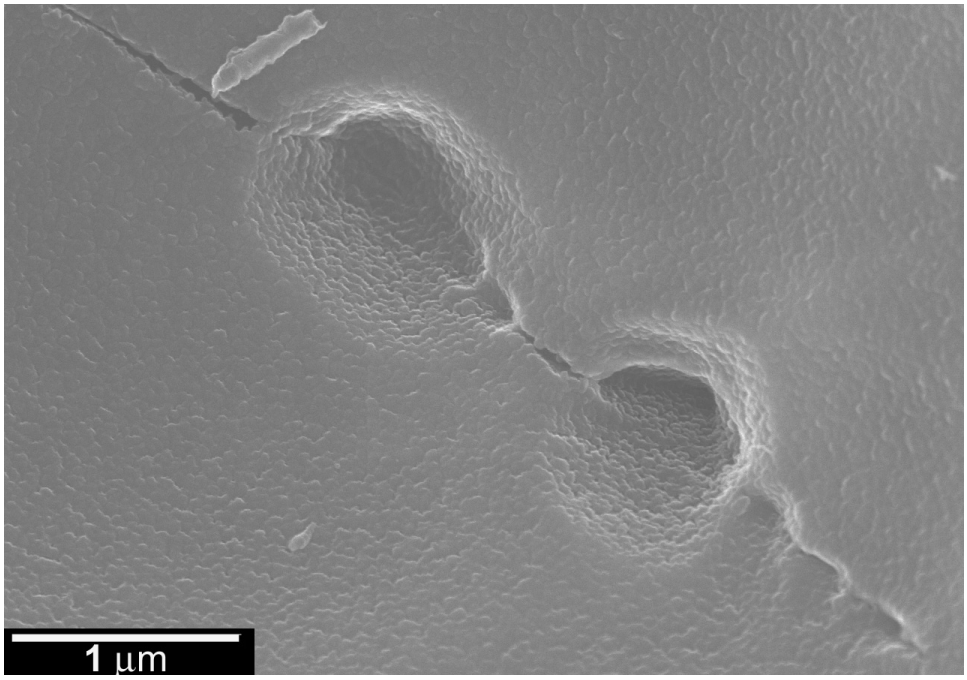

Figure 4-34. CVD diamond ET 100 treated at 1500 ^{o}C in 0.5 Pa O_2 for 120 min to a 12% weight-loss. Formation of craters along the cracking (30 kx).

4.5 SEM and TEM of Diamond Films Oxidized in $6x10^{-10}$ Pa O_2

CVD diamond films ET100 are treated in flowing helium gas at temperatures of 1003, 1303, and 1478°C for 600 min. The oxygen partial pressure of the carrier gas helium is $6x10^{-10}$ Pa. The oxygen concentration is only $1x10^{-14}$ of the pressure at 95 kPa O_2. In order to appreciate the slow reaction at such low oxygen partial pressure, the heat-treat time is set much longer, to 600 min. Figures 4-35 to 4-39 contain the micrographs taken from diamond exposed to $6x10^{-10}$ Pa O_2 at 1478 °C for 600 min. Figure 4-35 is a micrograph showing a relative large area of the surface. Instead of having etching features, the surface of the diamond film is fully covered by a layer of carbon. There are no pits or dents on the surfaces at all. The cracks likely result from the lattice mismatch of carbon and diamond. Figures 4-36, 4-37, and 4-38 are the micrographs taken from a side view (cross-sectional) so the carbon layer can be examined easily. The carbon layer is uniform with a thickness of ~ 1 μm. Figure 4-39 gives fine details of the carbon layer at 100 kx. The layer is granular. The individual granule has a diameter between 30 and 60 nm. It is of great interest to find out if the carbon layer is amorphous or crystalline. TEM combined with selected-area electron diffraction is used to investigate the crushed carbon layer. Figure 4-40 is a TEM image along with the electron diffraction pattern. The layer is amorphous as indicated by the diffusive rings in the electron diffraction pattern.

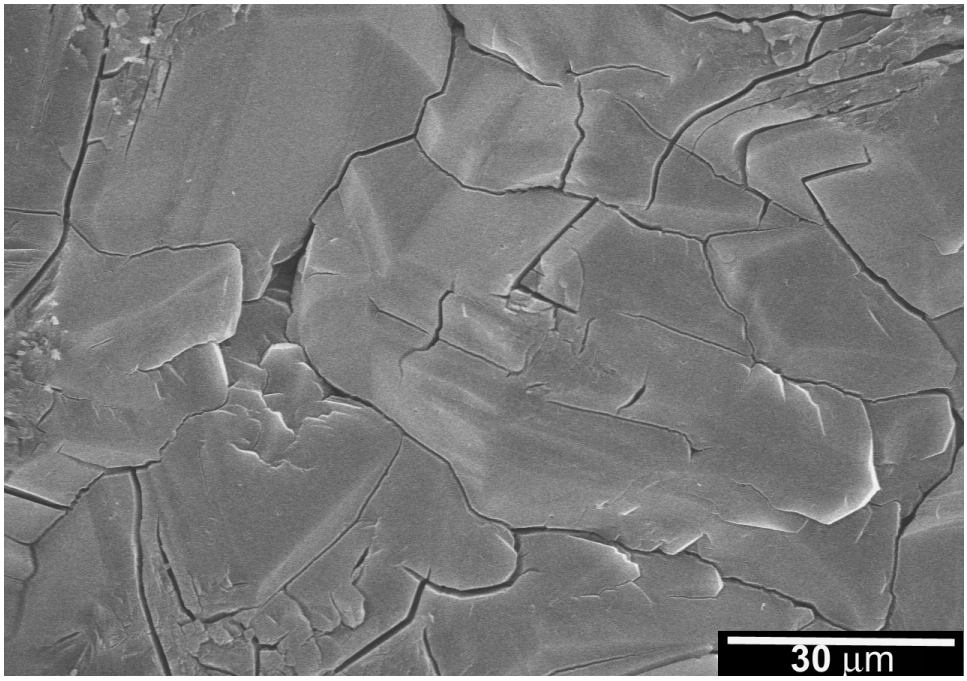

Figure 4-35. CVD diamond ET100 treated at 1478 ^{o}C in 6x10^{-10} Pa O_2 for 600 min (1 kx).

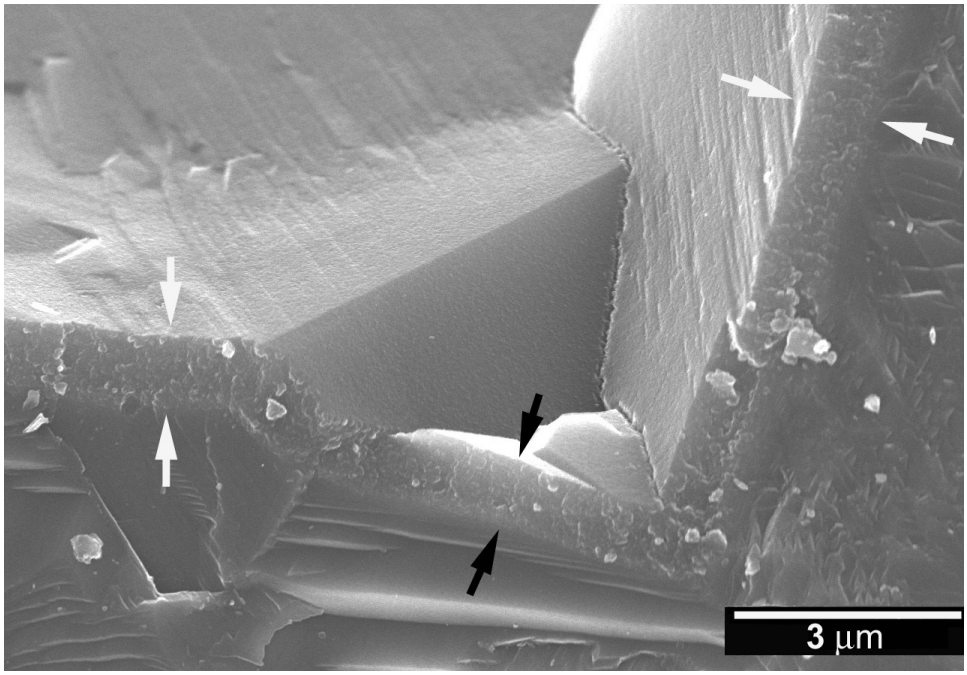

Figure 4-36. CVD diamond ET 100 treated at 1478 ^{o}C in 6x10^{-10} Pa O_2 for 600 min. Diamond film is uniformly covered by 1-µm-thick carbon. The sharp corners of the diamond facets are preserved.

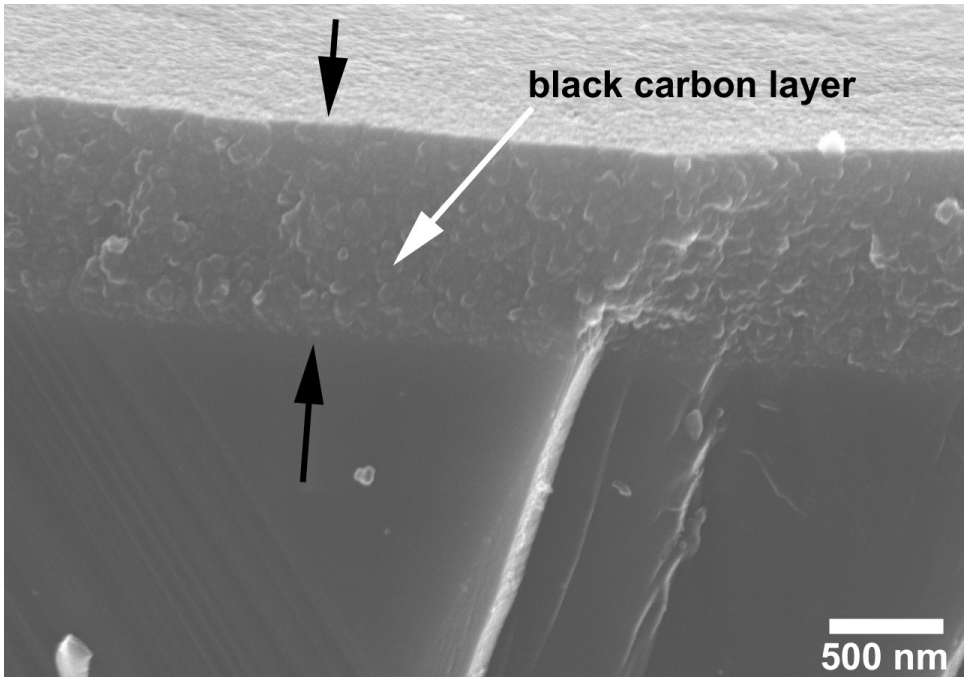

Figure 4-37. CVD diamond ET100 treated at 1478 ^{o}C in 6x10^{-10} Pa O_2 for 600 min. Carbon layer formed on top of the diamond (30 kx).

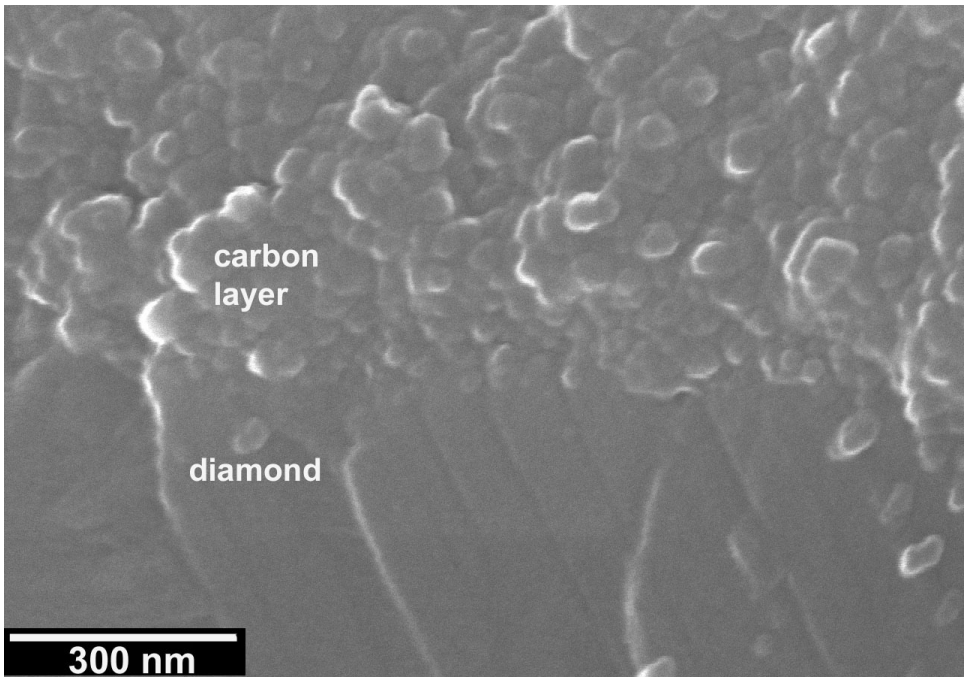

Figure 4-38. CVD diamond ET100 treated at 1478 ^{o}C in 6x10^{-10} Pa O_2 for 600 min. A closer view of the interface between diamond and carbon layer at 100 kx.

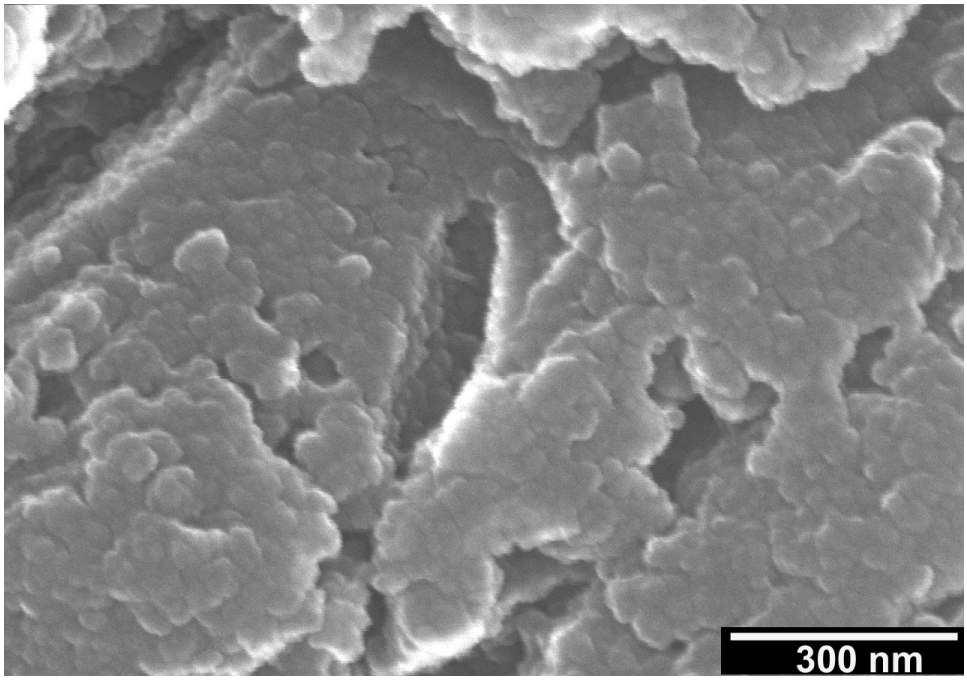

Figure 4-39. CVD diamond ET100 treated at 1478 ^{o}C in 6x10^{-10} Pa O_2 for 600 min. A top view of the microstructure of the carbon layer formed on diamond (100 kx).

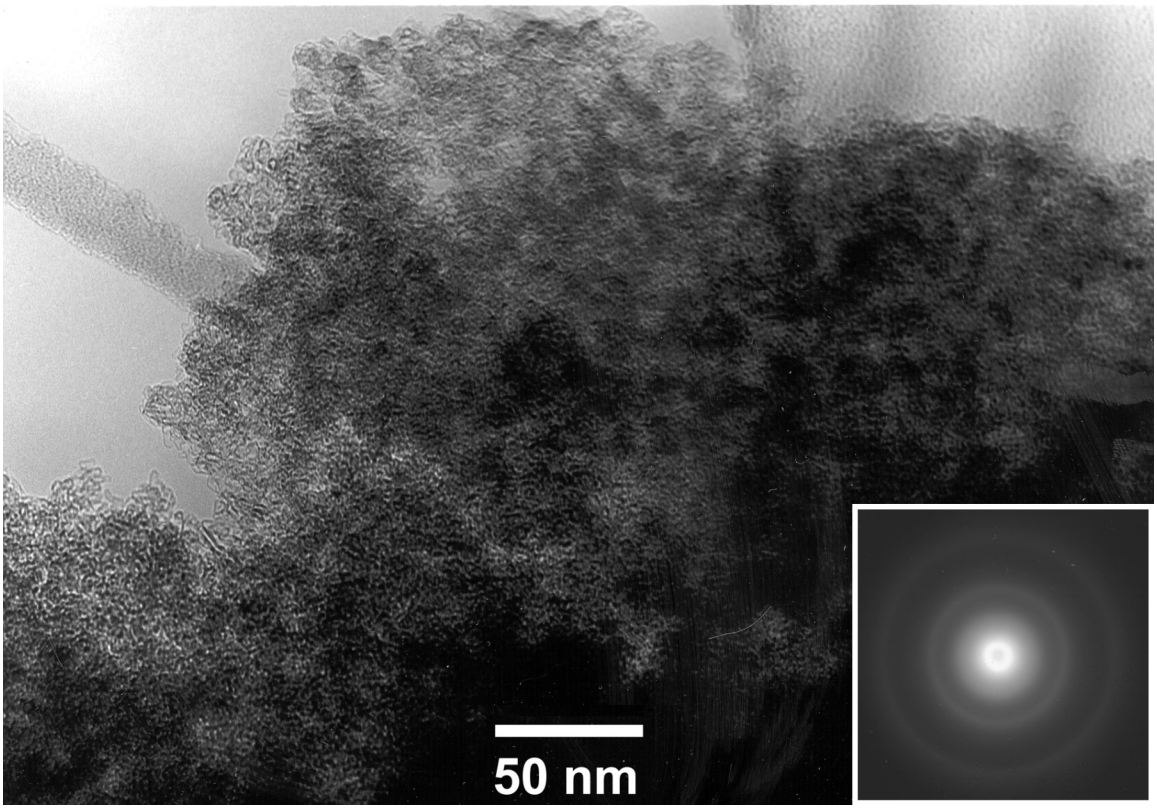

Figure 4-40. TEM image (at 400 kx) and electron diffraction pattern of the carbon layer formed during the treatment of CVD diamond ET 100 at 1478 ^{o}C in 6x10^{-10} Pa O_2 for 600 min. The blur diffraction rings at the corner suggest the amorphous nature of the carbon layer.

4.6 Oxidation of sp^2-Bonded Carbon at 600 ^oC in 95 kPa O_2

Highly oriented pyrolytic graphite (HOPG) is a crystalline form of sp^2-bonded carbon, and glassy carbon is an amorphous form of sp^2-bonded carbon. HOPG and glassy carbon are chosen as reference materials in the current study for the sake of comparison with sp^3-bonded diamond films. Oxidation of HOPG and glassy carbon is undertaken at 600 ^oC in 95 kPa O_2 for 170 min. After 170 min, glassy carbon reaches a 2 % weight-loss, whereas HOPG is more severely oxidized to a 12% weight-loss. The weight-loss of CVD diamond ET100, HOPG and glassy carbon is compared after exposure to 95 kPa O_2 at 600 ^oC for 130 min. The weight-loss of diamond is 12 % versus 8% for HOPG and 1.8% for glassy carbon. The weight-loss clearly indicates that glassy carbon is the most resistant to oxidation, followed by HOPG and then diamond. Figure 4-41 contains a micrograph of oxidized glassy carbon at 2 % weight-loss. The surface is full of curvy "ruts" and "craters". The fine features of the surface can be appreciated in the micrographs given in Figures 4-42 and 4-43, which are taken at higher magnifications. These "ruts" and "craters", 3 to 5 μm wide, have smooth walls as compared with the surrounding areas. Their formation is quite intriguing and it is a subject deserves further investigation.

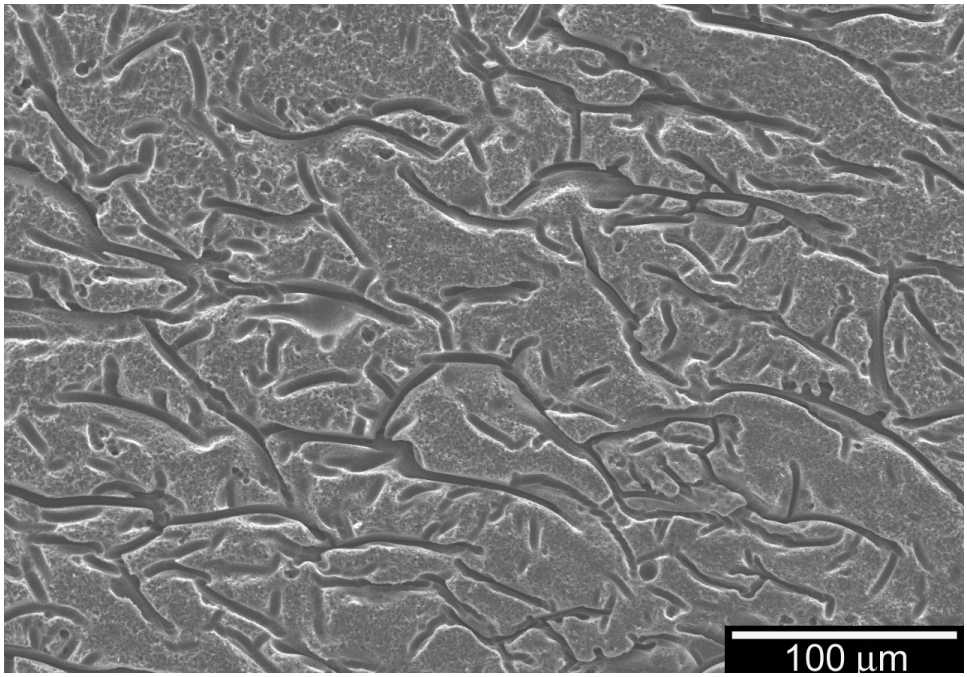

Figure 4-41. Glassy carbon treated at 600 ^{o}C in 95 kPa O_2 for 170 min to a 2% weight-loss. The oxidized surface is full of "ruts" (300 x).

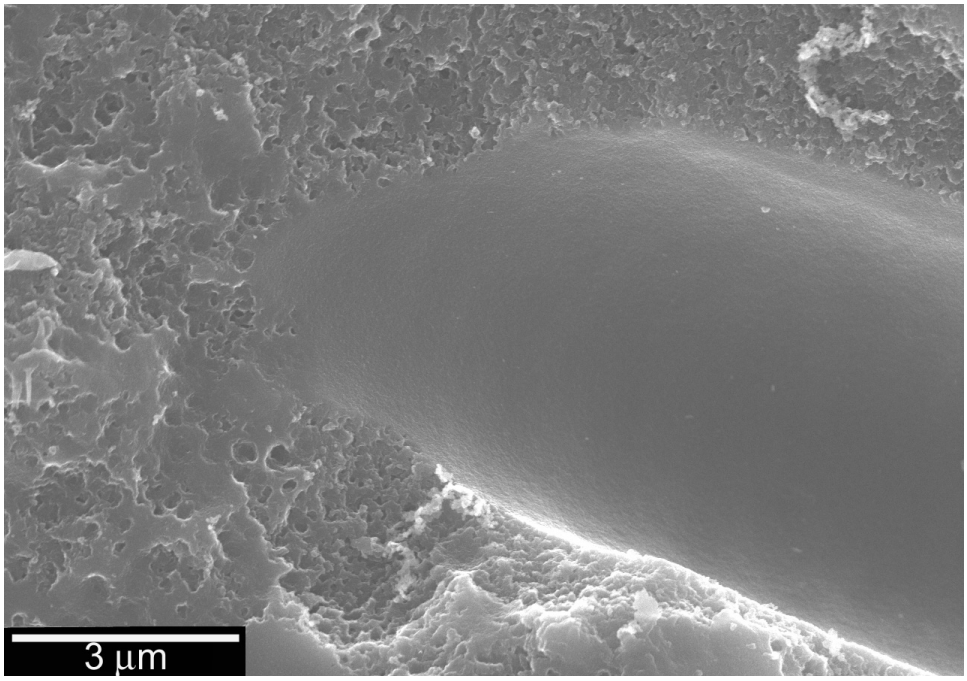

Figure 4-42. Glassy carbon treated at 600 ^{o}C in 95 kPa O_2 for 170 min to a 2% weight-loss. A closer view of a tip of a "rut" and the etched surrounding area (10 kx).

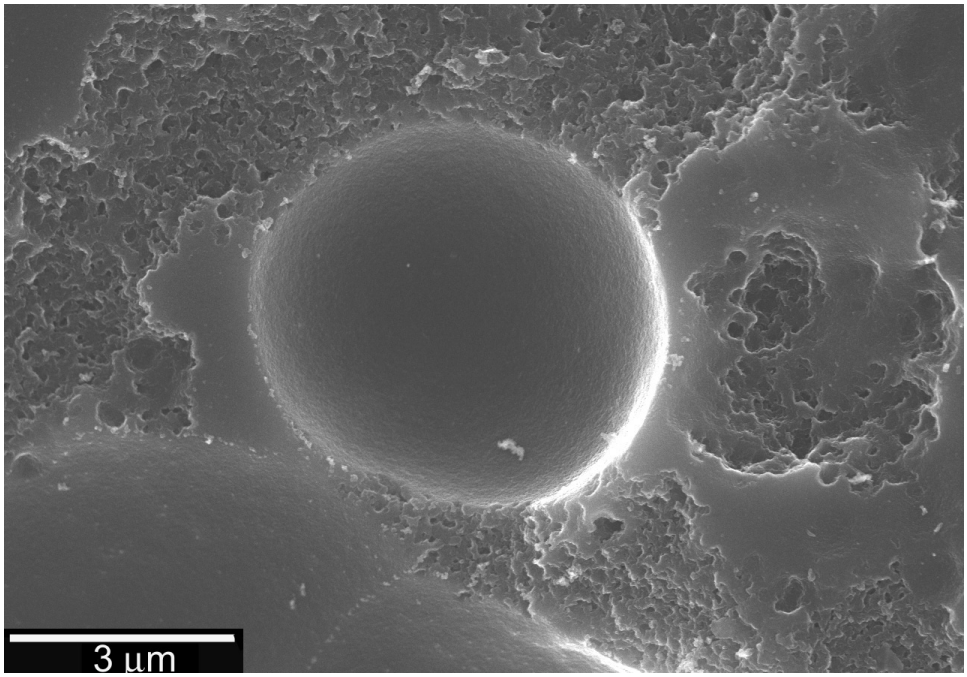

Figure 4-43. Glassy carbon treated at 600 ^{o}C in 95 kPa O_2 for 170 min to a 2% weight-loss. A closer view of a crater and the etched surrounding area (10 kx).

Figure 4-44 contains a micrograph of oxidized HOPG. The surface of the HOPG oxidized to a 12 wt % weight-loss is full of pits; however the graphene layers remain smooth and intact, Figure 4-44. A micrograph featuring the etched pit is given in Figure 4-45 at 100 kx. Oxidation exclusively occurs by forming a pit and expanding it deeper and wider, layer by layer. Unlike the oxidized glassy carbon, the pits on HOPG have well-defined straight and sharp-turning edges. The microstructure of oxidized HOPG observed in the current study is consistent with the oxidation behavior of HOPG, in which oxidation occurs preferentially at the edge site, not on the graphene layers. Hennig reports that the oxidation rates at edge sites are at least 20 times higher than on the graphene layers.[4] The preferential oxidation of HOPG on different sites inspires us to propose an oxidation mechanism of diamond in Section 6.4.

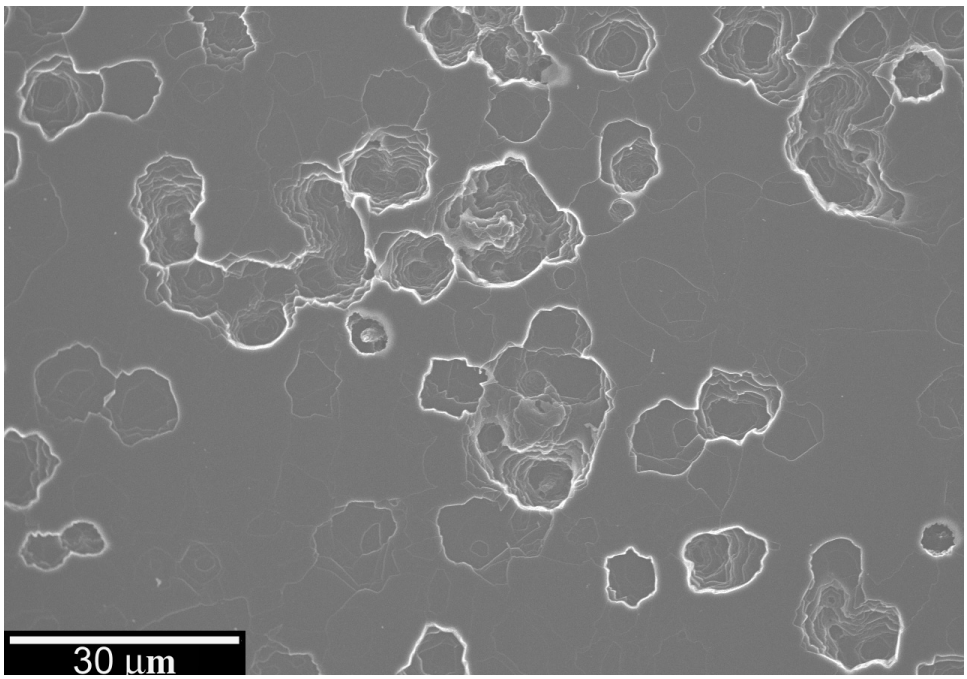

Figure 4-44. HOPG treated at 600 ^{o}C in 95 kPa O_2 for 170 min to a 12% weight-loss. The surface is full of etch pits (1 kx).

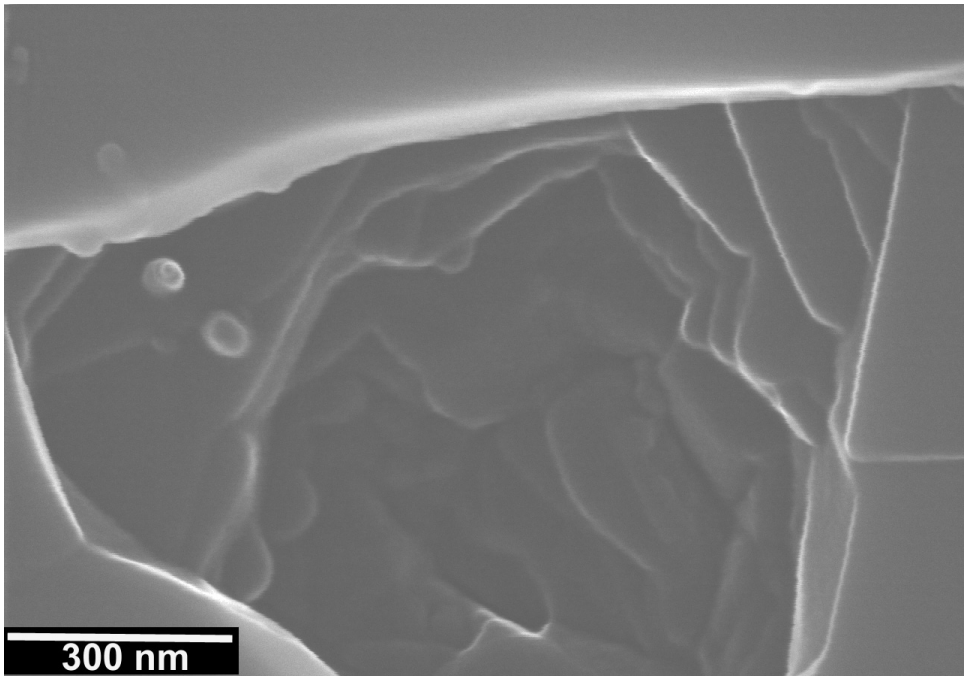

Figure 4-45. HOPG treated at 600 ^{o}C in 95 kPa O_2 for 170 min to a 12% weight-loss. The well-defined edges of the pits follow certain crystalline directions (100 kx).

4.7. Discussion and Summary

The "nodules" appearing on the diamond surfaces under 95 kPa O_2 are interesting features. Although no experiments have been undertaken to determine whether the nodule is crystalline or amorphous, computer simulation suggests that a partially oxygen chemisorbed surface (60% coverage) is amorphous with an sp^3 hybridization state (in Section 7.6.1). Backed up by Sappok and Boehm, and Matsumoto, et al.'s findings, we assume that the surface coverage is approximately 50% at 550 and 575 ^oC in 95 kPa O_2.[5-6] These researchers report that surface coverage is approximately 50% or more at temperatures higher than 550 ^oC. Therefore, we propose that these nodules are the objects that are amorphous carbon with an sp^3 hybridization state.

References

1. Powder Diffraction File (PDF-2), Database Sets 147; Diamond, ICDD# 6-675. International Center for Diffraction Data, Newtown Square, Pennsylvania, 1997.

2. W. Zhu, H.-S. Kong and J.T. Glass, *Diamond Films and Coating: Development, Properties, and Applications*; pp. 244-338. Edited by R.F. Davis. Noyes, Park Ridge, NJ, 1992.

3. K.J. Gray, Norton Diamond Film, Northboro, Massachusetts, 1999, Private Communication.

4. G.R. Hennig, "Surface Oxides on Graphite Single Crystals," *Proc. Conf. Carbon, 5th*, **1** 143-6 (1962).

5. R. Sappok and H.P. Boehm, "Chemie der Oberflache des Diamanten - II. Bildung, Eigenschaften und Struktur der Oberflachenoxide," *Carbon*, **6** [5] 573-88 (1968).

6. S. Matsumoto, H. Kanda, Y. Sato and N. Setaka, "Thermal Desorption Spectra of the Oxidized Surfaces of Diamond Powders," *Carbon*, **15** [5] 299-302 (1977).

5 AUGER AND XPS STUDY OF CVD AND NATURAL DIAMOND

5.1. Auger and XPS study of CVD and Natural Diamond treated in 95 kPa O_2

Oxidation of diamond involves a heterogeneous gasification process. Oxygen, water vapor, and carbon dioxide are but a few of the species that react with diamond surfaces, yielding CO(g) and CO_2 (g). Of interest are the active sites for oxidation on the surface and the possibility of surface reconstruction from an sp^3 to an sp^2 bond character. Identification of the surface active sites, the activity of specific crystallographic facets, and the extent to which surface conversion is involved in the oxidation process is key to the fabrication and design of diamond materials. It has long been argued whether oxidation of diamond is associated with graphitization, in other words, the change of surface from an sp^3 to an sp^2 bond character.[1] [2] [3] Evans and Phaal observe "black carbon" on oxidized natural diamond at 66 Pa O_2, but no "black carbon" forms if the diamond oxidizes in atmospheric pressure oxygen.[2] The oxidation behavior of CVD diamond differs from that of the single crystal diamond due to the structural imperfection as a consequence of either preferential crystal growth or incorporation of hydrogen into the CVD diamond.[3-9] Previous Auger and X-ray photoelectron spectroscopy studies are carried out on the clean and hydrogenated diamond surfaces.[1, 10-13] Changes in the detailed Auger spectra from diamond as compared to those from graphite and amorphous carbon are reported by Lurie and Wilson,[12] Pate,[1] and Ramaker.[13] XPS work on carbons in various chemical environments are reviewed by McFeely Kowalczyk, Ley, Cavell, Pollak, and Shirley,[11] and Carlson.[14] These researchers show that C 1s binding energy is sensitive to chemical shifts (chemical environments); therefore, the presence of oxygen

on the carbon surface (sp^3- or sp^2-bonded) could be tracked by the change of its binding energy.

Auger and XPS techniques are combined in examining oxygenated CVD diamond surfaces. Based upon the Auger and XPS findings, the issue of surface oxidation and phase transition of diamond is discussed in this chapter. Reported in this section are the findings of CVD diamond and natural diamond treated at elevated temperatures in 95 kPa O_2. The details of the materials and experimental procedures are given in Sections 3.1 and 3.2.2, respectively.

5.1.1 Results — Auger and XPS study on diamonds treated in 95 kPa O_2

Figure 5-1 contains the Auger spectra of natural diamond, CVD diamond, HOPG and glassy carbon. Spectra of CVD diamond are collected from atomically clean surfaces and specimens were treated in oxygen at temperatures of 420, 550, and 575 ^oC.

Although it is difficult to give a full and unambiguous interpretation of the Auger transition in solids, a comparison between the Auger fine structures and predominant features in the band structure is possible. Ramaker shows that theoretically, carbon KVV Auger lines shapes are the convolution of the main peak generated by the normal KVV process as well as up to four satellite peaks due to the resonant electron excitations.[13] Peak shifts observed in the diamond spectra are mainly due to charging, which mask the subtle change of peak position caused by the change of valence band structure [12 11]. We

thus limit our discussion to the change of line shapes of A_0 at 275 eV and the major satellite peak A_1 at ~ 262 eV.

The three natural diamond spectra, collected from as-received surfaces of {111}, {110}, and {100}, are quite similar. All the CVD diamond have similar A_0 and A_1, yet the kinetic energy shifted in a range from 270 to 277 eV. Diamond treated at 420 and 500°C is covered by chemisorbed oxygen without oxidation. Full oxygen coverage is achieved at 420 °C,[15] whereas diamond treated at 550 and 575 °C is oxidized.[9] Regardless of various surface conditions, the line shapes of CVD diamonds are akin to those of the natural diamond. Spectra of HOPG and glassy carbon are very alike and the kinetic energies are 275 eV.[16] The major difference between natural diamond and sp^2-bound carbon (HOPG and glassy carbon) is in A_1. The oxygen-chemisorbed and oxidized CVD diamond do not adopt the sp^2 bond character.

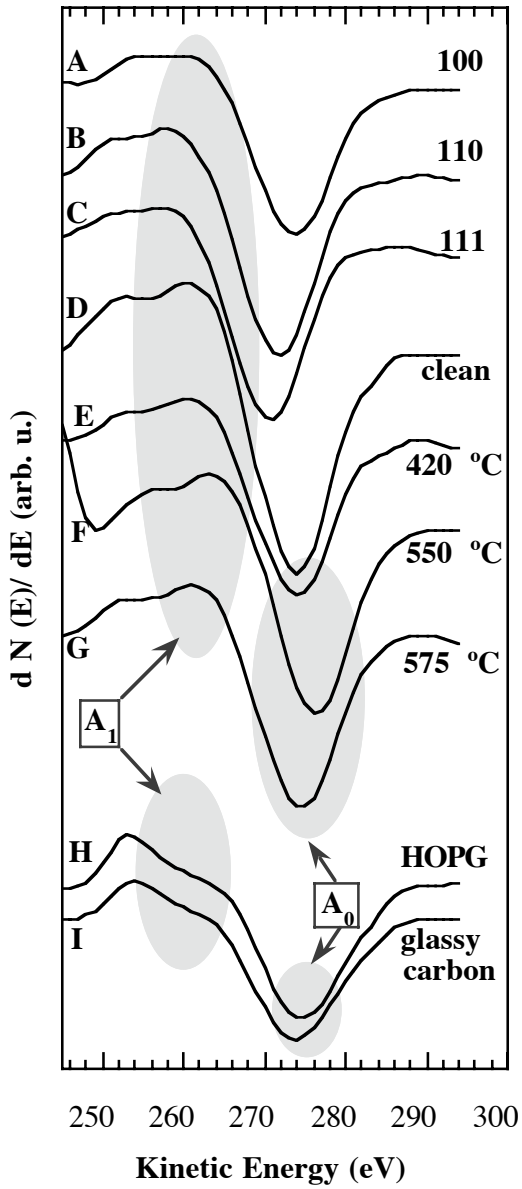

Figure 5-1. Auger spectra of natural diamond (A to C), CVD diamond (D to G), HOPG (H) and glassy carbon (I). A_0 is the main peak and A_1 is the satellite peak which shows the significant difference between sp^3- and sp^2-bound carbons.

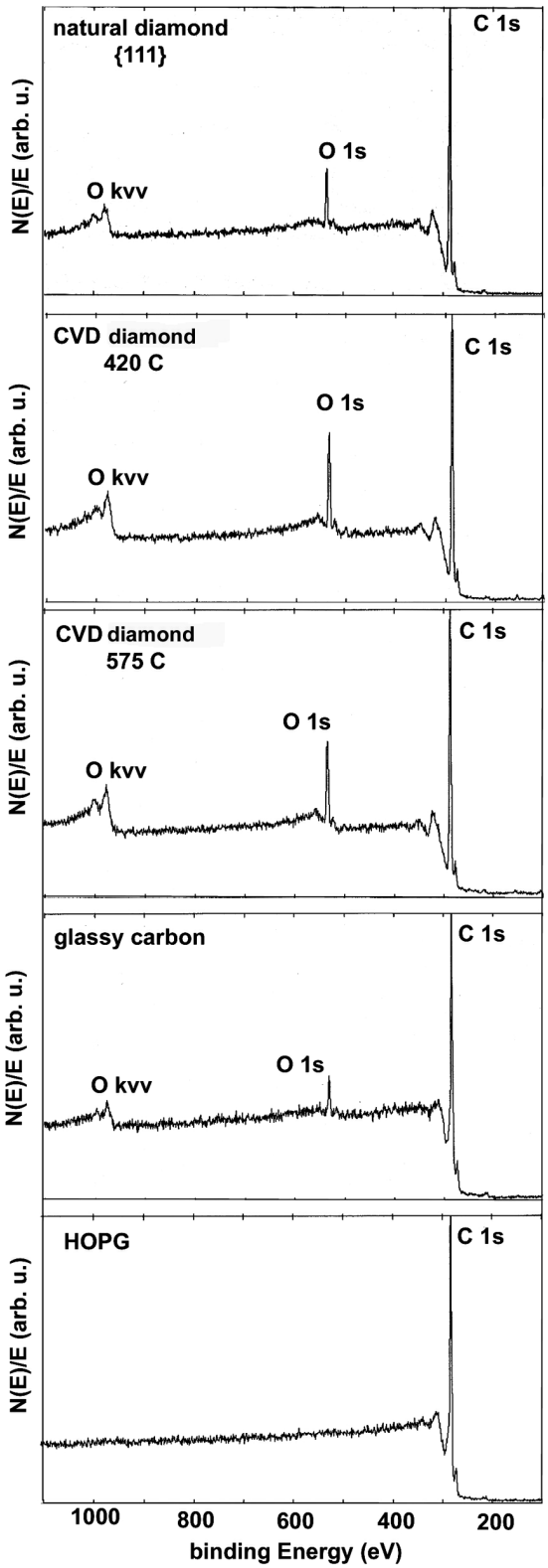

Figure 5-2. XP spectra of natural and CVD diamond, HOPG and glassy carbon. There is no oxygen on the {0002} of HOPG. The O 1s peak of glassy carbon is less intense than that of natural or CVD diamond.

No evidence of reconstruction from sp^3 to sp^2 (or phase transformation from diamond to graphite) can be found in the Auger spectra.

The XP spectra are presented in Figure 5-2. Oxygen peaks exist in all of the CVD and natural diamond spectra. Prior to the XPS study, these specimens are all exposed in air, yet there is no oxygen peak on HOPG. Diamond has stronger O 1s peaks than glassy carbon does. This indicates that there is more chemisorbed oxygen on the diamond, in other words, more surface active sites. The C1s binding energies are tabulated in Table V–1. The C1s of HOPG measured in the current study is 283.0 eV, which is lower than the well-accepted value at 284.5 eV.[17] CVD diamond has the highest binding energy of 287.3 eV on average. The values of natural diamond are lower, of 285.69 eV, whereas HOPG and glassy carbon have the lowest of 283.01 and 284.24 eV, respectively. HOPG has the narrowest C 1s peak of 1.48 eV while diamond has an FWHM from 1.85 to 2.06 eV. After ion sputtering for 30 s, the oxygen peak disappears, but C 1s peaks are all broadened (FWHM data in Table 5-1). Sputtering cleans off the surface and lowers the binding energy of the entire diamond. The binding energy of CVD diamond decreases from 287.3 to 285.8 eV in average. The binding energy of natural diamond drops to 283.0 eV which is the same as HOPG. Sputtering does not change the energy of HOPG. The binding energy of glassy carbon decreases from 284.24 to 283.60 eV. Therefore, its final value is still higher than that of HOPG.

Table V-1. XPS: A Comparison of C 1s Binding Energies

List of specimens		As-Prepared specimens		After 30 s sputter	
		C1s (eV)	FWHM (eV)	C1s (eV)	FWHM (eV)
CVD diamond	CH_3OH-rinsed	287.15	1.91	285.74	2.55
	O_2 @ 420 ^oC	286.93	1.85	285.03	2.40
	O_2 @ 500 ^oC	287.36	2.00	286.12	2.55
	O_2 @ 550 ^oC	287.65	2.00	285.96	2.52
	O_2 @ 575 ^oC	287.45	2.00	286.13	2.30
natural diamond	100	--	--	283.24	2.31
	110	--	--	282.88	2.40
	111	285.69	2.06	282.85	2.08
sp^2-Carbons	HOPG	283.01	1.48	283.04	2.00
	glassy carbon	284.24	1.85	283.60	2.15

The C1s energy of carbon compounds sensitively reflects the chemical environment of the carbon.[14, 18] It is reported that if the pure graphite has a C1s of 284.5 eV, then the binding energy of carbonyl is about 287-288 eV, and 286 to 287 eV for alcohols.[17] As shown in the Auger spectra and XPS, oxygen is the major specie on the diamond and glassy carbon. It is found by Sappok and Boehm using IR that the chemisorbed oxygen and hydrogen form hydroxyl, carbonyl (-C=O), CH_2-group, and ether-type C-O group.[19] Therefore, the chemical shift induced by these groups should show in the peak position as well as peak overlaps (hence broader peaks). The C1s from well-defined, clean {0001} of HOPG could be considered as a "single peak". Hence, the FWHM of HOPG, 1.48 eV, can be set as a standard for the current study. The broader peaks of diamond could imply that there are more chemisorbed species than those sp^2-bound carbons.

Clean surfaces are obtained using ion sputtering. Nevertheless, it induces peak broadening ubiquitously (Table 5-1), which is known as a "smearing effect" of band structure by the ion bombardment [20]. If sputtering does not cause a peak shift, the peak shift could be attributed to the elimination of chemisorbed species. The C1s binding energy of natural diamond after sputtering is very close to that of HOPG. Nonetheless, the binding energy of CVD diamonds is 2 eV higher than that of HOPG. This could imply that the electronic structure of CVD diamond is inherently different from that of natural diamonds. The XPS findings suggests that the transition of diamond to graphite during oxidation is not in favor because the diamond surface is more active.

5.1.2 Discussion of Auger and XPS Results — 95 kPa O_2

Graphite and diamond are the two common allotropes of carbon. Graphite is the thermal equilibrium phase under room temperature and pressure whereas diamond is metastable. It is found by Bansal,et al.[21] and Mastumoto, et al.[15] and confirmed in this study that the surface of diamond is much more active than that of sp^2-bonded carbons, i.e., graphite or glassy carbon. We propose that diamond minimizes its surface energy by either chemisorption or through surface reconstruction to an energy-favorable configuration, sp^2. Phase transition and oxidation can be a competing process depending upon oxygen partial pressure, temperature, defect concentration and specific crystal facets. Although retaining diamond structure via chemisorption is less thermodynamically stable, it could be kinetically favorable at high oxygen partial pressure, if the activation energy of chemisorption could be decreased by structural imperfection. Nevertheless, energy minimization may be achieved by surface reconstruction to an sp^2 configuration at low

oxygen partial pressure and high temperature. Our simulation work in Chapter 7 suggests that surface reconstruction to an sp^2 is more energetically favorable.

There is no evidence of diamond surface reconstruction to sp^2 from current Auger and XPS findings. This is consistent with our proposal, since the oxygen pressure is high (95 kPa) and heat treatment temperatures (420 to 575 °C) are relatively low, thus the surface energy of the CVD diamond is decreased by chemisorption of oxygen. Our study of the oxidation of CVD diamonds at low oxygen partial pressure and higher temperatures is presented in Section 5.2.

5.1.3 Conclusions

To date, all the oxygenated specimens are prepared at 95 kPa O_2. Auger KVV line shapes of oxidized (550 and 575 °C) and oxygenated (420 and 500 °C) CVD diamonds are more similar to that of natural diamond than either HOPG or glassy carbon. XPS is more sensitive to the change of surface chemisorbed species. CVD diamonds with surface absorbents had the highest binding energy of 287.3 eV in average. Natural diamond has a lower energy of 285.69 eV whereas HOPG and glassy carbon have the lowest binding energy of 283.01 and 284.24 eV, respectively. The {0001} of HOPG has the narrowest C 1s peak of 1.48 eV and least active surface. Sputtering cleans off the chemisorbed species and lowers the binding energy of all the diamonds. The binding energy of CVD diamonds decrease from an average of 287.3 to 285.8 eV and the binding energy of natural diamond drops to 283.0 eV, which is the same as HOPG. It is

concluded that under an oxygen pressure of 95 kPa, direct oxidation of CVD diamond occurs without phase transition.

5.2. Oxidation of CVD diamonds under 10^{-9} Pa O_2

Diamond is a material with extremely high surface energy. According to Harkins' calculation based upon bond strength, the surface energy is 5.50 J/m^2 on diamond (111) surface, as compared to 1.20 mJ/m^2 on silicon (111) surface.[22] In contrast, the surface energy of graphite {0001} is as low as 0.07 J/m^2.[23] Our own simulation study finds the diamond (111), (110), and (100) surfaces have the surface energies of 6.703, 7.146, and 8.636 J/m^2, respectively (Table VII-6). In a recent paper, Howe and Jones propose that diamond minimizes its surface energy via two possible mechanisms: either oxygen-chemisorption or relaxation to an sp^2 configuration, and each is governed by the partial pressure of oxygen.[24] As presented in the previous section, our Auger work on diamonds treated at elevated temperatures in 95 kPa O_2 supports in part this concept. At atmospheric oxygen pressure, only chemisorption occurs without surface reconstruction to the sp^2 configuration. Chemisorption and surface reconstruction to sp^2 occur simultaneously in oxygen partial pressure from 0.5 to 15 Pa at elevated temperature. The question is what happens on the diamond surface at very low oxygen pressure at less than 10^{-9} Pa (more precisely, 6×10^{-10} Pa) at temperatures from 1000 to 1500 ^{o}C? In this section, it describes the Auger investigation on diamond surfaces after these heat treatments. The bond nature of diamond on the surface is determined from the line shape of Auger spectra at the first satellite region around 260 eV.

5.2.1 Results and Discussions — Diamonds treated in 10^{-9} Pa O_2

The materials and experimental procedures are given in Chapter 3. Figure 5-3 is the Auger spectra of CVD diamonds and glassy carbon. Spectra of CVD diamond are collected from as-received (AR) surface as well as heat-treated specimens. Carbon has two core electrons and four valence electrons. Therefore carbon KLL transition is specified as KVV through the context of this section.

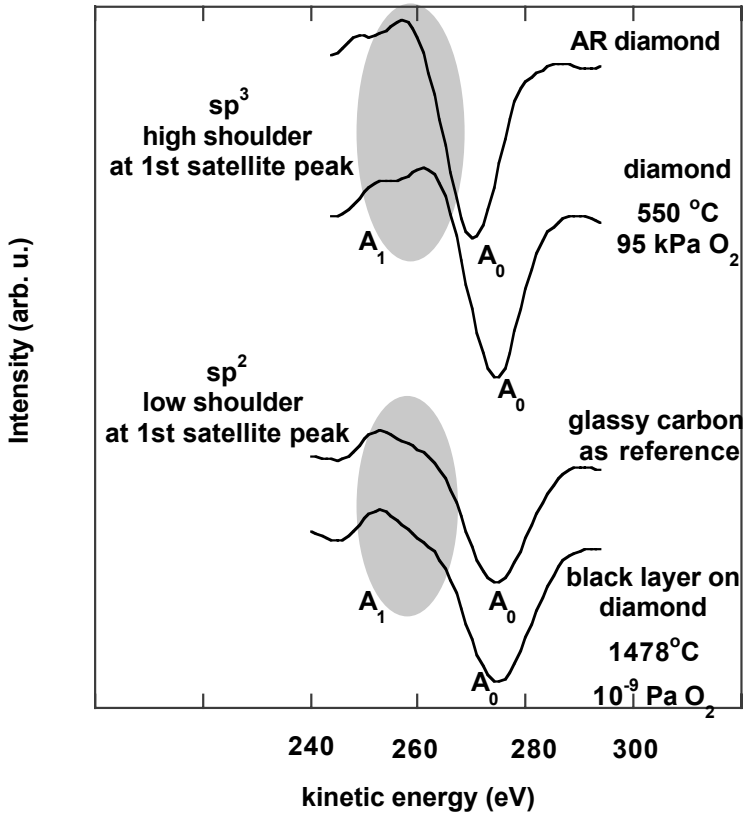

Figure 5-3. Auger spectra of CVD diamonds and glassy carbon. Difference of bond character is shown in the first satellite peak A_1. Heat treatment in low oxygen partial pressure leads to a surface reconstruction to sp^2 bond character.

Because of the complexity of Auger transition in solids, a full and unambiguous interpretation is still pending, yet a comparison between the Auger fine structure and predominant features in the band structure is possible. Ramaker shows that theoretically, carbon KVV (KLL transition is specified as KVV in context) Auger line shapes are the convolution of the main peak generated by the normal KVV process as well as up to four satellite peaks due to the resonant electron excitations.[13] Peak shifts observed in the diamond spectra are mainly due to charging. Charging masks the subtle change of the main peak position (A_0) caused by the change of valence band structure.[11, 12] However, the peak shape of the first satellite peak (A_1) still truthfully reflects the bonding information. We thus limit our discussion to the line shape of the major satellite peak, A_1, at ~ 262 eV.

The diamond spectra, collected from diamond treated at 550 ^{o}C in 95 kPa O_2, are quite similar to those of the as-received specimen. The high shoulder of A_1 is the signature of the sp^3 bond character.[24] We know that diamond is oxidized after being isothermally treated at 550 °C for 170 min.[9] The similarity of line shapes between as-received and oxidized diamonds implies that a direct oxidation from sp^3-bonded carbon occurs.

In contrast, spectra of diamond treated at low oxygen pressure (< 10^{-9} Pa O_2) are similar to those of glassy carbon reference. The lower shoulder at A_1 is the significant feature of sp^2-bound carbons. This finding clearly shows that after heat treatment at 1478^{o}C in 10^{-9} Pa O_2 for 600 min, the surface of diamond is reconstructed from sp^3 to sp^2. Evidence of

reconstruction from sp^3 to sp^2 is also observed from the change of appearance: a layer of black carbon, up to 3 μm thick, is formed on the diamond surface.

We propose that diamond minimizes its surface energy by either chemisorption or through surface reconstruction to an energy-favorable configuration, sp^2. Surface reconstruction and direct oxidation can be a competing process depending upon oxygen partial pressure, temperature, and energy on specific crystal facets. The driving force of these transitions is thought to be the high surface energy of diamond. The Auger study on the oxidized diamond proves the fact that reconstruction does occur. Our computer simulation study leads to the same conclusions.

5.2.2. Summary

CVD diamond film ET100, is isothermally treated in oxygen at two conditions: 1) 550 ^{o}C/95 kPa O_2 for 170 min; and 2) 1478 ^{o}C/ 10^{-9} Pa O_2 for 600 min. The diamond films are then investigated using Auger electron spectroscopy. Auger spectra of oxidized diamonds are compared with that of glassy carbon. It is suggested that diamond minimizes its surface energy by: 1) oxygen-chemisorption and retaining sp^3 character at high pressure (95 k Pa O_2); and/or 2) surface reconstruction to an sp^2 character at low pressure (< 10^{-9} Pa O_2).

References

1. B.B. Pate, "The Diamond Surface: Atomic and Electronic Structure," *Surf. Sci.*, **165** [1] 83-142 (1986).

2. T. Evans and C. Phaal, "The Kinetics of the Diamond-Oxygen Reaction," *Proc. Conf. Carbon, 5th*, **1** 147-53 (1962).

3. K. Miyata and K. Kobashi, "Air Oxidation of Undoped and B-Doped Polycrystalline Diamond Films at High Temperatures," *J. Mater. Res.*, **11** [2] 296-304 (1996).

4. M. Alam and Q. Sun, "The Kinetics of Chemical Vapor Deposited Diamond-Oxygen Reaction," *J. Mater. Res.*, **8** [11] 2870-8 (1993).

5. K. Tankala, T. DebRoy and M. Alam, "Oxidation of Diamond Films Synthesized by Hot Filament Assisted Chemical Vapor Deposition," *J. Mater. Res.*, **5** [11] 2483-8 (1990).

6. A. Joshi, R. Nimmagadda and J. Herrington, "Oxidation Kinetics of Diamond, Graphite, and Chemical Vapor Deposited Diamond Films by Thermal Gravimetry," *J. Vac. Sci. Technol., A*, **8** [3] 2137-42 (1990).

7. C.E. Johnson, M.A.S. Hasting and W.A. Weimer, "Thermogravimetric Analysis of the Oxidation of CVD Diamond Films," *J. Mater. Res.*, **5** [11] 2320-5 (1990).

8. C.E. Johnson, J.M. Bennett and M.P. Nadler, "Oxidation of Diamond Windows," *J. Mater. Res.*, **10** [10] 2555-60 (1995).

9. J.Y. Howe, L.E. Jones and D.W. Coffey, "The Evolution of Microstructure of CVD Diamond by Oxidation," *Carbon*, **38** [6] 931-3 (2000).

10. T.W. Haas, J.T. Grant and G.J. Dooley III, "Chemical Effects in Auger Electron Spectroscopy," *J. Appl. Phys.*, **43** [4] 1853-60 (1972).

11. F.R. McFeely, S.P. Kowalczyk, L. Ley, R.G. Cavell, R.A. Pollak and D.A. Shirley, "X-Ray Photoemission Studies of Diamond, Graphite, and Glassy Carbon Valence Bonds," *Phys. Rev. B: Solid State*, **9** [12] 5268-78 (1974).

12. P.G. Lurie and J.M. Wilson, "The Diamond Surface II. Secondary Electron Emission," *Surf. Sci.*, **65** 476-98 (1977).

13. D.E. Ramaker, "Chemical Effects in the Carbon KVV Auger Line Shapes," *J. Vac. Sci. Technol., A*, **7** [3] 1614-22 (1989).

14. T.A. Carlson, *Photoelectron and Auger Spectroscopy*; pp. 193-200. Plenum, New York, 1975.

15. S. Matsumoto, H. Kanda, Y. Sato and N. Setaka, "Thermal Desorption Spectra of the Oxidized Surfaces of Diamond Powders," *Carbon*, **15** [5] 299-302 (1977).

16. *Handbook of Auger Electron Spectroscopy*, 3rd ed.; pp. 30-1. Edited by C.L. Hedburg. Physical Electrons, Inc., Eden Prairie, Minnesota, 1995.

17. *Handbook of X-Ray Photoelectron Spectroscopy*; p. 40. Edited by J. Chastain and R.C. King Jr. Physical Electronics Inc., Eden Prairie, Minnesota, 1995.

18. M. Thompson, M.D. Baker, A. Christie and J.F. Tyson, *Auger Electron Spectroscopy*; pp. 219-22. John Wiley & Sons, New York, 1985.

19. R. Sappok and H.P. Boehm, "Chemie der Oberflache des Diamanten - I. Benetzungswarmen, Elektronenspinresonanz und Infrarotspektren der Oberflachen-Hydride, -Halogenide und -Oxide," *Carbon*, **6** [3] 283-95 (1968).

20. S. Hofmann, *Practical Surface Analysis by Auger and X-Ray Photoelectron Spectroscopy*, 1st ed.; p. 161. Edited by D. Briggs and M.P. Seah. John Wiley & Sons, New York, 1983.

21. R.C. Bansal, F.J. Vastola and P.L. Walker Jr., "Kinetics of Chemisorption of Oxygen on Diamond," *Carbon*, **10** [4] 443-8 (1972).

22. W.D. Harkins, "Energy Relations of the Surface of Solids I. Surface Energy of the Diamond," *J. Chem. Phys.*, **10** 268-72 (1942).

23. R.J. Good, L.A. Girifalco and G. Kraus, "A Theory for Estimation of Interfacial Energies. II. Application to Surface Thermodynamics of Teflon and Graphite," *J. Phys. Chem.*, **62** [11] 1418-21 (1958).

24. J.Y. Howe, L.E. Jones and D.N. Braski, "An Auger and XPS Study on CVD and Natural Diamonds," *Mater. Res. Soc. Symp. Proc.*, **593** 453-8 (2000).

6 KINETIC STUDIES OF OXIDATION OF CVD DIAMOND FILMS

Presented in this section are the results from the kinetic study of diamond oxidation. A list of all the TGA runs is compiled in Appendix I. Data presented in this chapter are plotted as percentage burn-off. Burn-off, which is the weight-loss due to oxidation, is normalized to the remaining weight of specimen. Burn-off data are subsequently plotted as a function of heat treatment time at isothermal conditions. The difference between percentage burn-off and percentage weight-loss should be emphasized. The former is normalized to the remaining weight, whereas the latter is normalized to the initial weight. The graphs in these figures are all plotted from time zero, which is the point that the run reached its targeted isothermal temperature.

The study of diamond oxidation is undertaken under the following conditions that vary specifically as a function of oxygen partial pressure:

1. High pressure: 95 kPa UHP O_2 with a flow rate of 70 sccm. The isothermal temperatures studies under high pressure conditions are:
   420, 500, 515, 530, 550, 575, 600, and 625 ^{o}C
2. Low pressure: 0.4 (2 Pa of air) to 18 Pa O_2 (90 Pa of air)
   The isothermal temperatures studies under low pressure conditions are:
   750, 850, 1000, 1300, 1400, and 1500 °C
3. $6x10^{-10}$ Pa O_2 in atmospheric pressure of helium with a flow rate of 50 sccm. The isothermal temperatures studies under very low pressure conditions are:
   1003, 1303, and 1478 °C

Results of experiments under 95 kPa and $6x10^{-10}$ Pa O_2 are presented in Sections 6.1 and 6.2. The results of 0.4 to 18 Pa O_2 are presented in Sections 6.3. The two extreme oxidation conditions are presented first in order to comment on the range of behavior.

6.1 Kinetic Studies of Oxidation under 95 kPa O_2

The isothermal oxidation behavior of CVD diamond film ET100 in 95 kPa O_2 flowing at 70 sccm, at 515, 530, and 550 ^oC is given in Figure 6-1. Weight-loss as an indication of oxidation is first observed at 515 ^oC. The noise level is high because of the low mass loss over a long time frame. In other words, the rates are low enough to be at the edge of the instrument limits. The weight-loss is confirmed using SEM in which preferential oxidation occurs on {111} of diamond at these temperatures, Figure 4-19. Oxidation rates are very low at these temperatures. A rate of $1.33 \times 10^{-5} min^{-1}$ is measured at 0.2 % burn-off at 515 ^oC. Figure 6-2 contains the isothermal oxidation profiles in O_2 at 550, 575, 600, and 625 ^oC. Oxidation rates in varying partial pressures of O_2 are tabulated in Table 6-1. All rates are measured and compared at approximately 0.2 % burn-off level to allow comparison of rates obtained at all the conditions. Rates of HOPG and glassy carbon at 600 ^oC in 95 kPa O_2 are included in this table as well. HOPG and glassy carbon are the crystalline and glassy form of carbon with the sp^2 bond character. Under 600 ^oC in 95 kPa O_2, diamond has the highest rate followed by HOPG, with glassy carbon the lowest. Oxidation behavior of diamond films is compared to glassy carbon and HOPG at 600 ^oC, Figure 6-3. Both diamond and HOPG bear non-linear oxidation behavior whereas oxidation of glassy carbon is linear.

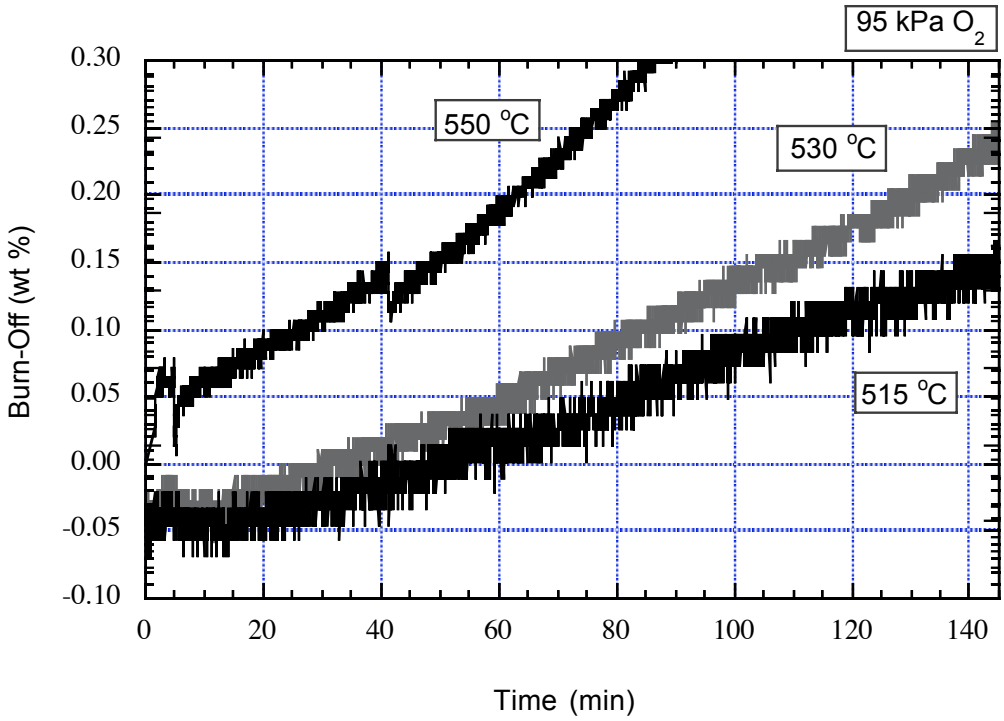

Figure 6-1. Isothermal oxidation of CVD diamond film ET100 in 95 kPa O_2 flowing at 70 sccm, 515, 530, and 550 °C. Oxidation initiates at 515 °C.

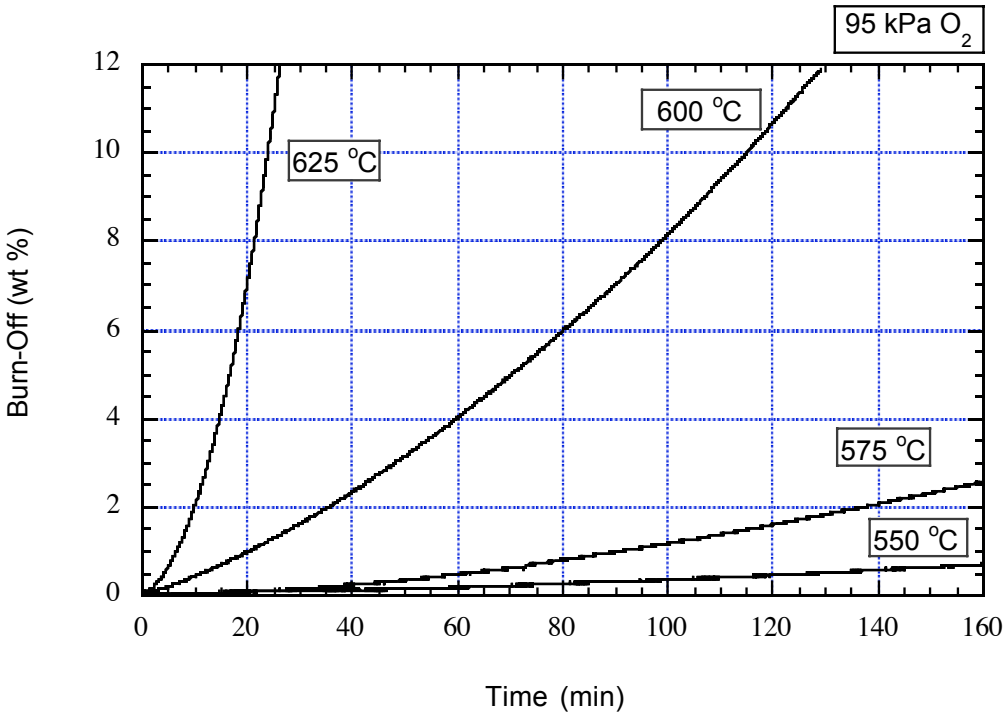

Figure 6-2. Isothermal oxidation of CVD diamond film ET100 in 95 kPa O_2 flowing at 70 sccm at 550, 575, 600, and 625 ^{o}C. Oxidation rates accelerate with increasing burn-off level.

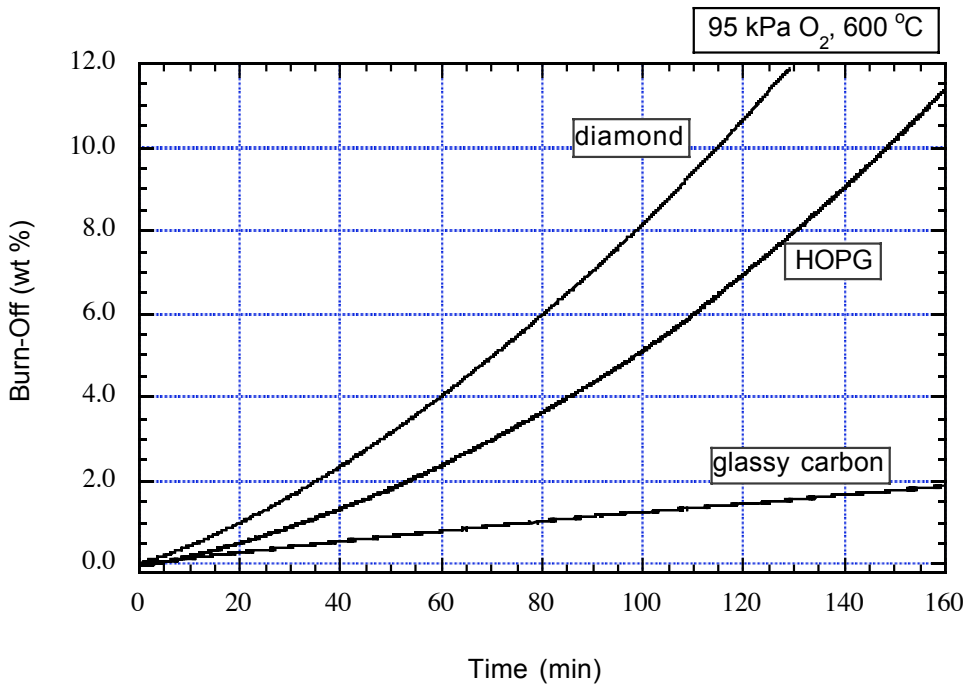

Figure 6-3. Isothermal oxidation of CVD diamond film ET100, HOPG and glassy carbon in 95 kPa O_2 flowing at 70 sccm at 600 °C. CVD diamond is the most vulnerable whereas glassy carbon is the most resistive to oxygen attack.

The rates of CVD diamond oxidation increase as a function of temperature, Table 6-1. For instance, the rate at 625 °C, 1.49 x $10^{-3}$$min^{-1}$, is more than 100 times that at 515°C, 1.33 x $10^{-5}$$min^{-1}$. Oxidation rate is not a linear function of either time or burn-off. Oxidation increases with burn-off levels. For instance, at 625 °C, the oxidation rate was 1.49 x 10^{-3} at 0.2 % burn-off, 3.4 x 10^{-3} at 5% burn-off, and 0.31 min^{-1} at 25% burn-off, Figure 6-2. The raw weight-loss data in mg of an isothermal oxidation run at 625 °C, plotted as a function of time, is given in Figure 6-4. It is obvious in this format of plot that oxidation levels off after a total weight-loss of 31.10 mg out of the initial weight of 33.86 mg. The same set of data, is plotted again in % burn-off, as a function of time in Figure 6-5. It is clearly illustrated using this format that oxidation of CVD diamond at

625 ^{o}C in 95 kPa O_2 is a two-stage process. The first stage is a slow oxidation up to 10% burn-off (equivalent to 10 % weight-loss), followed by a second stage of fast consumption of material up to 50 % burn-off (equivalent to 90% weight-loss), Figure 6-5. The micrographs of remaining materials are given in Figure 4-10.

Table VI-1. Oxidation Rates of CVD Diamond and Carbon at Approximately 0.2 wt % Burn-Off in a Wide Range of Oxygen Partial Pressures

Pressure of O_2 (Pa)	Temperature (^{o}C)	Oxidation Rate min^{-1})
95 k	515	1.33×10^{-5}
95 k	530	2.71×10^{-5}
95 k	550	3.66×10^{-5}
95 k	575	9.87×10^{-5}
95 k	600	1.47×10^{-4} (glassy carbon)
95 k	600	2.91×10^{-4} (HOPG)
95 k	600	4.41×10^{-4}
95 k	625	1.49×10^{-3}
12-18	850	1.12×10^{-4}
0.4	1000	1.01×10^{-4}
14	1000	6.97×10^{-5}
0.6	1300	2.02×10^{-4}
0.6-1.6	1400	3.01×10^{-4}
1.2-1.0	1500	7.58×10^{-4}
0.5	1500	2.78×10^{-4}
10^{-9}	1003	1.71×10^{-5}
10^{-9}	1303	2.13×10^{-5}
10^{-9}	1478	4.07×10^{-5}

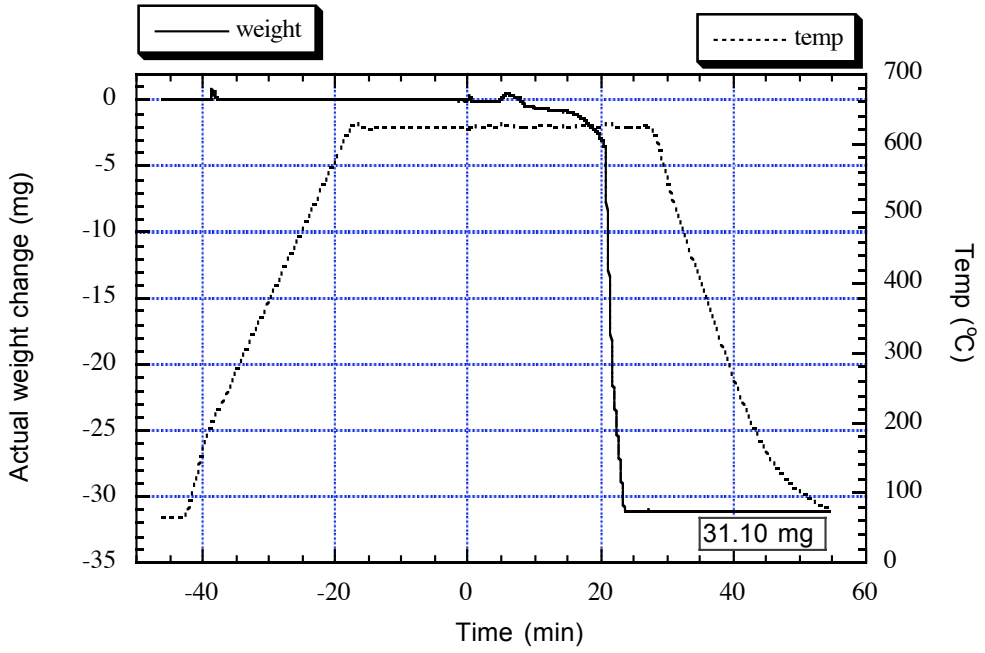

Figure 6-4. Raw data from the isothermal oxidation of CVD diamond film ET100 in 95 kPa O_2 flowing at 70 sccm at 625 °C. Sample is heated and stabilized in helium; UHP O_2 is then introduced at time zero. The initial sample mass is 33.86 mg. Oxidation levels off after a total loss of 31.10 mg (90 % weight-loss).

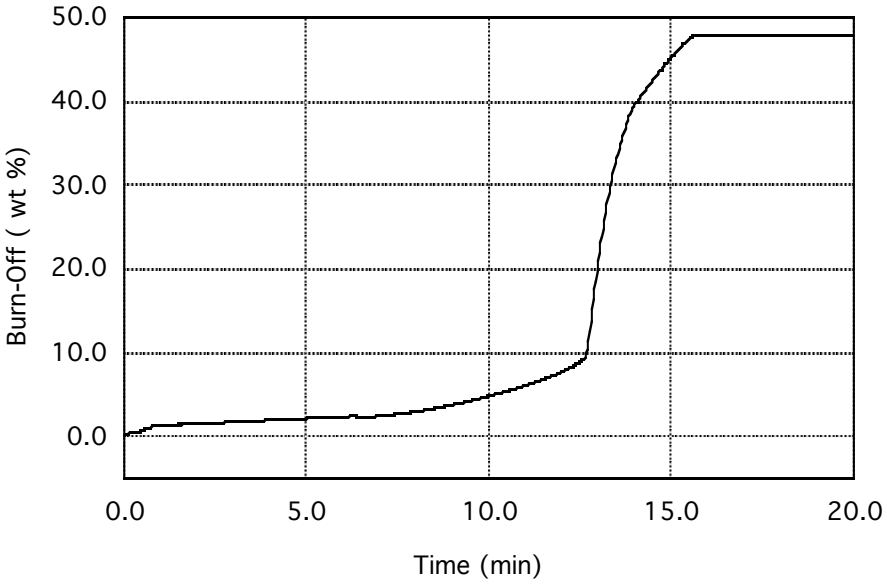

Figure 6-5. Isothermal oxidation of CVD diamond film ET100 at 625 °C in 95 kPa O_2 flowing at 70 sccm. Oxidation is a two-stage process at this temperature.

Figure 6-6 contains the burn-off data at 0.2 % burn-off plotted in an Arrhenius format. Apparent activation energy of diamond oxidation, E_a, is the slope of the curve in Figure 6-6, which the logarithm of oxidation rate at 0.2 % burn-off is plotted against the reciprocal of absolute temperature. Since the curve is not a straight line, E_a therefore is temperature dependent. E_a is 153 kJ/mol if obtained from 515, 530, and 550 ^oC. It increases to 310 kJ/mol if the data of 550 to 625 ^oC (four data points) are used. But the energy decreases to 293 kJ/mol when using data at 575, 600, and 625 ^oC only. A non-linear ln(rate) ~ 1/K relationship at those temperatures suggests a change of the oxidation mechanism.

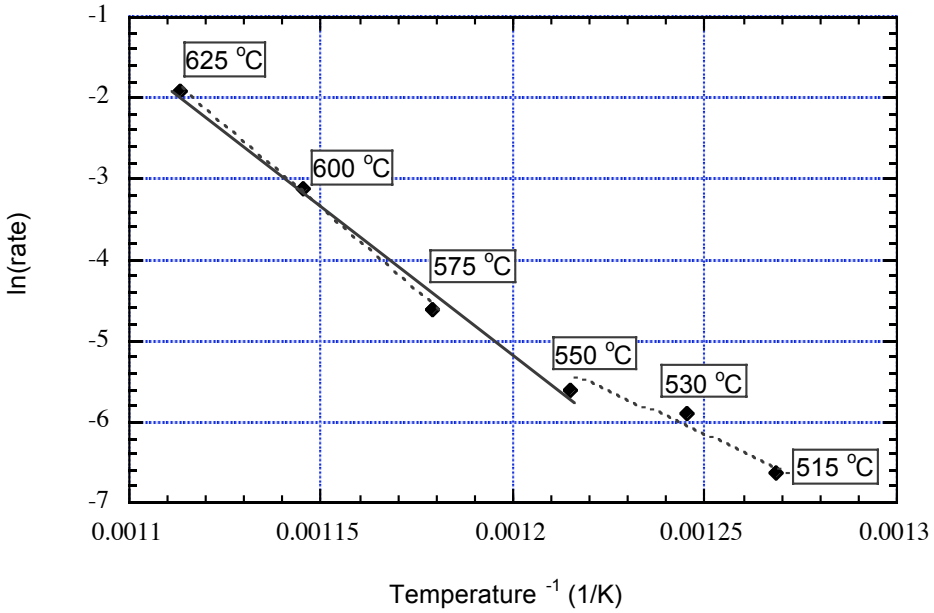

Figure 6-6. Arrhenius behavior for the oxidation of diamond at 0.2 wt % burn-off at 95 kPa O_2 with a flow rate of 70 sccm. E_a is 293 kJ/mol using 575, 600, and 625 ^oC data, 310 kJ/mol from 550 to 625 ^oC data, and 153 kJ/mol from 515 to 550 ^oC.

6.2 Oxidation of Diamond at $6x10^{-10}$ Pa O_2

Diamond surfaces reconstruct to an sp^2 bond character at oxygen partial pressures of $6x10^{-10}$ Pa. At this low oxygen partial pressure, initial oxidation occurs at temperatures as low as 1003 ^oC. The lowest temperature of heat treatment is 1003 ^oC; nonetheless, it does not imply that this is the lowest temperature of oxidation under these conditions. The oxidation rate is 1.71 x 10^{-5} min^{-1} at 1003 ^oC in $6x10^{-10}$ Pa O_2. The rate at 515 ^oC in 95 kPa O_2 is 1.33 x 10^{-5} min^{-1}. Figure 6-7 presents a graph that percentage of burn-off is plotted as a function of heat treating time at 1003, 1303, and 1478 ^oC. The rate data of this figure, extracted at 0.2% burn-off, are tabulated in Table 6-1. Oxidation behavior is linear indicating that it is the oxidation of amorphous carbon. Recall in Figure 6-3 that glassy carbon has a linear oxidation behavior at 600 ^oC in 95 kPa O_2. Oxidation as a function of oxygen partial pressure at 1500 ^oC is presented in Figure 6-8. The partial pressure range of oxygen explored is $6x10^{-10}$ Pa to 1.1 Pa. Oxidation rates increase with oxygen partial pressure. SEM and TEM observations (Figures 4-35 to 4-40) indicate that amorphous carbon forms and covers the surface of diamond film in the partial pressure range of 10^{-9} Pa O_2 at temperatures from 1000 to 1500 ^oC. Hence, the oxidation behavior of diamond film under these conditions no longer occurs on the sp^3-bonded surface, but on surfaces that have reconstructed to an sp^2 bond character. The carbon on these surfaces is amorphous.

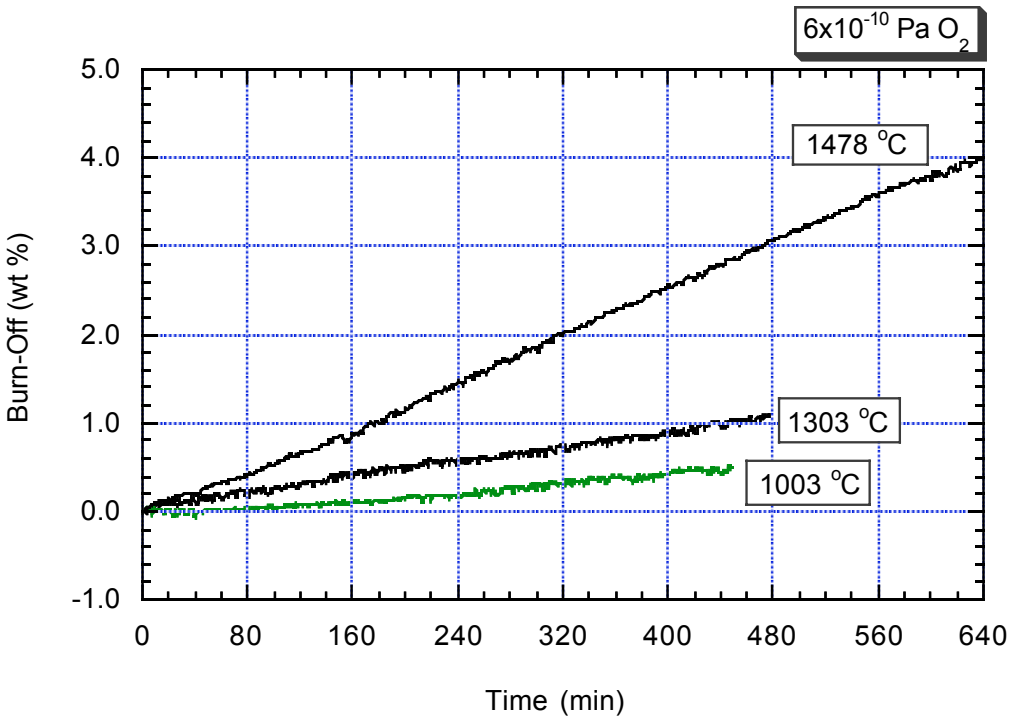

Figure 6-7. Isothermal oxidation of CVD diamond film ET100 in $6x10^{-10}$ Pa O_2, carried by He flowing at 50 sccm, at 1003, 1303, and 1478 °C. Oxidation behavior is linear.

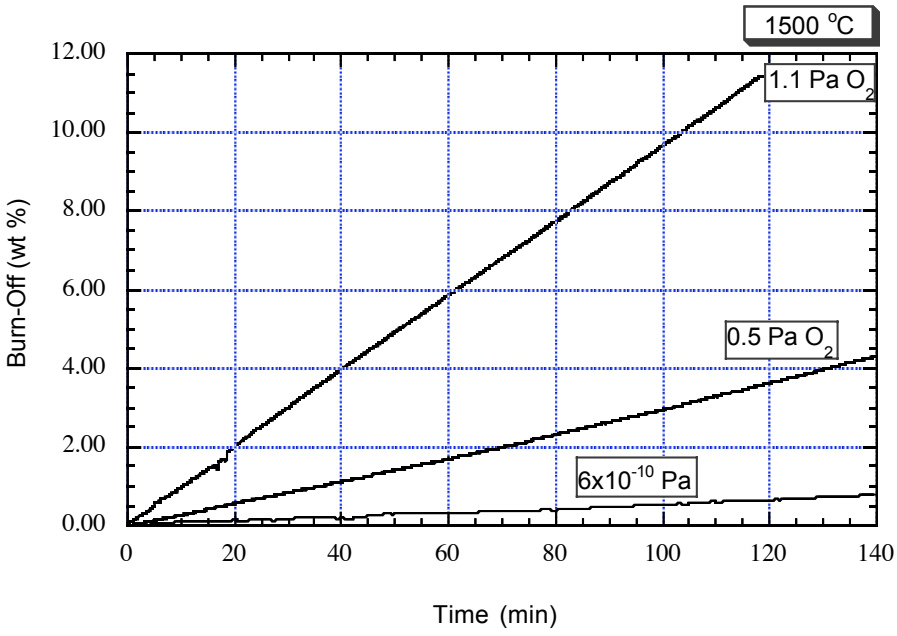

Figure 6-8. Isothermal oxidation of CVD diamond ET 100 as a function of oxygen partial pressure at 1500 °C.

Rates data taken at both 0.3 and 0.5 % burn-off in O_2 pressure of less than 10^{-9} Pa are plotted as a function of reciprocal temperature in the range between 1000 and 1500 ^oC in Figure 6-9. Although the author is reluctant to extract the slope from these data points in Figure 6-9, slopes are given for the sake of comparison with the data at 95 kPa. E_a is 30 kJ/mol at 0.3 % burn-off and 36 kJ/mol at 0.5% burn-off. Even with the large statistic error, activation energy of 30 kJ/mol is drastically less than that of 310 kJ/mol at 95 kPa around 600 ^oC range (Table VI-2).

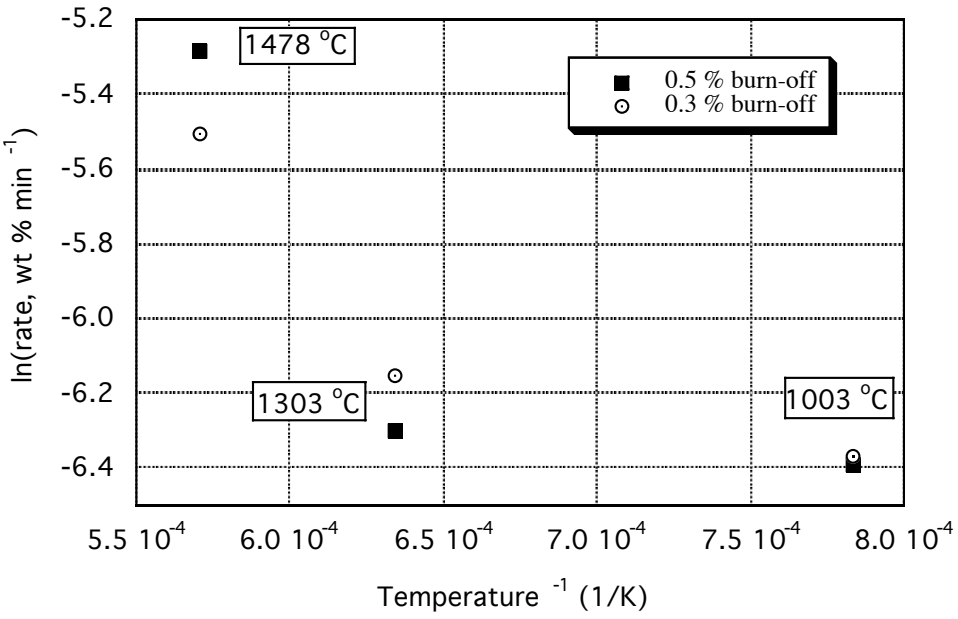

Figure 6-9. Logarithm of rates at both 0.3 and 0.5 % burn-off vs. reciprocal absolute temperature at $6x10^{-10}$ Pa O_2. E_a is 30 kJ/mol at 0.3 % burn-off data and 36 at 0.5 % burn-off.

Table VI-2. Activation Energy, E_a, of Diamond Oxidation
(Rate data at 0.3 % burn-off, unless otherwise specified)

Oxygen partial pressure (Pa)	Temperature range (^oC)	E_a (kJ/mol)
95 k	515 to 550	153
95 k	550 to 625	310
1.0	1300 to 1500	152
$6x\ 10^{-10}$	1003 to 1478	30 (at 0.3 % burn-off)
$6x\ 10^{-10}$	1003 to 1478	36 (at 0.5 % burn-off)

6.3 Oxidation under Oxygen Partial Pressure of 0.5 to 18 Pa

Isothermal heat treatments of CVD diamond ET 100 are undertaken from 750 to 1500°C in this pressure range. There is no observable weight-loss at 750 ^oC. Oxidation and phase transition occur from 850 °C and higher. Figure 6-10 contains a graph of the isothermal oxidation of CVD diamond ET100 as a function of temperature (at 1300, 1400, and 1500 ^oC) at ~ 1 Pa O_2. The rate data of this figure, extracted at 0.2 % burn-off, are tabulated in Table 6-1. The oxidation rates are linear and increase with increasing temperature. Figure 6-11 contains a graph that the burn-off data at 0.2 to 0.3 % burn-off plotted in an Arrhenius format from temperature range 1300 to 1500 ^oC. E_a is 152 kJ/mol. The oxidation behavior falls somewhere in between as compared to that under two extreme conditions, i.e., at 95 kPa and $6x10^{-10}$ Pa O_2.

It is observed that the substrate side of the diamond film has a reaction with the Pt crucible, which is attributed to the reaction between platinum and the residual silicon on the substrate side (The CVD film is grown on a silicon substrate and then is removed from the substrate). The impact of silicon on the oxidation behavior of diamond is not assessed in the current study.

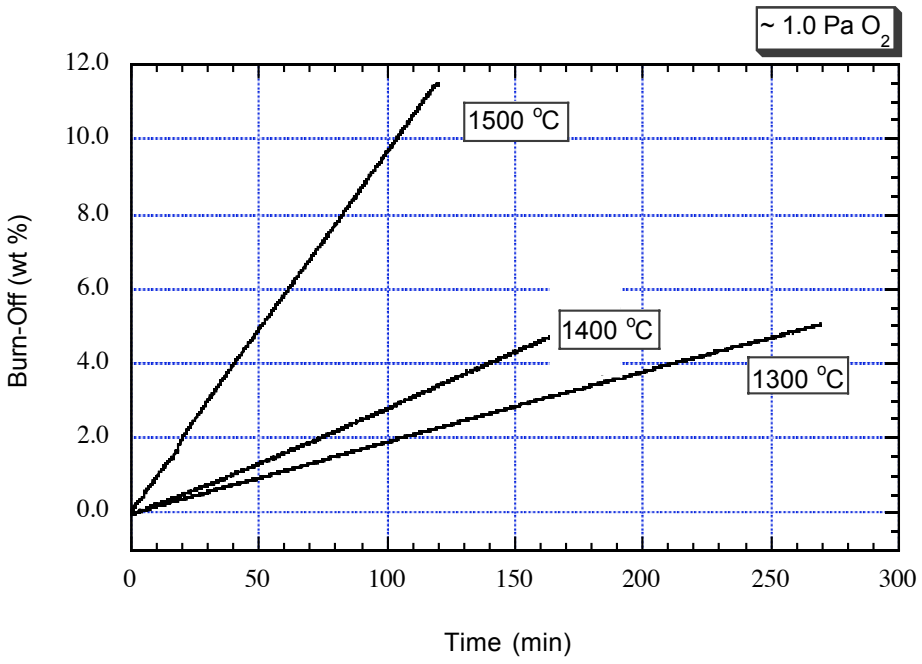

Figure 6-10. Isothermal oxidation of CVD diamond ET 100 as a function of temperature from 1300 to 1500 °C at about 1 Pa O_2.

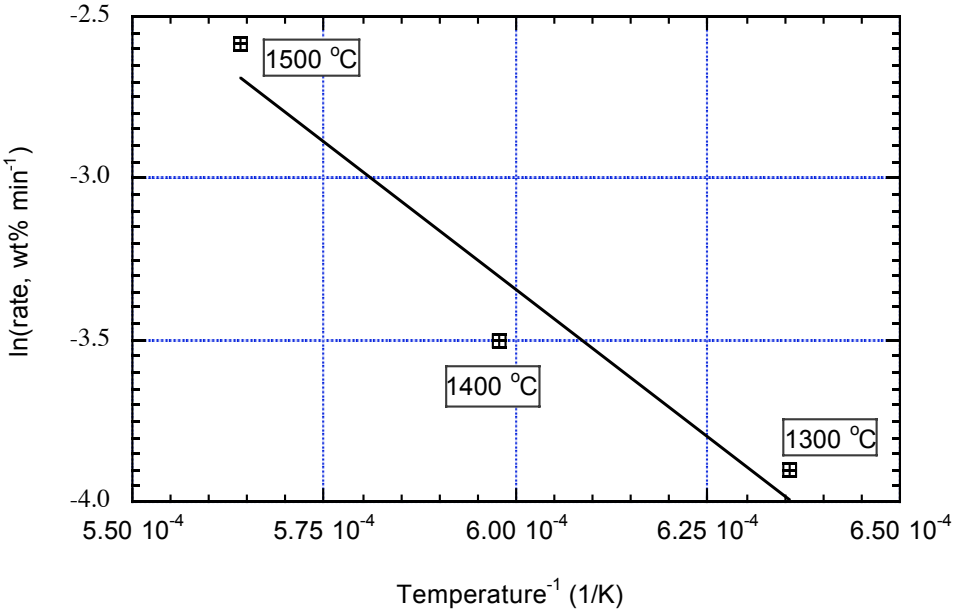

Figure 6-11. Logarithm of rates at 0.2 to 0.3 % burn-off vs. reciprocal absolute temperature at oxygen partial pressure of about 1.0 Pa. E_a is 152 kJ/mol.

6.4 Discussion and Summary

Total surface area (TSA) and active surface area (ASA) are widely used terms in studying kinetics of oxidation of carbon materials. It is the active surface area, not the total surface area, that plays an important role in carbon oxidation. For instance, in graphite, the edge sites of the sp^2-bonded carbon layers are considered active surface area. The oxidation rate at the edge sites is at least 20 times higher than that of at the non-edge sites.[1] In many cases, the increase of oxidation rate during oxidation is a consequence of increasing active surface area. It seems logical to use the concept of ASA/TSA to interpret the oxidation of diamonds. We hereby propose that {111} are the ASA in oxidation of diamond materials. Oxidation of diamond under 95 kPa is much faster than that of the sp^2-bonded carbon. This is due to the larger active surface area to begin with. ET100 is terminated by {111} and {100}. The area of {111} is estimated to be 50% of the TSA. When oxidation proceeds, more {111} is converted from {100}; hence there is an increase of oxidation rate. A scenario of diamond oxidation at 95 kPa can be plotted as:

- The first stage is the break-in part when oxygen attacks {111} and {100} surfaces. During this very early stage, oxidation is controlled by the defects.
- The second stage: Oxidation proceeds on {111}, and the {111}-faceted pits formed on {100}.

At 95 kPa, when oxygen is abundant, the surface is partially covered by chemisorbed oxygen. Oxidation is a chemically controlled process where activation energy is as high as 310 kJ/mol. At low oxygen partial pressure, phase transition from sp^3 to sp^2 becomes

prominent. Diamond surface is covered by sp^2-bonded black carbon. Thus, oxidation of diamond becomes the oxidation of amorphous carbon. Oxidation of amorphous sp^2-bonded carbon under these conditions is mass transport controlled with a low activation energy of 30 to 36 kJ/mol.

Previous attempts have been made (including ours) to relate the amount of available dangling bonds to the reactivity of diamond surfaces.[2-4] This simple model treats bonds like sticks, without seeing the image of the electrons occupying the space. Instead, in order to find out the reactivity of the oxygen and diamond reaction, the density and distribution of electrons on the diamond surfaces ought to be taken consideration, which is better to be calculated using density functional theory (DFT) methods. The computational findings using DFT are presented in the following chapter.

References

1. G.R. Hennig, "Surface Oxides on Graphite Single Crystals," *Proc. Conf. Carbon, 5th*, **1** 143-6 (1962).

2. R. Sappok and H.P. Boehm, "Chemie der Oberflache des Diamanten - I. Benetzungswarmen, Elektronenspinresonanz und Infrarotspektren der Oberflachen-Hydride, -Halogenide und -Oxide," *Carbon*, **6** [3] 283-95 (1968).

3. R.C. Bansal, F.J. Vastola and P.L. Walker Jr., "Kinetics of Chemisorption of Oxygen on Diamond," *Carbon*, **10** [4] 443-8 (1972).

4. J.Y. Howe, L.E. Jones and D.W. Coffey, "The Evolution of Microstructure of CVD Diamond by Oxidation," *Carbon*, **38** [6] 931-3 (2000).

7 SIMULATION STUDY OF DIAMOND SURFACES

7.1 Background of Simulation Methods

Atomistic simulations are capable of calculating structural and dynamical properties of materials. Such studies have become increasingly important as part of the research effort in chemistry, materials research, and the life sciences. Figure 7-1 contains a chart of the possible computational approaches. In order to select an approach, the first decision must be made between force field methods and quantum mechanical approaches. If electron properties are the interest of study, then force field methods should not be chosen because they are unable to compute electronic properties. The next choice among the quantum mechanical methods is between ab initio and semi-empirical. Semi-empirical methods, although much less time-consuming (less expensive), require careful control of inherent approximation and parameters. On the other hand, the ab initio approach provides more reliable results. The Hartree-Fock method considers each electron and its interactions with all other electrons and nuclei. Thus a system is described by a set of one-electron wave functions. This precise approach gives reliable results but limits the capability to handle only of 50 carbon-like atoms. By using point or space group symmetry, Hartree-Fock methods can also handle one-, two-, and three-dimensional periodicity as well. However, Hartree-Fock method itself do not address the correlations and exchange forces that exist in the solids. Density functional theory is a means to take the correlations and exchange forces into consideration and a review is given in the following section.

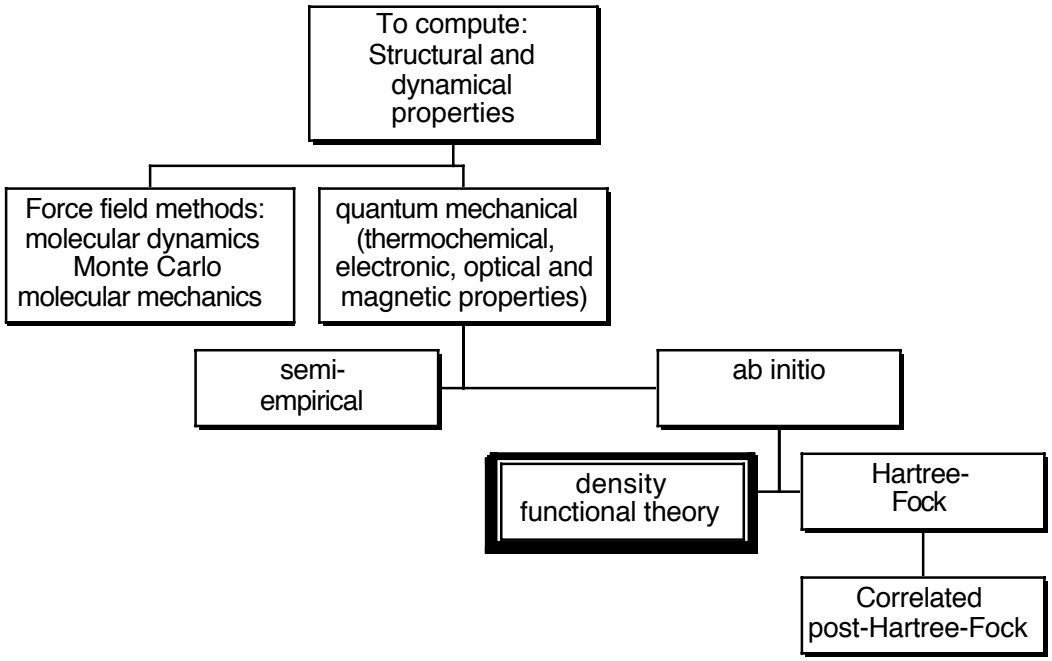

Figure 7-1. The Computational Approaches

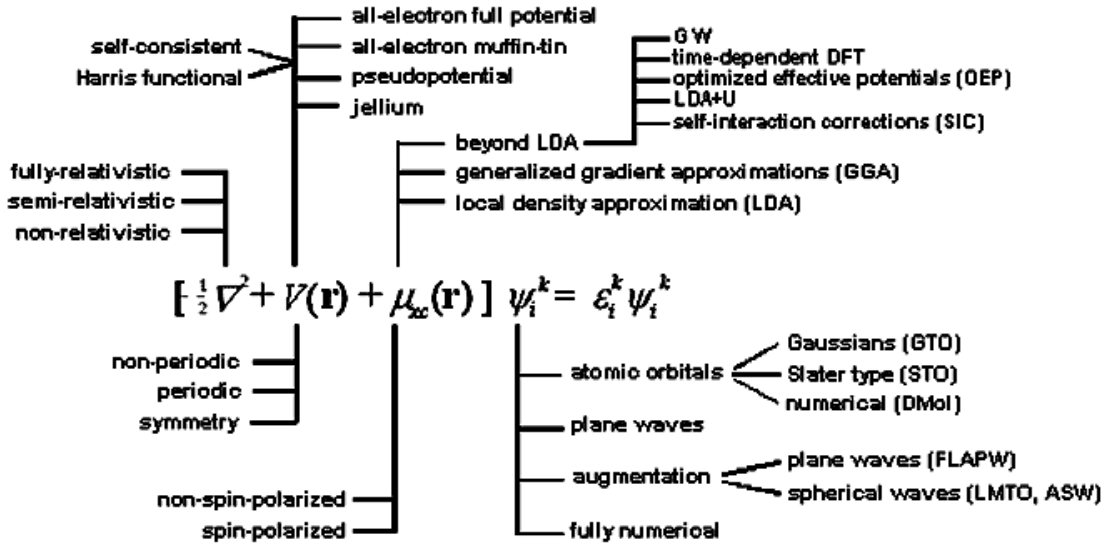

Figure 7-2. DFT Implementations by Wimmer [1]

7.2 Density Functional Theory and CASTEP

7.2.1 Density Functional Theory

The existence of *correlations and exchange forces* between the particles presents the main difficulty in treating solids in quantum mechanics.[2] The positions and motions of the particles that make up solids or molecules are correlated when the particles interact with each other and exert forces upon while they move. The electrons are Fermions that follow the Pauli Exclusion Principle: the electron motion is correlated, with two parallel-spin electrons tending to avoid each other, thereby creating an exchange-correlation hole.[3] A breakthrough in the calculation of the energy of collections of atoms and the forces on each particle was developed by Kohn and Sham in the 1960's.[4] They showed that a mean-field theory can be applied to describe correlation and exchange forces. Their method is referred to as density functional theory (DFT).

The concept of DFT, which expresses the total energy of a system as a functional of the total electron density, was introduced shortly after the formulation of quantum mechanics in the mid 1920's. Kohn and Sham's equations, which are the foundation of accurate calculations, are actually the effective one-electron Schrödinger equations of DFT (Figure 7-2). The total energy is decomposed into three terms, as presented in the square bracket of Figure 7-2, as: 1) the kinetic energy of electrons; 2) the Coulomb potential due to classical electrostatic interactions among all the charges in the system; and 3) the exchange-correlation potential that describes all many-body exchange interactions. In a periodic system, the wave functions are described by an additional quantum number, **k**, where $\hbar k$ is the momentum of the electron in the crystal. The solutions to these equations

enable access to the total energy as a functional of nuclear position. From these solutions, all the properties can be derived. Although the form of Kohn-Sham equations is exact, the actual expressions of the exchange-correlation interactions are unknown. Therefore, the Kohn-Sham functional must be supplemented by an approximation for the exchange and correlation term. DFT methods are named after the particular type of these approximations, such as local density approximation (LDA), general gradient approximation (GGA), local spin density approximation (LSDA), and gradient-corrected LSDA (GGS).

In the local density approximation, proposed by Kohn and Sham, a homogeneous electron gas having density ρ substitutes the true electron density locally. In other words, E_{xc} for a non-uniform charge distribution is approximated at a given position by the value of E_{xc} corresponding to a system of uniform charge density. The value of this uniform charge density is known, and this value has the same charge density as that at the site in the real charge distribution. Equation 7-1 describes the LDA as:

$$E_{xc}^{h}[\rho(x)] = \int dx \cdot \rho(x) \cdot \varepsilon_{xc}^{h}[\rho(x)] \qquad (7\text{-}1)$$

where $E_{xc}^{h}(\rho)$ is the exchange-correlation energy of a homogeneous electron gas with density ρ.

LDA remained the only choice of approximation E_{xc} for many years. Density Functional Theory (DFT) was used only by the physics community while most chemists remained extremely skeptical. Early DFT calculations predicted binding energies very poorly—

typically overestimating them by 30% — although molecular geometries and vibrational frequencies are predicted to within 1 or 2% of the correct values. The main reason for the error in binding energies is the very crude approximation used to determine the effects of electron-electron interactions: the assumption that the interaction energy at any point in space depended only on the electron density at that point, taking into account nothing about variations in density. The generalized gradient approximation (GGA) is one of the approaches to correct exchange-correlate functionals. Introducing terms that depend on the gradient of the density gives binding energies that can be predicted as accurately as molecular geometries and vibrational frequencies.[5] Using the gradient correction barely influences local properties such as bond lengths or vibration frequencies, yet it significantly improves global changes in the energy in cases such as a molecule binding on a surface, or two atoms forming to make a molecule. As a result, many chemists are beginning to exploit DFT calculations, which have been very successful for the calculations on elements in the first row of the periodic table. For these reasons, GGA has been selected for this study.

7.2.2 An Overview of CASTEP

Computer simulation is carried out using the CASTEP module of Cerius2®, running on an SGI Octane workstation. CASTEP®, an acronym for CAmbridge Sequential Total Energy Package, is a commercial software package originally developed by the Theory of Condensed Matter Group at the University of Cambridge.[6] It performs total energy calculations that solve quantum mechanical equations for the electronic states of systems

® Cerius2 is a software developed by Molecular Simulations Inc., San Diego, CA.

containing arbitrary arrangements of atoms. CASTEP calculates the ground state energy and charge density of the system, allowing any physical quantity that is related to total energies (e.g., lattice constants, elastic constants, geometric structure, binding energies) to be computed. It is general enough to be applicable to the full range of molecular, solid state, and surface problems found in the materials sciences.[7] It has been applied to a wide range of materials science problems in areas including calculations on diamond.[8-11]

CASTEP calculations are carried out on periodically repeating cells or boxes, usually referred to as "supercells". The dimension of the supercell may be the same as the unit cell. It can also set to be larger than the unit cell. Supercells can host not only crystalline species, but also species without periodicity, e.g., an oxygen molecule. The only input to a calculation is a starting geometry for the system under consideration and the atomic numbers of the constituent atoms. In the method, core electron potentials are replaced by pseudopotentials, which are the effective potentials that act only on the valence electrons in the system. The electronic wavefunctions are expanded in terms of a plane wave basis set, and electron-electron interactions are described using density functional theory. Combining the use of pseudopotentials and plane wave basis sets makes it rather easy to calculate the forces on all of the atoms in a system. This renders efficient optimization of atomic/ionic configurations, a critical point when performing calculations on complex systems, as it is rare that atomic geometry is precisely known.[7]

7.3 Literature Review on Computational Study of Surface Reaction of Diamond

The majority of the computational studies on diamond have been on the simulation of vapor phase diamond growth using molecular mechanical approaches. Limited simulation studies on diamond surfaces have been carried out using quantum mechanical approaches as well molecular dynamics methods.

7.3.1 Molecular Dynamics Simulation Study on Diamond

Molecular dynamics (MD) simulation is basically an exercise in statistical physics which follows the time evolution of a system, or an ensemble of atoms, that represents the structure of materials. The atoms are placed in a simulation box with certain boundary conditions. Positions and velocities (from which their temperature is determined) are updated iteratively as a function of time. New values are calculated by a short timestep (for instance, a femtosecond per step and 250,000 to millions of steps in total), based upon Newton's Second Law, using the forces that apply on the atoms obtained from a given interatomic potential model. Structural analysis can be performed by averaging over a number of timesteps at the final temperature. The accuracy of an MD simulation is determined by three major factors: 1) accuracy of the interatomic potential model; 2) size of the simulation box; and 3) methodology or process that is applied to create the structure of interest, which influences the final simulated structure.[12]

MD simulation methods are categorized after the methods of obtaining the force constants, either empirical or ab-initio. Using an ab-initio molecular dynamical approach, DeVita, Galli, Canning, and Car proposed a microscopic model for the early stages of the

graphitization process.[13] They find that a well-defined diamond/graphite interface forms during the transition. The interfaces are highly chemically active sites as suggested by the electronic properties of the atoms there.

The graphitization of diamond (111) surface was studied using an ab initio MD method by Kern and Hafner.[14] They claimed that graphitization could occur at temperatures between 3500 to 3900 K on a flat (111) surface and as low as 2500 K on a reconstructed (111) surface with a step.

7.3.2 Quantum Mechanical Study – Semi-Empirical Approach

Davidson and Pickett studied the diamond surfaces using the tight-binding method.[15] The band structure of (100), (110), hydrogenated diamond (111) surfaces, as well as the (111) surface with a (2x1) reconstruction, which is comprised of π bonded chains in the first two surface layers, were calculated. After reconstruction, the bare (110) and (100) surfaces have bond lengths comparable to those of graphite, whereas the hydrogen-terminated (110) has C bond lengths of ~ 1.52Å. In a follow-up paper, the authors reported that the bare diamond (111) surface with a surface step becomes sp^2 bonded near a step.[16] The spontaneous graphitization is associated with a large increase in spacing between the surface layers, while adding hydrogen onto the surface forces the carbon atoms to revert back to sp^3 bonding.

7.3.3 Quantum Mechanical Study of Diamonds Using Density Functional Theory

Inspired by the models of surface reconstruction that are applicable to silicon, Pandey proposed a dimerized-chain model for the reconstruction of the diamond (111)-(2x1) surface using tight-bonding-theory.[17] Pandey claims that this chain-model is supported by Himpsel, Eastman, Heimann, and van der Veen's photoemission spectroscopy data and LEED patterns.[18]

Kern and Hafner investigated surfaces of diamond using both quantum mechanical and molecular dynamical approaches.[19] Ab initio local-density-functional calculations of the clean diamond (110) show that the clean surface relaxes to a structure where the chains in the first two planes are straightened so that the bond lengths are shortened, but the bond angles increase. The relaxed (110) surface is metallic with a very low density of states at the Fermi level, whereas the hydrogenated (110) maintains a structure almost the same as the bulk, and the surface is semi-conducting. The surface energies of the as-cleaved and relaxed low index facets are also given in their paper. Relaxation reduces energies of the (100) and (111) surfaces by 50%. Their local-density-functional calculations on the stepped (111) surfaces indicate that the relaxation leads to an sp^2 bonding near the step, and is restricted to the immediate environment of the step only.[20] It is also calculated that hydrogen stabilizes the flat (111) surfaces but exposure of the (111) surface to atomic hydrogen can roughen the surface as the energy gained by forming an extra C-H bond is larger than the step-formation energy.

Clark, Ackland, and Crain predicted the theoretical stability limit of diamond at ultrahigh pressure, using CASTEP.[5] They claim that GGA is superior to LDA in terms of the accuracy of binding energies and equilibrium lattice parameters. The lattice parameter is calculated to be 3.55 Å using GGA, but 3.51 Å using LDA. Compared to the experimental data of 3.57 Å, GGA gives a more accurate result. It is concluded that at pressures above 5.0 Mbar (500 MPa), a distorted rhombohedral cell containing eight atoms is the stable structure for diamond.

Robertson and Rutter studies the electron affinity (EA) of diamond and diamond-like carbons with various surface terminations, using CASTEP.[8-10] A supercell with eight or ten layers of carbon is used with a vacuum layer of 8 to 10 Å on top. The exchange-correlation is described mostly by LDA. They report that the reconstructed clean diamond (100) and (111) surface have a positive EA of 0.5 and 0.35 eV, respectively, yet the hydrogenated surfaces have negative EA of about 2 eV. The oxygenated (100) surfaces are found to be strongly EA positive, + 2.6 eV for the more stable ether configuration and +3.6 eV for the less stable ketone configuration. The authors claim that according to their brief test, the results do not change significantly when GGA is applied.[9]

Investigation of the oxidation of diamond (100) surfaces was undertaken using CASTEP by Tamura, et al. (a total of eleven co-authors).[11] Generalized gradient approximation (GGA) is the method used to describe the exchange-correlations. Ether, hydroxyl, and ketone structures are found to be stable on this surface. They predict that the ether

structures are expected to form at the initial stage of oxidation on (100); then the formation of the ketone structures becomes easier as the coverage of oxygen increases.

7.3.4 Quantum Mechanical Study of Diamond Using Hartree-Fock Methods

A detailed description of the Hartree-Fock theory can be found in elsewhere.[21] In general, the Hartree-Fock method is a good base-level theory which gives reasonable predictions of structure and vibrational frequencies of stable molecules and some transition states.[22] Yet it is insufficient for accurate modelling of the energetics of reactions and bond dissociation. This insufficiency arises primarily from the fact that the Hartree-Fock method includes exchange exactly only for a single Slater determinant wave function, but neglects a full treatment of the electron correlation. Crystal solids are the systems where correlation-exchange interaction is of great importance.[23] However, this insufficiency can be eliminated if DFT is incorporated into the calculation.

CRYSTAL© is a program that uses Hartree-Fock linear combination of atomic orbitals (LCAO) computational scheme. The latest version of CRYSTAL is capable of undertaking ab initio calculation on crystalline materials at either Hartree-Fock (HF) or DFT level. Pere, Gelizé-Duvignau, and Lichanot compare structure factors and charge density in diamond calculated using Hartree-Fock and DFT methods.[24] They report that both HF and DFT methods calculate the structure factors with an excellent accuracy, while the best agreement with experimental data is obtained using the HF approach.

© by R. Dovesi, C. Pisani, C. Poetti, M. Causa, V.R. Saunders, available through the Quantum Chemistry Program Exchange, Indiana University, Bloomington, IN (http//qcpe.chem.indiana.edu).

In DFT calculations, the GGA approach yields better results than LDA. In charge-density maps, it is found that the HF approach enhances the calculated bond charge around the bond mid-point with respect to the DFT scheme.

Gaussian® is another popular code that is being widely used by chemists.[25] Gaussian uses a non-periodical system in the Hartree-Fock limit. Due to its inability to handle a crystalline system, simulation studies of diamond using Gaussian code tend to be manipulative in nature. Instead of considering the crystal surface as a periodic system, a small cluster of diamond, usually of less than 25 carbon atoms, is singled out as a starting model. The dangling bonds of the carbon atoms are saturated by forming C-H bonds.

Larsson, Lunell, and Carlsson studied adsorption of hydrocarbons on the diamond (111) surface using the Gaussian code.[26, 27] Clusters of $C_{22}H_{27}$, $C_{13}H_{21}$, and C_4H_9 were used as templates for the (111) surface. The electron correlation effects were corrected using second-order Møllet-Plesset theory (MP2) on the relative adsorption energies. Møllet-Plesset perturbation theory is a means to describe electron correlation. It adds higher excitations to HF theory as a non-iterative correction. The MP2 method is one of the least time-consuming ways to improve on HF method prior to the widespread of DFT methods.[21, 22] The adsorption energies are found to be in the order: $C_2H\bullet$ > H• and CH_2 (singlet) > CH• > CH_2• (triplet) > CH_3• > C_2H_2. The $C_2H\bullet$ species is predicted to adsorb more strongly onto the H-terminated diamond (111) surface than does H•.

® Gaussian is a quantum mechanical simulation package developed by Gaussian Inc., Pittsburgh, PA.

Hukka, Pakkanen, and D'Evelyn investigated chemisorption of hydrogen,[28] fluorine, chlorine, HF, and HCl on diamond (100) 2x1 surfaces,[29] using Gaussian. Clusters consisting of nine carbon atoms in four separate layers were used as templates of the diamond (100) 2x1 surface for these chemisorption cases. The bond lengths of C-H, C=C, C-X (X may be H, F, Cl), and XCC-H are determined based upon this C_9H_{13} cluster. They state that their work provides upper and lower bounds on the C=C dimer bond lengths and C-X bond energies. Nonetheless, they agree that larger clusters or slabs are needed for fully-converged results.

Skokov, Weiner, and Frenklach studied the energetics and vibrational spectra of oxygenated diamond (100) surfaces using Gaussian as well as a semi-empirical MD approach.[30] They point out that calculations based upon small clusters are not always able to provide upper and lower bounds to real energies. They thus move on to study the energetics of (100) surfaces using MD based upon a model with 360 carbon atoms in 10 (100) layers. They report that the (100) surfaces containing hydroxyl and ether-like oxygen bonds are found to be energetically more favorable than surfaces with a ketone structure. Hydrogen bonds are predicted to form among chemisorbed oxygenated species, which is important in stabilizing the chemisorbed layers.

7.4 Philosophy of Computational Study

Computers do not "think". Computers merely carry out what has been asked. *"Garbage in, garbage out"*, although a far less elegant statement, has been the unofficial maxim of simulation study for a long time. Simulations deal with models. It is all about using the

appropriate method to treat reasonable models. A model should be the simplified reality yet reflect the characteristics of the system. A computational study would be marginally meaningful if the conclusions are drawn from a model which hardly resembles the real system. In the current study, the key characteristic of diamond surfaces is the periodicity of the lattice. A simulation method should be capable of handling a model with surfaces and periodicity. Our simulation investigation is a practice of this philosophy of computational study.

7.5 Simulation Approach of the Current Study

Simulation is carried out using CASTEP on an SGI Octane work station. The calculation is undertaken using GGA-PW91 (general gradient approximation, the Perdew-Wang method).[31, 32 33] The Perdew and Wang method is a GGA based on real-space cutoff of the spurious long-range components of the second-order gradient expansion for the exchange-correlation hole. The PW91 method is tested to be better than LDA on a wide variety of systems including atoms, molecules, solids, and surfaces.[33] The strategy of the computational work is to build a supercell with various surface conditions and perform a geometry optimization with respect to the total energy. A relaxed structure is the final one when the energy converges to a minimum. The supercell is built to be large enough to allow relaxation, yet small enough to be computationally economical (smaller cells demand less CPU time, therefore, use fewer computational resources).

The images of three supercells, denoted (111), (110), and (100) (representing different surfaces), are given in Figure 7-3, and the cell contents and cell parameters of these cells

are tabulated in Table VII-1. Modeling is carried out using these cells. The cells are set to be big enough to allow ample degeneracy of periodicity. Giving as an example, in order to study the surface relaxation and oxygen-chemisorption, a super cell of 54 carbon atoms in total is built with six (111) layers; each layer contains 9 carbon atoms (see Figure 7-3). There is 10 Å of vacuum on top of the (111) surface. The cell dimensions are 7.543, 7.543, and 14.619 Å, in the *a*, *b*, and *c* directions, respectively (Table VII-1). The [111] of the original unit cell coincides with the *c* axis of the supercell; the cell angle γ is 120^{o}. Thus an infinite 3-D lattice is constructed in a way that it can also be visualized as stacks slabs (infinite in 2-D) with 10Å of vacuum in between. The vacuum space of 10 Å is large enough to ensure that there are no interactions between adjacent slabs.

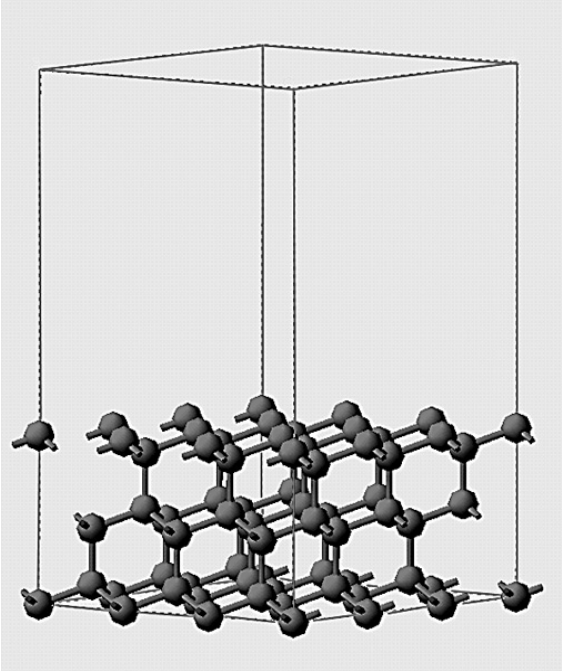

(a)

Figures 7-3 (b) and (c) are on the next page.

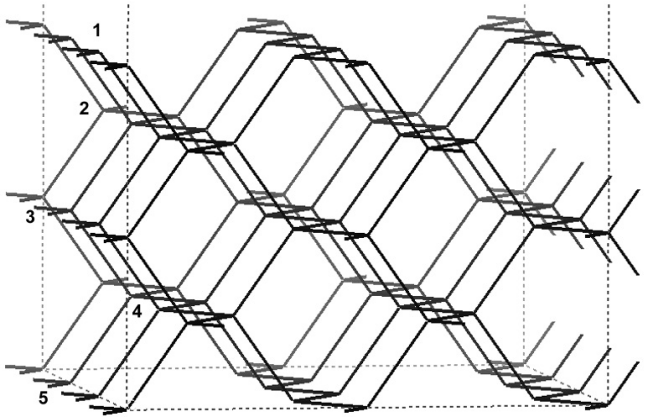

(b)

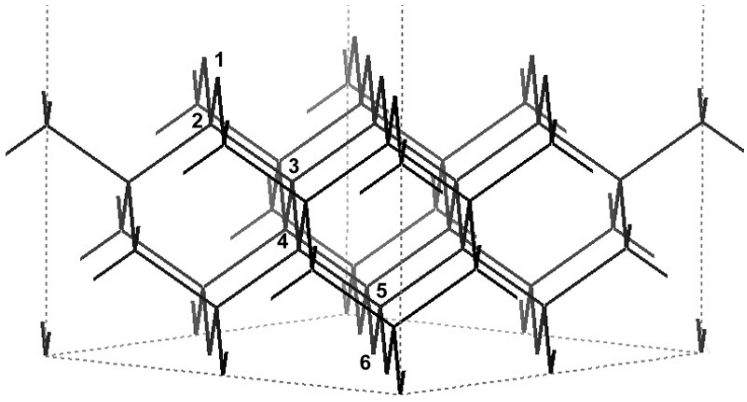

(c)

Figure 7-3. Diamond (111), (110) and (100) supercells used as templates for surface relaxation or chemisorption. (a) The (111) cell with 10 Å of vacuum; (b) The (110) cell; and (c) The (100) cell. The vacuum space of the (110) and (100) cells is not shown in (b) and (c) . The layers of carbon are numbered in (b) and (c).

The (110) and (100) supercells are constructed in a similar manner (Table VII-1). These supercells are the templates on which chemisorbed species, mostly oxygen in the current study, can be deliberately added to the top layer. Geometry optimization is then performed on these starting models. The final structure is the one with the lowest energy.

The energetics of surface relaxation and oxygen-chemisorption on diamond surfaces have been calculated. A schematic of oxidation mechanism for diamond is given in Figure 7-4. This is a simplified mechanism in which the first step involves carbon chemisorption and the second step is the desorption. The energetics of just the first step is calculated in the current study, in other words, only the chemisorption study is undertaken, which is illustrated as the shaded area in Figure 7-4. The oxygen chemisorption can be described as a two-step process. The first step is the dissociation of oxygen molecule to two oxygen atoms, Equation 7-2. The second step is the chemisorption of the oxygen atom on the surface, Equation 7-3.

$$O_2 \rightarrow 2O \qquad (7\text{-}2)$$

$$C_{diamond} + 1/2\ O_2 \rightarrow C(O)_{diamond} \qquad (7\text{-}3)$$

The energetics described by Equation 7-2 is literally the heat of formation, for which the dissociation enthalpy of the oxygen dimer and the hydrogen dimer at 0 K were cited from Journal of Physical and Chemical Reference Data: the formation of H from 1/2 H_2 is 216.035 kJ/mol at 0 K,[34] and the formation enthalpy of O from 1/2 O_2 is 246.790 kJ/mol at 0 K.[35] The energy of each term in Equation 7-3 is calculated using CASTEP.

Table VII-1. Cell Parameters and Contents of Diamond and Graphite Supercells

cell	a (Å)	b (Å)	c (Å)	γ (°)	V (Å^3)	layers	atom/layer
d (111)	7.543	7.543	14.619	120	720.436	6	9
d (110)	7.112	7.543	16.286	90	873.733	5	12
d (100)	14.445	7.123	7.123	90	734.038	6	8
g(0001)	7.380	7.380	18.00	120	849.015	3	18

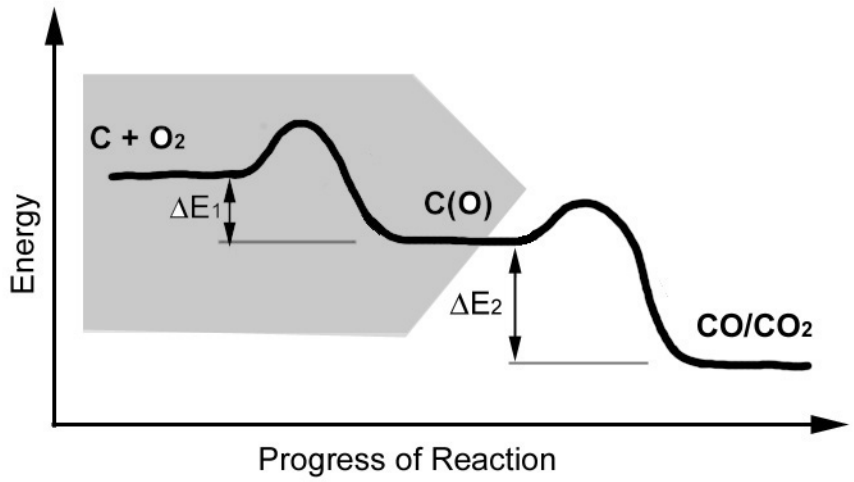

Figure 7-4. A schematic of the reaction between diamond and oxygen. The shaded part of the reaction is the topical area of current research.

The oxygen and hydrogen molecules are also treated in periodic systems as if the dimer occupies space in the supercell. The dimer is put in a box (supercell) which is big enough for the dimer to be regarded as isolated in a vacuum. The box for the oxygen dimer is a 15x15x15 $Å^3$ cube and the box to host the hydrogen dimer is an 18x18x18 $Å^3$ cube. For the sake of comparison, the surface energy of graphite (0001) and hydrogen-chemisorption on the diamond (111) surface are calculated as well.

All the CASTEP jobs can be categorized into six groups, as listed below. Details of each job can be found in Appendix II, where all the CASTEP jobs are compiled.

- Diamond (111) surface

  Relaxation of the clean surface

  Fully covered by oxygen

  With 1 oxygen atom (11% coverage)

  With 2 oxygen atoms (22% coverage)

  With 6 oxygen atoms (67% coverage)

  The bulk energy calculation (single point energy)
- Diamond (110) surface

  Relaxation of the clean surface

  Fully covered by oxygen

  The bulk energy calculation (single point energy)
- Diamond (100) surface

  Relaxation of the clean surface

  Fully covered by oxygen

The bulk energy calculation (single point energy)

- Graphite (0001) surface

  Relaxation of a clean (0001) surface

  Graphite bulk (single point energy)

  Single point energy calculation on the cell with clean (0001) surfaces

- Oxygen dimer
- Hydrogen dimer

Geometry optimization calculation is performed in all the relaxation runs as well as on the cells with chemisorbed species. Single point energy calculations are used to obtain the energy of a system, without any change of the geometry. All the cells, excluding graphite, are treated as insulators. Graphite is more appropriately treated as a metal in this simulations because graphite is by nature a semi-metal. In the CASTEP calculation, the "metal" setting specifies that partial occupancies should be used for electronic band close to the Fermi level. It also requires better sampling of the Brillouin Zone, therefore, yielding more accurate results for metallic materials and semiconductors with odd number of valence electrons.

Surface energies are calculated using the following equation:

$$E_s = (E_{surface} - E_{bulk})/(2 \cdot A) \qquad (7\text{-}4)$$

Where E_s is the surface energy; $E_{surface}$ is the energy of a system with a surface; E_{bulk} is the energy of a system without surface; and A is the area of the newly created surface.

Values of E_{bulk} result from single point energy calculations. The bulk energy of diamond is obtained by multiplying the energy of a single atom by the number of atoms. Because the energy difference between bulk graphite and graphite surface is very small, the energy of the bulk graphite was calculated directly based upon a bulk supercell of graphite. E_s is the difference of the bulk and the one with two surfaces. The models used for this calculation are given in Figure 7-5.

Heat of chemisorption is calculated by:

$$E_c = E_{final} - (E_{clean} + 1/2\ n \cdot E_{O\text{-}dimer} - n \cdot E_{disso}) \qquad (7\text{-}5)$$

where E_c is the heat of chemisorption; E_{final} is the energy of the final (relaxed) structure with chemisorbed oxygen atoms; E_{clean} is the energy of the structure with clean surfaces that is obtained from single point energy calculation; n is the number of oxygen atoms (the number of oxygen dimers is a half of n); $E_{O\text{-}dimer}$ is the energy of the oxygen dimer; and E_{disso} is the dissociation energy of the oxygen dimer.

The terms included in the parentheses represent the energy of the reactants while the E_{final} is the energy of the products. The heat of chemisorption is the difference between the products and the reactants.

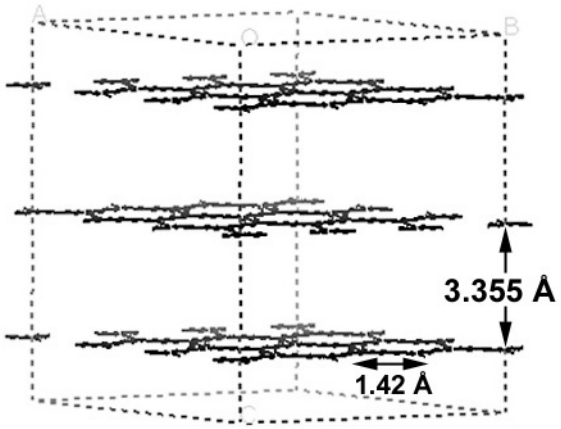

(a)

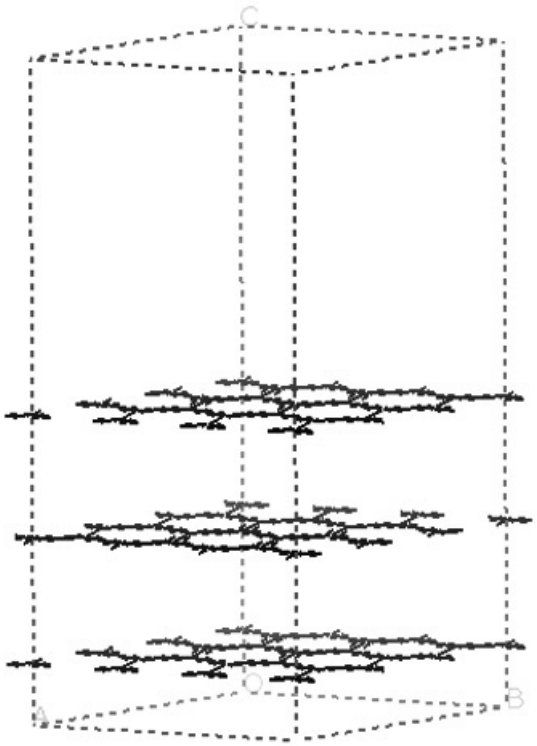

(b)

Figure 7-5. Graphite (0001) supercells: (a) the cell represents bulk graphite; and (b) the cell represents (0001) surfaces with 9.61 Å of vacuum above the top layer. The energies of the cells are obtained from single point energy calculation. The surface energy is the difference between the two structures that is normalized to the newly created surface area.

7.6. Results

7.6.1 Relaxation and Oxygen-Chemisorption on Diamond (111) Surface

Relaxation of clean diamond (111) surface

Cell dimensions and cell contents of the (111) supercell are described in Section 7.5.2 and Table VII-1. Carbon atoms in unrelaxed diamond have a sp^3 bond character and the covalent bonds are arranged in a tetrahedral manner. The bond length is 1.54 Å and the bond angle is 109.5°. Relaxation of the diamond (111) surface leads to a structure similar to graphite (0001). Carbon atoms of graphite (0001) are sp^2-hybridized and arranged in a planar manner, with a bond length of 1.42 Å and a bond angle of 120° within each carbon layer, Figure 7-5. The interlayer spacing of ideal graphite is 3.355 Å. After relaxation, the original six layers of diamond (111) flatten and reduce to three flat layers of carbon with an interlayer spacing of 3.41 Å, Figure 7-6. The bond lengths between the carbons within each layer are given in Figure 7-7. The C-C bond length is 1.45 Å and the bond angle increases to 120°. The C-C bond length and interlayer spacing of the relaxed structure are larger than in crystalline graphite but fall well within the range of amorphous carbon. The relaxation energy is calculated to be -81.12 kJ/mol. This suggests that the clean diamond (111) surface spontaneously relaxes to an amorphous carbon structure which is energetically more favorable.

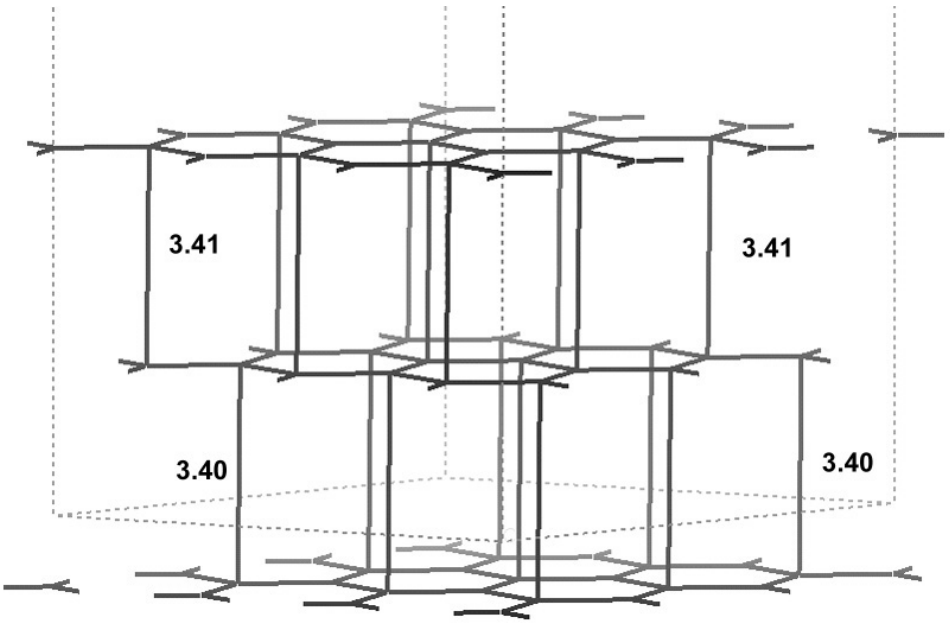

Figure 7-6. A diamond supercell with clean (111) surfaces after relaxation. Six layers of atoms (refer to Figure 7-3) flatten to three layers. The interlayer spacing increases to 3.41 and 3.40 Å, respectively. The intra-layer bond lengths are given in Figure 7-7.

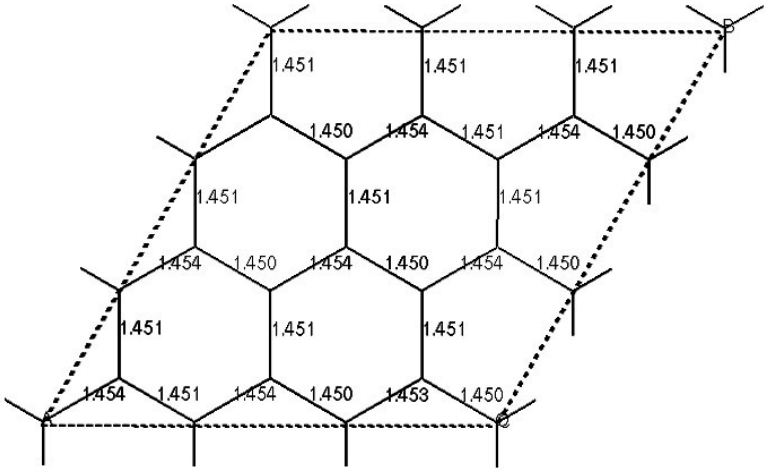

(a) Top layer

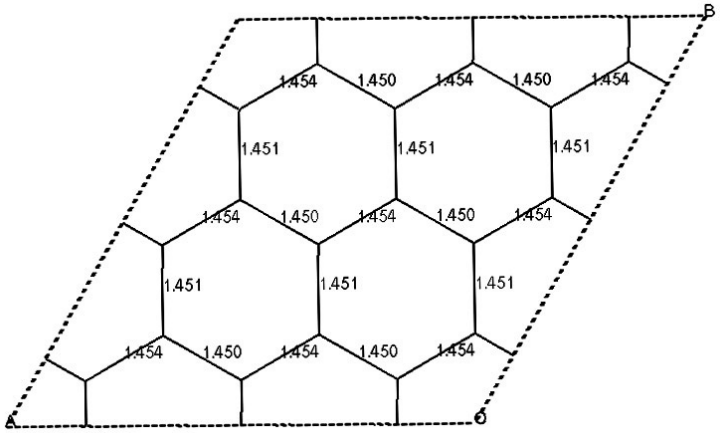

(b) mid-layer

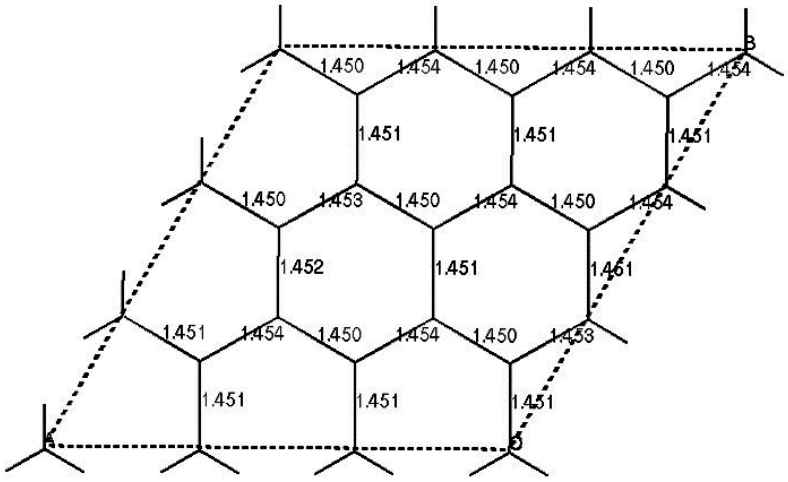

(c) bottom layer

Figure 7-7. A reconstructed clean (111) cell. (a) The top layer, (b) the middle layer, and (c) the bottom layer. Bond lengths reduce from 1.54 Å to 1.45 Å.

Chemisorption on the Diamond (111) Surface

Simulations are carried out on (111) surfaces with 11, 22, 67, and 100% oxygen-coverage. The (111) supercell has 9 carbon atoms on the top layer which implies that there are nine available sites for chemisorption. A 100 % coverage is obtained by placing 9 oxygen atoms on the top layer and forming C-O bonds. Adding one oxygen on the top layer results in a 11 % surface coverage, two oxygen atoms render a 22 % coverage, and six result in a 67% surface coverage. Presented in this section are the structural changes as a function of oxygen chemisorption. The energetics associated with the oxygen-chemisorption are presented later in Section 7.6.5.

The structure of the (111) cell with 100% O-coverage is given in Figure 7-8. The surface retains its sp^3 bond character if the surface is fully chemisorbed with oxygen, although the bond angles and bond lengths are distorted slightly (see Figure 7-8). If the atomic positions of the bottom layer are not fixed, the bottom surface, which is a clean surface free of chemisorbants, tends to deviate from a true sp^3 bond character. The bond length of the top, middle, and bottom reconstructed layers are given in Figure 7-9.

Figure 7-10 contains the structure of a (111) cell fully covered by chemisorbed hydrogen on the top surface. The sp^3 bond character can also be preserved by complete hydrogen-chemisorption (see Figure 7-10). If fully covered by oxygen or hydrogen, these C-O or C-H bonds are all perpendicular to the plane of the (111) layer. However, under partial oxygen coverage, the C-O bonds are canted (tilted with respect to the surface),

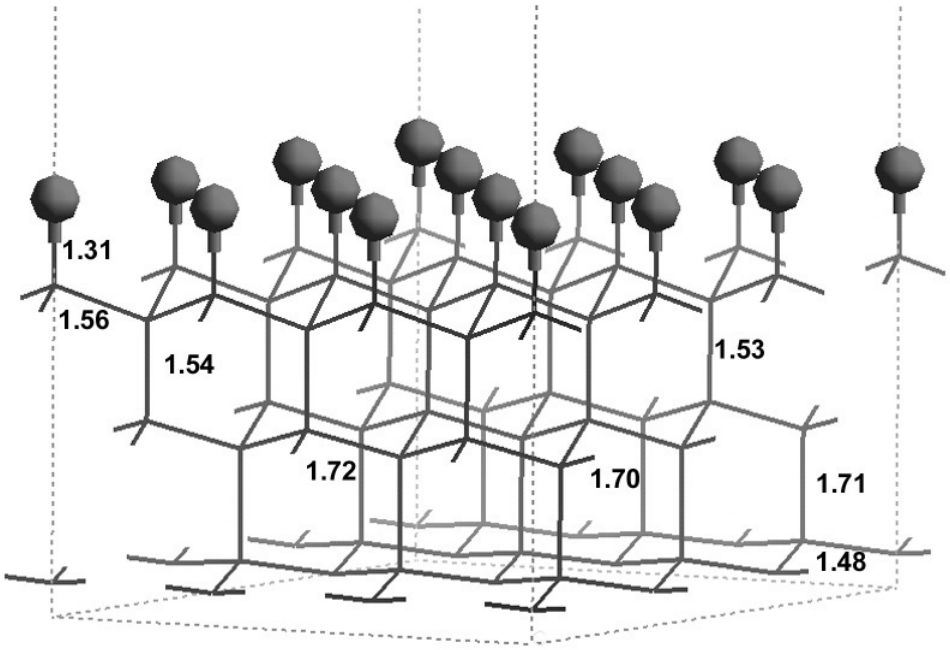

(a) (111) cell with relaxed bottom layer

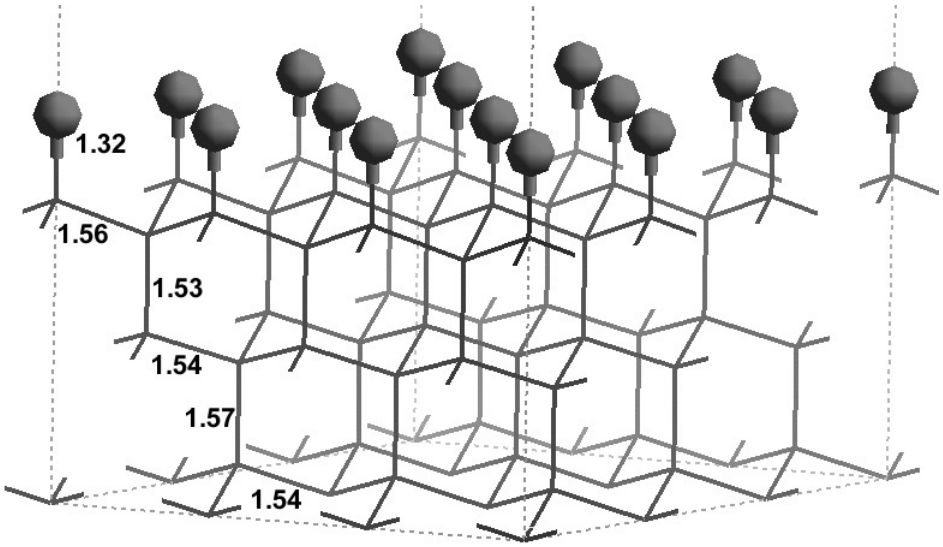

(b) (111) cell with fixed bottom layer

Figure 7-8. The (111) supercells: (a) with relaxed bottom layer and (b) with fixed bottom layer. Top layer: fully covered by chemisorbed oxygen (C-O bond length is 1.31-1.32 Å), and the sp^3 configuration is maintained.

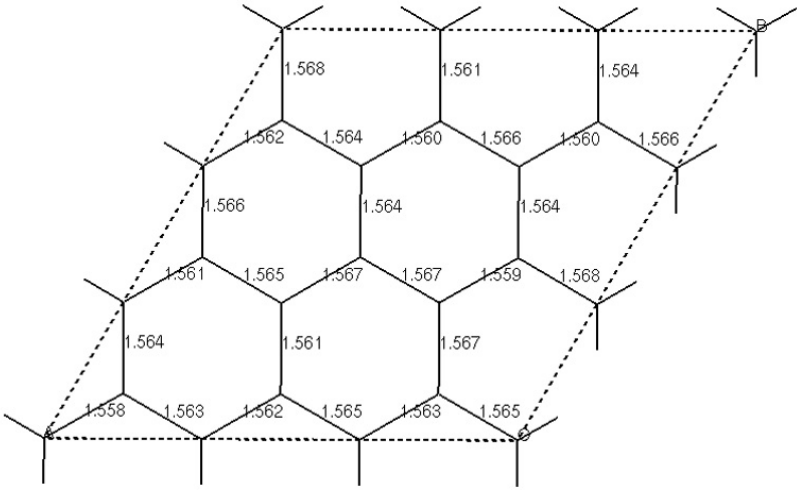

(a) Top layer

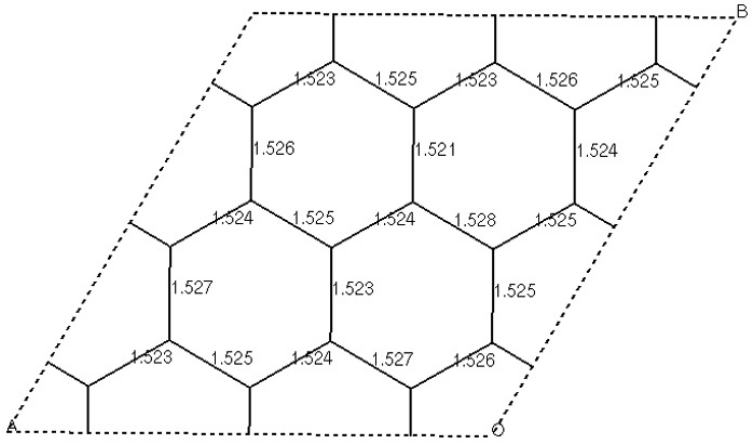

(b) mid-layer

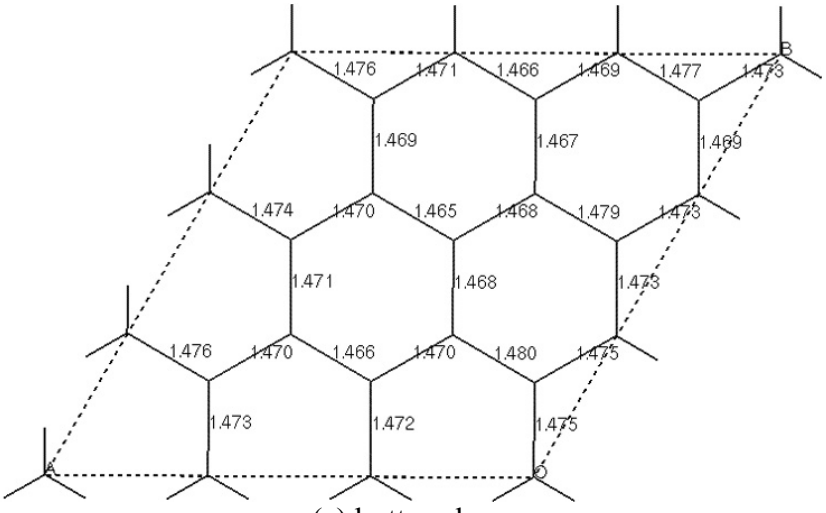

(c) bottom layer

Figure 7-9. A (111) cell with 100% O-coverage at top layer. (a) The top layer, (b) the middle layer, and (c) the bottom layer. Bond length of top, mid-, and bottom layers are 1.56, 1.52, and 1.47 Å, respectively.

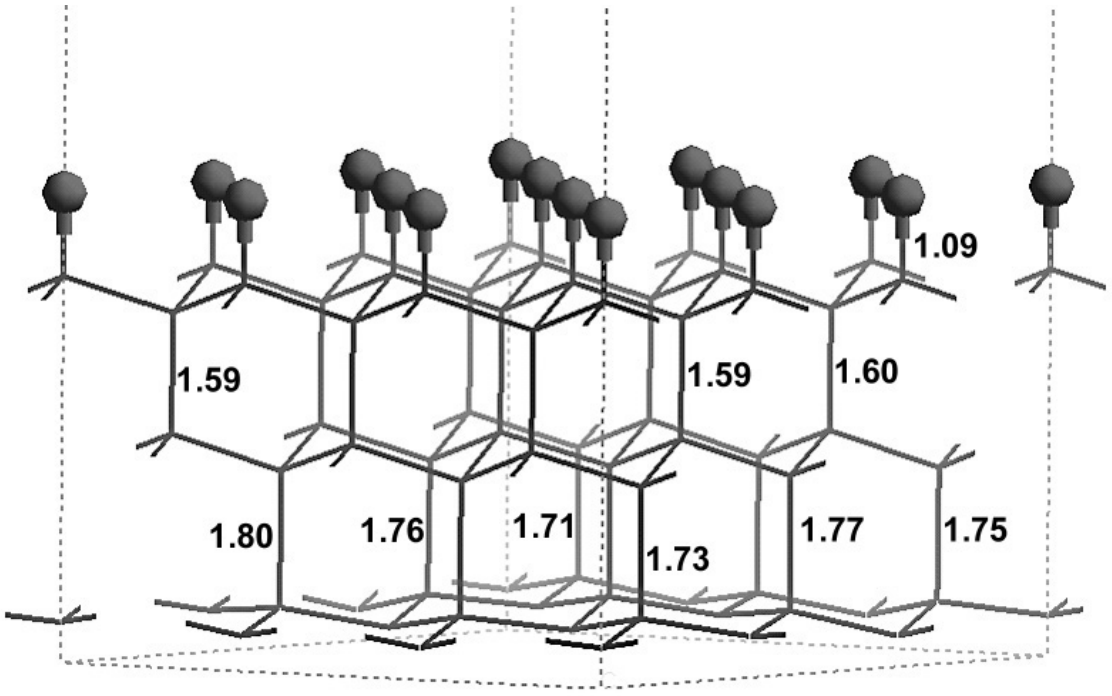

Figure 7-10. Relaxed (111) supercell that top layer is fully covered by chemisorbed hydrogen (C-H bond length is 1.09 Å). The sp^3 configuration is maintained. Bottom layer is a clean (111) with flattened layer and stretched interlayer spacing to 1.71Å.

introducing localized bond distortion and, thereby, lowering the structural symmetry. In other words, partial coverage of a surface with chemisorbed species does not prevent it from being amorphous. The structures of the (111) cells with 11, 22, and 67% O-coverage are given in Figures 7-11 through 7-16. Figure 7-11 contains two cells with 11% coverage: (a) is a cell which the lone chemisorbed oxygen atom sits in the center of the top layer; and (b) is the cell which the oxygen chemisorbs on a corner carbon atom. The different arrangements of oxygen on the surfaces yield different structures. The oxygen-at-the-center cell has an interlayer spacing of 3.42 Å, while it is 3.85 Å for the oxygen at-the-edge cell (see Figure 7-11). Yet the total energy of these two are very similar, –8859.28 and –8859.75 eV for the oxygen-at-the-center and oxygen-at-the-edge

cells, respectively. This converts to an energy difference of 0.8 kJ/mol of these 55-atom cells (54 carbon and 1 oxygen). The different structure has the similar energy suggests that structural diversity could be maintained, and possibly, lead to an amorphous structure.

The bond lengths in the top, middle, and bottom reconstructed layers of the cells with 11, 22, and 67% coverage are given in Figure 7-12, 7-14, and 7-16, respectively. Figures 7-13 and 7-15 contains the structures of the cells with 22 and 67% coverage, respectively. Canted C-O bonds are ubiquitous in these models. The change of bond length on various layers can be tracked by the values labeled in these figures.

Table VII-2 compiles the data for C-O (and C-H) bond angles and lengths. At 10 and 22% coverage, the C-O bond length is 1.48 Å, which is 13 % longer than that at 100% coverage. The angle of canting of C-O bond is 58.4 ^{o}. The angle of canting is defined as the angle between the C-O bond and the plane of the (111) layer. The distortion goes further into the second and third layer. The layers are shifted slightly, as indicated in Figures 7-11 and 7-13. In the case of 10% coverage, two models were studied, i.e., with the only oxygen placed at the center, and at the edge. The two models produce the same structure and nearly the same total energy after relaxation, despite the differences in oxygen location, Figure 7-11. At 22 % coverage, the two C-O bonds point in the same direction and the bond lengths are the same. The bond lengths and angles are the same for both 11% and 22% coverage conditions, at 1.48 Å and 58.4^{o}. The surfaces with 11 or 22% coverage closely resemble the reconstructed clean surface, which is sp^2-bonded

amorphous carbon. But with 67% coverage, the bond angles and lengths are quite different from the low coverage cases. The six C-O bonds of the 67% coverage point in various directions; the angle of canting varies from 80 to 84 ^{o}, and the bond lengths range from 1.38 to 1.46 Å. The carbon layers are shifted. The symmetry of the (111) cell with 6 oxygen atoms is drastically reduced. The simulation study shown here is based upon a (111) cell with a surface area of 7.54 x 7.54 $Å^2$. According to the electron density map, the surface with 67% coverage is akin to the surface of full coverage, i.e., having sp^3 bond character. In a scenario with more cells of partial coverage, the C-O bonds point in random directions and, it is reasonable to consider that the diamond surface is virtually amorphous.

The canting of C-O bonds at low coverage is an interesting phenomenon. Does canting imply that the ether type C-O-C bonding might be more favorable? It is possible. The experimentally measured C-O single bond length is 1.43 Å.[36] The canted C-O bonding makes the oxygen atom lean towards the flat carbon layer. Thus the C-O distance (not the bond length here) measured in the model with 11% O-coverage is 1.47Å, Figure 7-11. The C-O distances are 1.46 and 1.47 Å on the model with 22 % coverage, Figure 7-13. However, the C-O distance increases significantly in the model with 67% coverage, ranging from 1.97 to 2.49 Å, Figure 7-15.

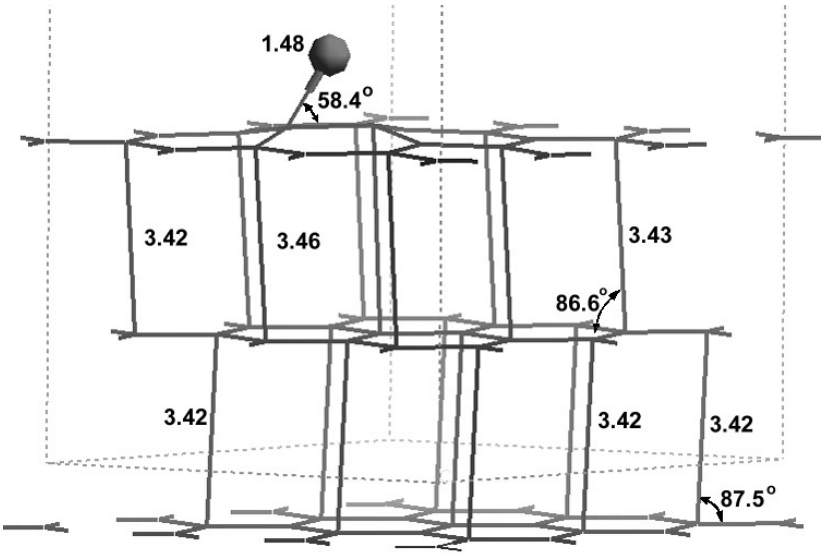

(a) Chemisorbed oxygen sits at the center of the (111) supercell.

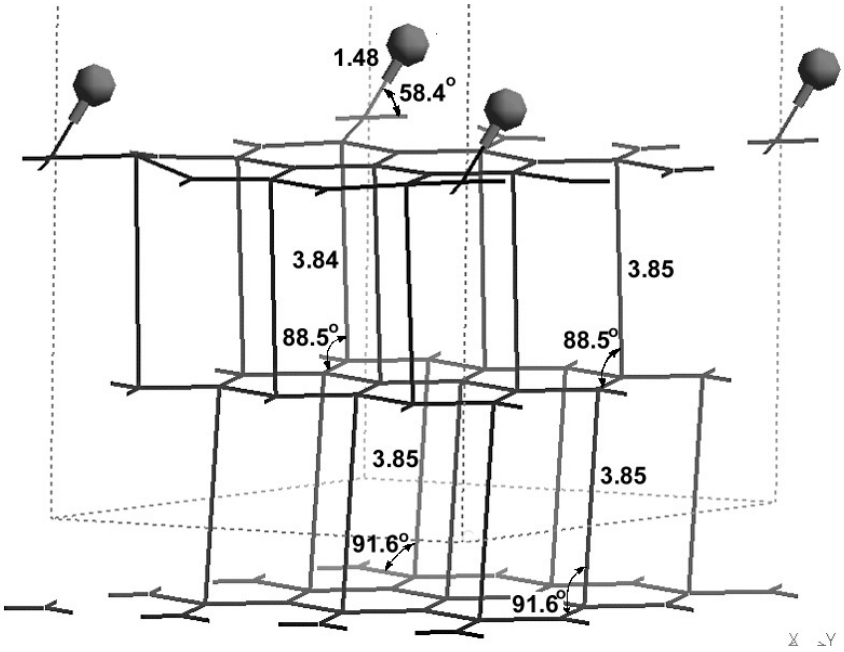

(b) Chemisorbed oxygen at the edge of the cell

Figure 7-11. Relaxed (111) supercell with one oxygen chemisorbed on top layer (11% coverage). C-O bond is canted by 58.4° with a 11% coverage. Partial coverage introduces distortion of the first interlayer spacing.

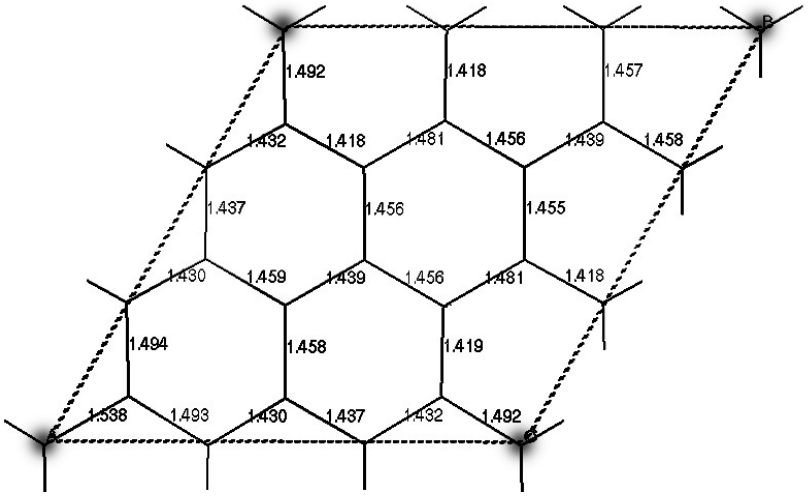

(a) top layer

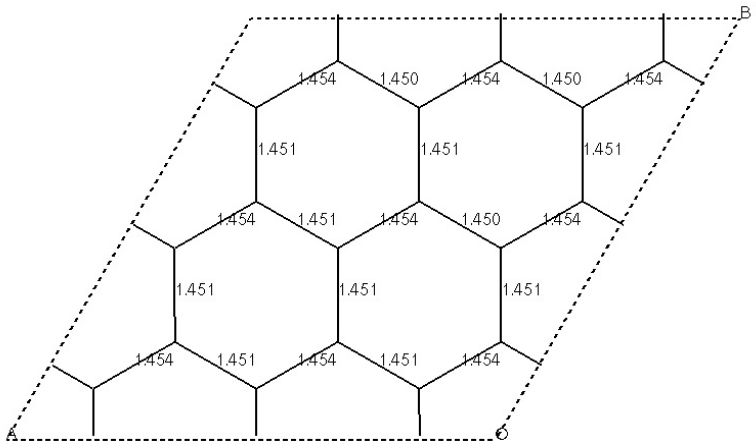

(b) middle layer

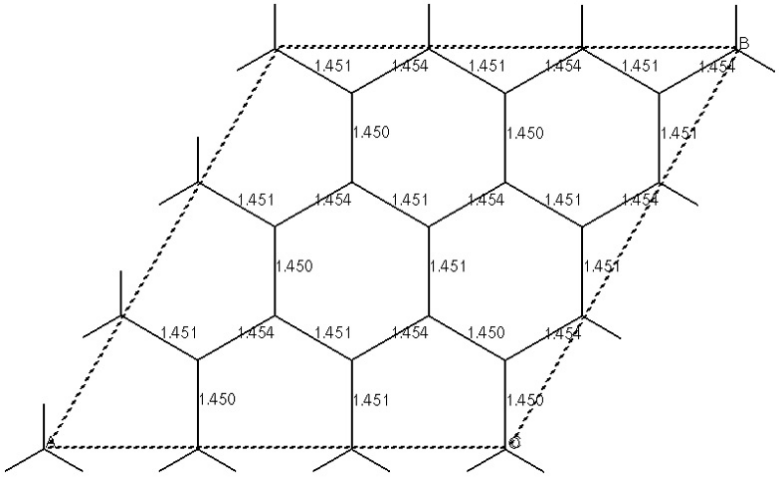

(c) bottom layer

Figure 7-12. A (111) cell with 11% O-coverage on top layer (labeled by blobs). (a) The top layer, (b) the middle layer, and (c) the bottom layer. Bond length difference is 9% on top layer but less than 1% for the rest.

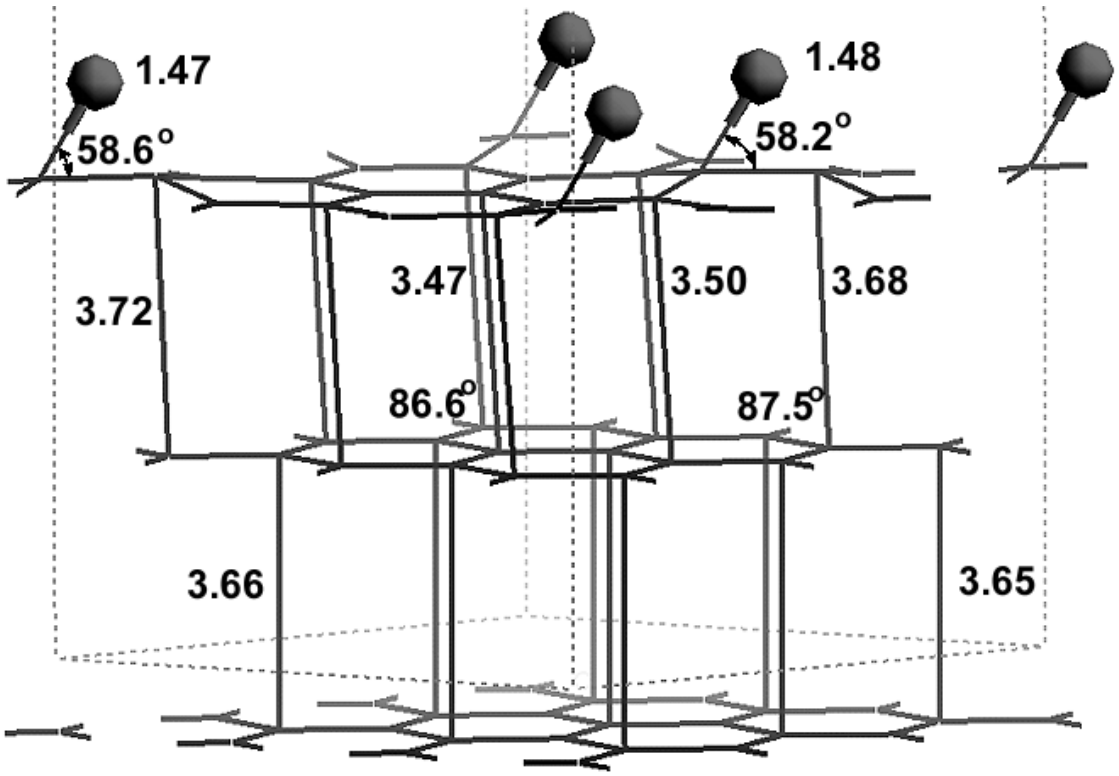

Figure 7-13. Reconstructed (111) supercell with two oxygen chemisorbed on top layer. C-O bond is canted by 58.4° with a 22% coverage. Partial coverage introduces distortion of the first interlayer spacing.

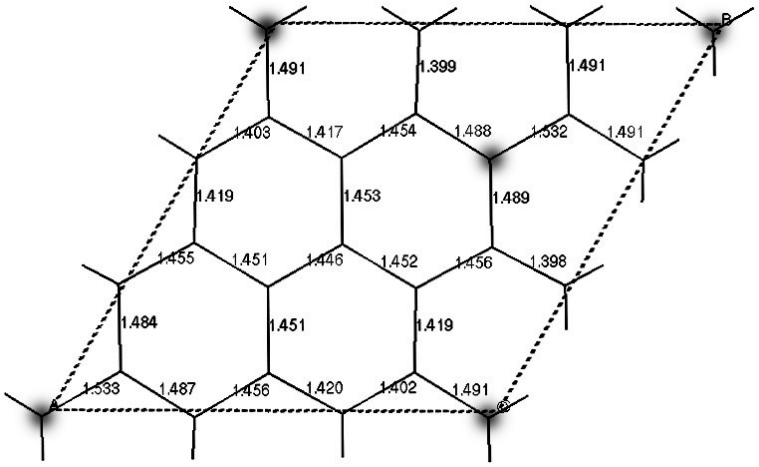

(a) Top layer

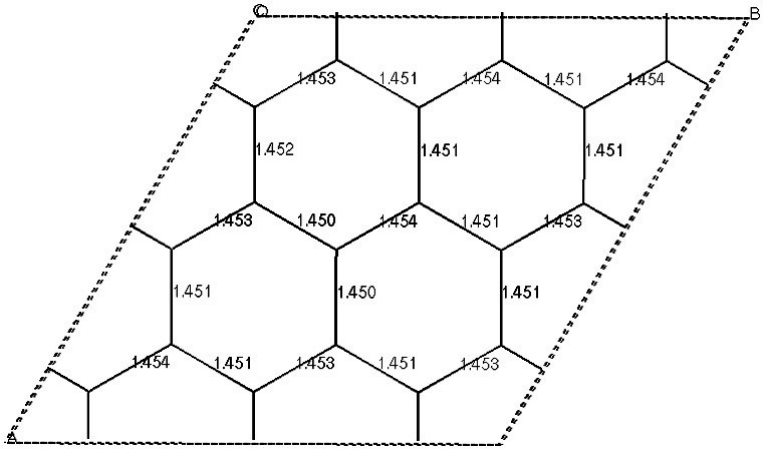

(b) mid-layer

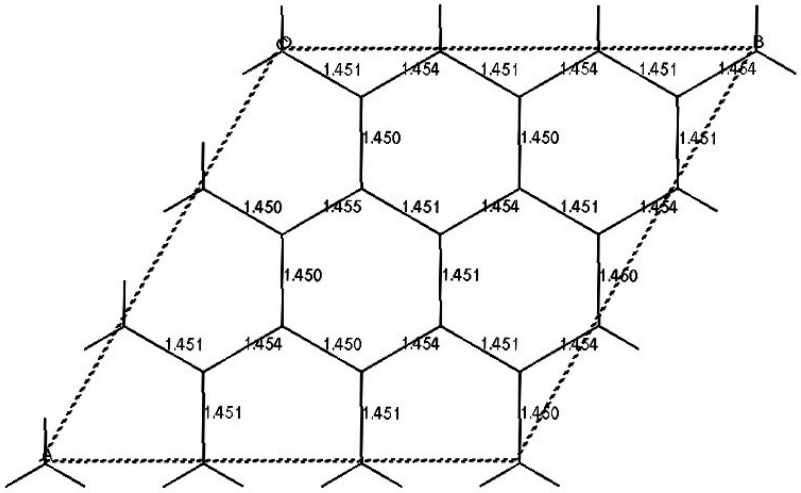

(c) bottom layer

Figure 7-14. A (111) cell with 22% O-coverage (labeled by blobs). (a) The top layer, (b) the middle layer, and (c) the bottom layer. Bond length difference is 9% within top layer.

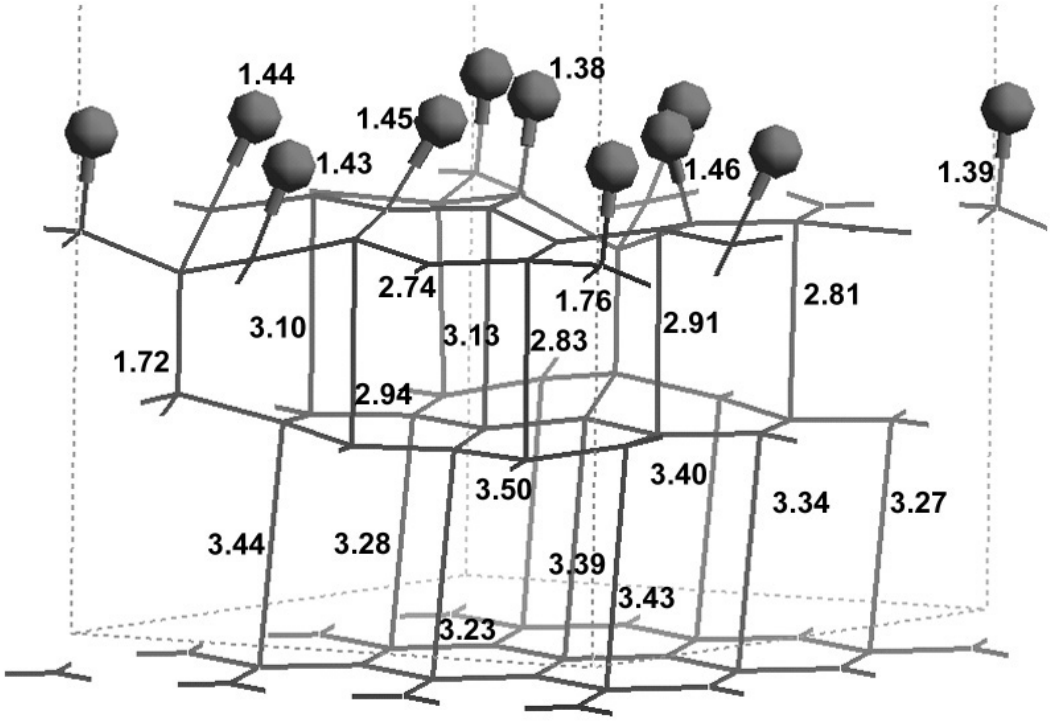

Figure 7-15. Reconstructed (111) supercell with six oxygen chemisorbed on top layer (67% coverage). The C-O bonds are canted along various directions ranged from 80 to 84 ^{o} with a 67% coverage. Partial coverage introduces distortion of bond angle and bond length of all carbon layers which significantly reduces the symmetry of the cell.

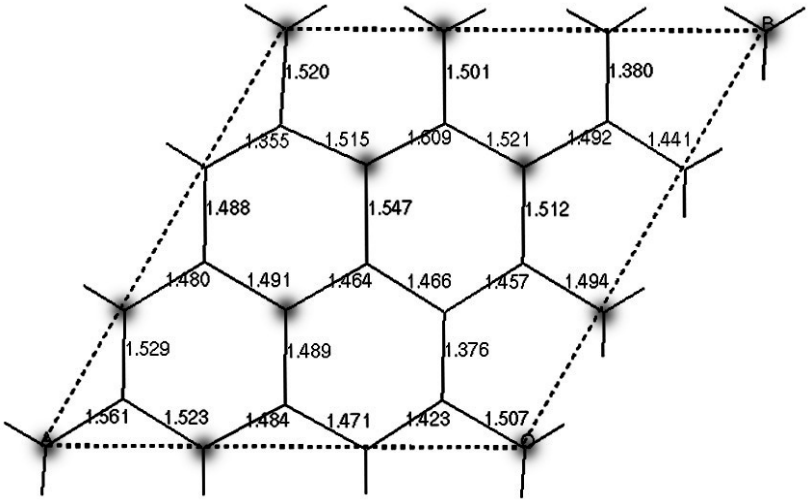

(a) Top layer

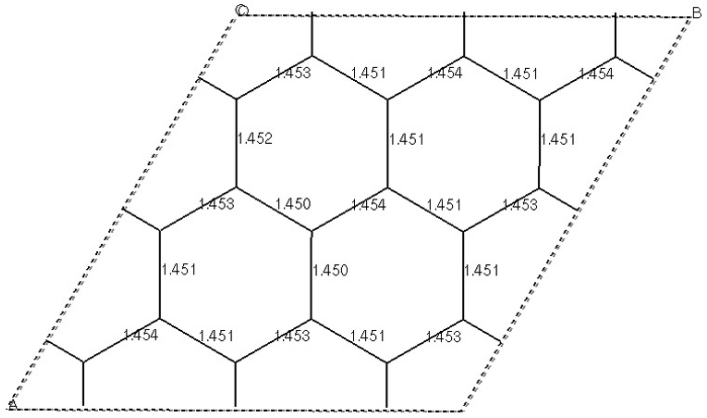

(b) mid-layer

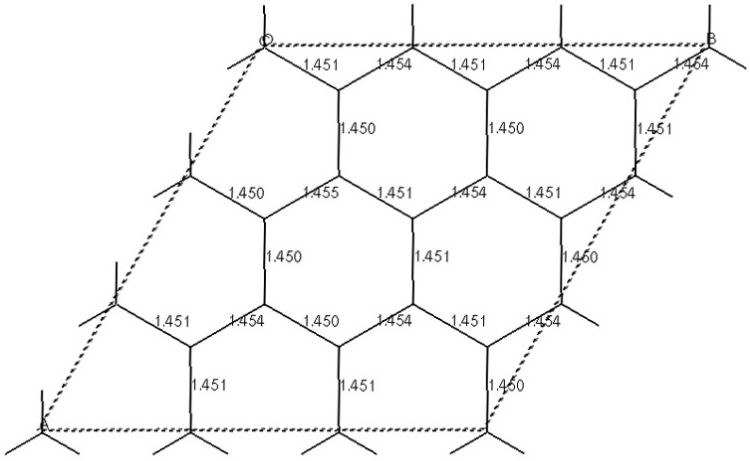

(c) bottom layer

Figure 7-16. The (111) cell with 67% O-coverage (labeled by blobs). (a) The top layer has 17% bond length difference, (b) the difference is 9% within the middle layer, and (c) less than 1% at the bottom.

Table VII-2. C-O Bond Lengths and Bond Angles on Diamond Surfaces

	% of coverage	Bond length (Å)	Angle of canting (^{o})
(111)	11 at the center	1.48	58.4
	11 at the edge	1.48	58.4
	22	1.48	58.2, 58.6
	67	1.38 – 1.46	varies from 80 to 84
	100	1.31	90
	100 (hydrogen)#	1.09	90
(100)	100	1.50	n/a
(110)	100	1.36	n/a
	100	1.46	n/a
experimental C-O bond length[36]		1.43	—

* Angle of canting is defined as the angle between the C-O bond and the plane of the first layer of (111).
# This is to emphasize that the surface is fully covered by chemisorbed hydrogen atoms, not oxygen.

7.6.2 Geometry Optimization — Fixed or Movable Bottom Layer

Before presenting the simulation findings on diamond (100) and (110) surfaces, it is of importance to discuss the difference in computational results due to the constraints applied.

Supercells with one surface fully covered by chemisorbed oxygen (the top layer) but with the other surface remaining clean (the bottom layer) are the starting models for the simulation of oxygen chemisorption. One set of geometry optimization is performed, allowing all the atoms to move freely, that includes those on the clean surface. These calculations are referred to as geometry optimizations with a movable bottom layer. Another set of calculations is undertaken with the constraints on the clean surface. With these constraints, the calculation is performed on a cell with a fixed bottom layer. The calculation with a movable bottom layer allows an unrestricted relaxation with respect to the total energy, whereas the calculation with fixed bottom layer simulates the conditions in which relaxation on the fifth or the sixth layer is strictly limited.

The total energies of the cells with 100% O-coverage are tabulated in Table VII-3. As expected, the total energies of cells with a fixed bottom layer are slightly higher than the cells with a movable bottom layer. However, the biggest difference in energy, 5.71 eV, is found in the (111) cell, whereas the (100) cell bears the minimal difference of 0.14 eV. This suggests that (100) surface is least subject to surface reconstruction while (111) surface is the most subject to a such change. Another interesting observation is the formation of O-O bonds on the (110) surface; that is described in detail in Section 7.6.4.

Table VII-3. Total Energies of the Cell Converged with Movable and Fixed Bottom Layer

ID	Cell content	Total Energy (eV) movable layer	Total Energy (eV) Fixed layer	Difference in Total Energy (eV)
(111)	54 C + 9 O	-12318.718	-12313.004	5.714
(110)	60 C + 12 O	-14553.910	-14549.886	4.024
(100)	48 C + 8 O	-10945.209	-10945.067	0.142

7.6.3. Relaxation and Oxygen-Chemisorption on Diamond (100) Surface

Relaxation of Clean Diamond (100) Surface

Relaxation of the clean diamond (100) surface is also studied by running geometry optimization routines. Figure 7-17 contains the structures of the (100) supercell with clean surfaces before (blue) and after (black) relaxation. The reconstructed structure bears a strong resemblance to the bulk structure. Figure 7-18 illustrates a relaxed (100) cell labeled with values of bond length and bond angle. Contrary to the drastic reconstruction of diamond (111) surface, there is a 3% change of bond length and a 5% change of bond angle on the (100) surface. The bond lengths and angles vary as a function of distance to the surface. For instance, the first layer has the shortest length of 1.50 Å, while the second layer has the longest of 1.59 Å, Figure 7-18. The third layer in the middle remains almost the same as the bulk structure. The sp^3 bond character is preserved on (100) after the relaxation.

Oxygen-Chemisorption on Diamond (100)

A 100% coverage of oxygen-chemisorption on diamond (100) is studied here. The relaxed structure is given in Figure 7-19. The values of bond length and bond angle of

each layer are tabulated in Table VII-4. The illustration and the numbers clearly indicate that no major change occurs in the structure as a result of chemisorption. At the bottom surface where no oxygen is chemisorbed and the carbons are allowed to move freely, the bond length shrinks slightly to 1.48 Å. The existence of bridging oxygen on the (100) does not influence the hybridization state, which is still sp^3.

7.6.4 Relaxation and Oxygen-Chemisorption on Diamond (110) Surface

Relaxation of Clean Diamond (110) Surface

Figure 7-20 contains the structure of the relaxed (110) cell with clean surfaces. Similar to (100), relaxation of the clean diamond (110) surface results in little change in either bond angle and bond length. The bond lengths and angles for the reconstructed cell are labeled in Figure 7-21. The most significant of these changes occurs on layers 1 and 5 (top and bottom). There is minimal variation of structure in the third layer, which is in the middle of the five layers. It is labeled in Figure 7-21 that on layer 3, the bond length is 1.54 Å and the bond angle is 107.6 ^{o}. These data are very close to that of the bulk structure of 1.54 Å and 109.5^{o}. The bonds can be separated into two sets. One set are those parallel to the surfaces or on the surfaces and they have shorter length from 1.41 Å on the surfaces to 1.54 Å in the middle of the cell. The second set includes those not parallel to the surfaces. They have longer bond lengths, from 1.51 Å near the surface to 1.68 Å at the center of the cell. Similar to the case of (100), the sp^3 bond character is preserved on (110) after the relaxation.

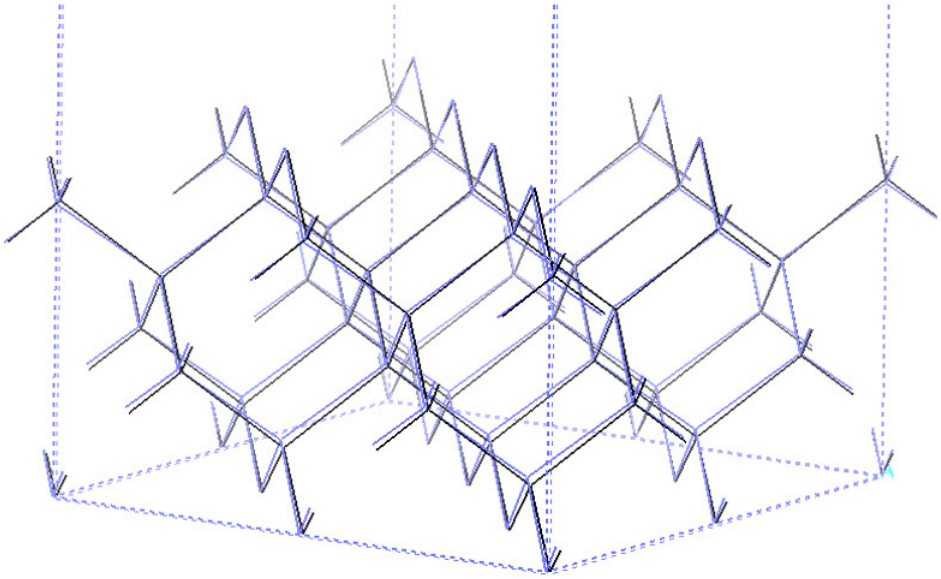

Figure 7-17. The (100) supercell with clean surfaces before (blue)* and after (black) relaxation. There is a minor change in structure as compared to the case of (111) surface.
* This structure would be in gray if printed out in a black-and-white setting.

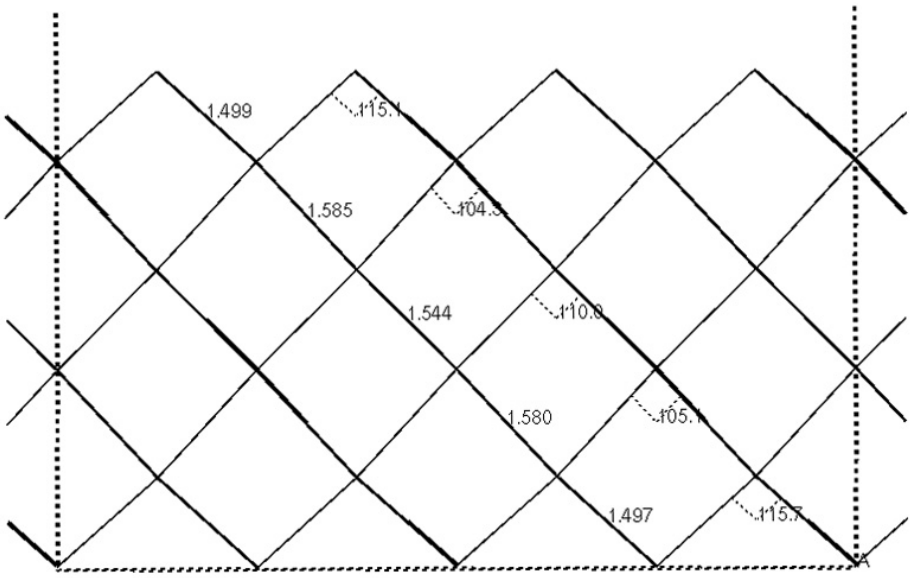

Figure 7-18. Values of bond lengths and bond angles of a relaxed (100) surface. The relaxed bond length is close to the bulk value of 1.54 Å, which is in the center of the cell.

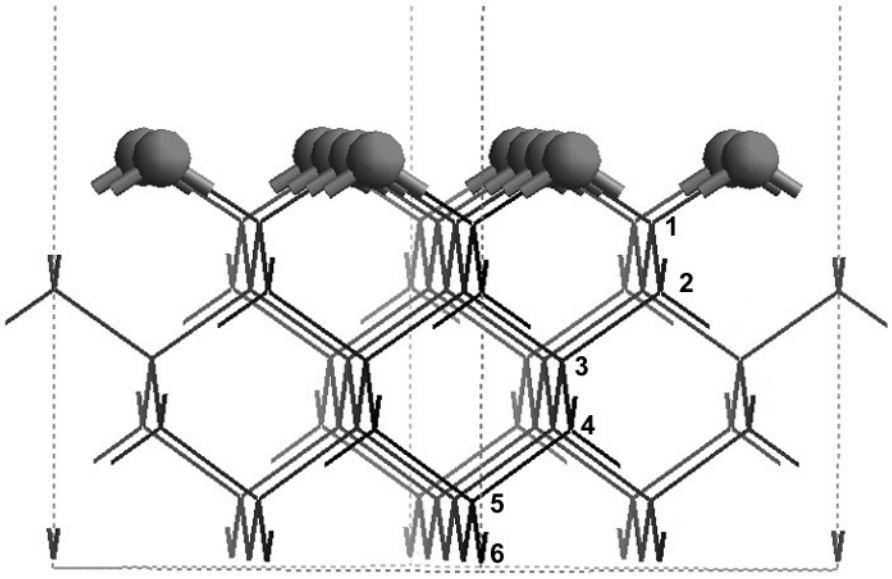

Figure 7-19. Relaxed (100) supercell whose top layer is fully covered by chemisorbed oxygen. The carbon layers are labeled and values of bond angle and length are given in Table VII-4.

Table VII-4. Bond Angle and Bond Length of (100) Supercells with 100 % Oxygen-Coverage (as refer to the structure shown in Figure 7-19)

Layer ID	Bond length (Å)	Bond angle ID	Bond angle* (degree)
	C-O-C bond: 1.500	1 (tetrahedron of 2 C and 2 O)	108/111/108/114
1-2	1.525-1.526	2	109/109.9/109/109.9
2-3	1.536	3	109/110.7/109.1/109.9
3-4	1.529	4	109.6/108.2/109.4/110.6
4-5	1.549	5	108.1/116.8/107.9/107.8
5-6	1.480-1.483		

* For each central carbon atoms (as marked by *) bonded to other four carbon atoms in diamond, there are six C-C*-C bond angles. Four out of six angles are cited here: Two of the angles that are perpendicular to (001) and two other angles. For example, in the second row, the Bond Angle ID reads "2". The values of four C-C2-C read "109/109.9/109/109.9".

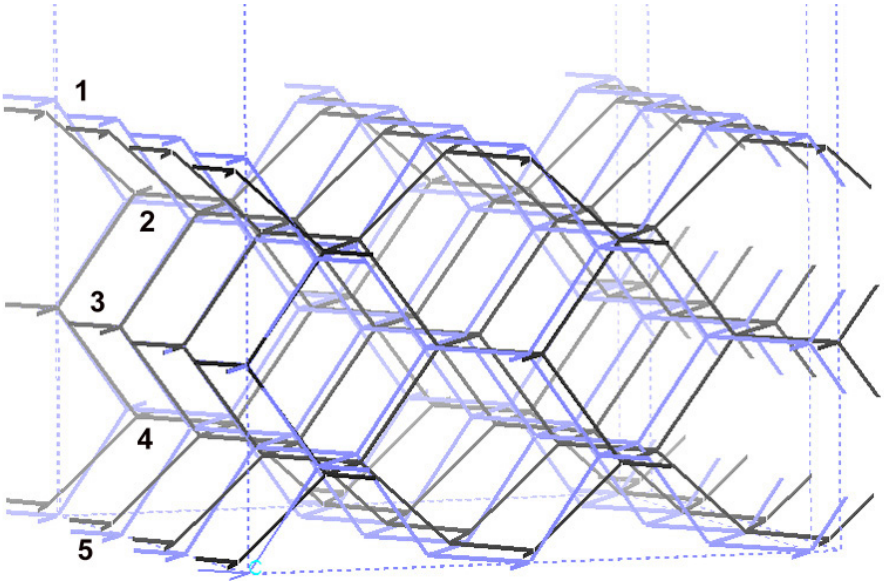

Figure 7-20. A (110) supercell with clean surfaces before (blue)* and after relaxation (black). There is minimal variation on layer 3.

* This structure would be in gray if printed out in a black-and-white setting.

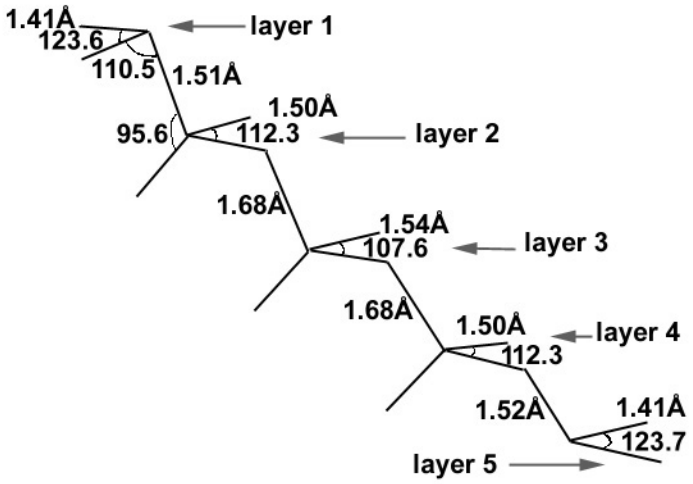

Figure 7-21. Bond lengths and bond angles of the reconstructed (110) cell (cell structure given in Figure 7-20 in black). Values are very close to that of the bulk form on Layer 3.

Oxygen-Chemisorption on Diamond (110)

Oxygen atoms are placed on every available site of the top (110) surface (100% coverage) whereas the bottom surface is free of absorbents. First, geometry optimization is carried out without any constraint on atomic positions. The (110) cell with chemisorbed oxygens, prior to and after relaxation, is given in Figure 7-22. Minimal change occurs in layer 3, which sits in the middle of the cell. Figures 7-23 and 7-24 contains the structure of relaxed (110) cells. The bond lengths and bond angles of C-O and C-C bonds are also marked on these figures. It is illustrated in Figure 7-23 (a) that, surprisingly, the twelve C-O bonds are divided into two sets. One set has a C-O bond length of 1.36 Å and the other of 1.46 Å. A top view of this cell down the *c* direction is also given in Figure 7-24 (a). The C-O bonds with of 1.46 Å are tilted away (having an angle of 15^{o}) from the *a* direction. The presence of two sets of C-O bond length causes two sets of O-O distance for its adjacent oxygen atoms. For one set, the O-O distance is 1.50 Å and for the other, it is much larger at more than 1.90 Å. The O-O distance of 1.50 Å is very close to the experimental data of O-O single bond length of 1.48 Å.[37] Thus, it is considered that a real O-O bond is formed between these two oxygen atoms.

Geometry optimization is also performed on a (110) cell with full O-coverage, under the conditions of a fixed bottom layer. The structure of the reconstructed cell is given in Figures 7-23 (b) and 7-24 (b). In this "fixed layer" version, all twelve C-O bonds have the same length at 1.46Å, Figure 7-23 (b). All the C-O bonds have an angle of 25^{o} away from the *a* direction. In contrast to the "movable layer" calculation, all six sets of O-O distances have the same value of 1.53 Å. The total energy of this model is –14549.88 eV.

Again, the O-O distance of 1.53 Å is close to the experimental data of 1.48 Å, the O-O single bond is formed. Figure 7-25 contains the image of the (111) cell fully covered by chemisorbed oxygen that viewed from *c* direction. Of note is that the O-O distance on the relaxed (111) surface is in the range of 2.50 Å, which is much larger than the usual O-O bond length of 1.43 Å, Figure 7-25. Therefore, the possibility of O-O bond formation is unique to (110) only.

With a 100% oxygen coverage, the sp^3 bond character of the (110) surface is preserved.

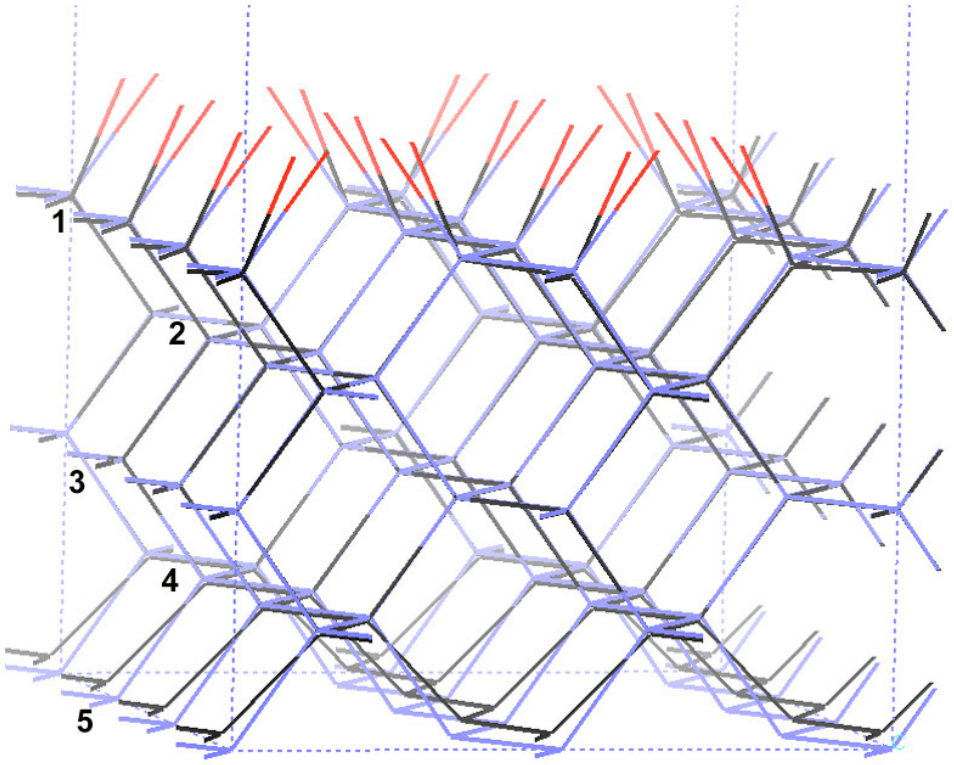

Figure 7-22. O-chemisorbed (110) supercell before (blue)* and after relaxation (black). Oxygen atoms are all in red. There is a minor change in structure as compared to that of the (111) surface.

* This structure would be in gray if printed out in a black-and-white setting.

8 DISCUSSION — THE OXIDATION OF DIAMOND

8.1. Is the Expression "Graphitization of Diamond" Appropriate?

Is the expression "graphitization of diamond" appropriate? No.

Many researchers use the term "graphitization of diamond", yet their studies involve the phase transition of diamond (reviewed in Section 2.5).[1-5] Before a discussion, whether this is a proper usage of the terms, let us take a look at the definition of graphitization by IUPAC, "A solid-state transformation of thermodynamically unstable non-graphitic carbon into graphite by means of heat treatment."[6] The following notes under the definition point out, "graphitization is also for the transformation of metastable diamond into graphite by heat treatment, … Such uses of the term graphitization are in line with the above definition. The use of the term graphitization to indicate a process of thermal treatment of carbon materials at T > 2500 K regardless of any resultant crystallinity is incorrect." This definition implies that graphitization of diamond is a proper term only if diamond transformation produces graphitic carbon. "Graphitic carbon" is defined by IUPAC as, "All varieties of substances consisting of the element carbon in the allotropic form of graphite irrespective of the presence of structural defects."[6] IUPAC emphasizes that the use of the term is justified only if three-dimensional hexagonal crystalline long-range order can be detected in the material by diffraction methods. Based upon these two definitions, the use of "graphitization of diamond" is proper only if the sp^2-carbon formed after the phase transition from diamond (sp^3-carbon) is crystalline.

Our study shows that the sp^2-bonded carbon, which results from a diamond phase transition, is amorphous. Two levels of structure are under consideration here: First, the electronic structure has an sp^2 hybridization state; and second, on a larger scale at atomic level, the arrangement of the atoms exhibits the lack of long range order. While many researchers either do not make the attempt to determine the crystallinity of the carbon,[4, 5, 7] or have not obtained sufficient proof of the crystallinity,[2, 3] it is incorrect to use the term "graphitization of diamond". One might argue that Evans and James prove that using electron diffraction technique, graphite forms after heating diamond pieces that are "thin enough for TEM observation" at 1600 to 1900 ^{o}C in a vacuum for 45 min.[1] However, one should also bear in mind that in order to be transparent to electron beams, the thickness of these specimens must be 1 μm or less. It is literally an annealing process by heating such a thin strap of carbon piece at temperatures exceeding 1600 ^{o}C for 45 min. Crystal growth can easily occur under these conditions. In the current study, CVD diamond ET100 is treated at temperatures between 1000 and 1500^{o}C in $6x10^{-10}$ Pa O_2 for 600 min. The heat treat temperature is set high enough to observe phase transition but low enough to inhibit crystal growth. Our findings are supported by other researchers' work: Hoffman, Bobrov, Fisgeer, Shechter, and Folman report that LEED pattern fades if sp^2-bonded carbon is formed on the surface of diamond.[8] Fading of LEED pattern suggests the disappear of the long range order. The change of a diamond surface to sp^2 carbon is more accurately described a phase transition and not graphitization.

8.2. Do oxidation and phase transition occur simultaneously?

Do oxidation and phase transition occur simultaneously?

Yes and No.

We say yes because it is observed that at certain conditions, direct oxidation of diamond (sp^3-bonded carbon) and phase transition of diamond occur on the same facet of diamond surfaces (refer to Section 4.4, and Figures 4-24 to 4-26). Direct oxidation leaves (111)-faceted pits and ruts on the surface without color change, whereas phase transition accompanied by blackening of surface, and oxidation of this sp^2-bonded carbon occurs after the transition. It is considered simultaneously, in a steric sense, that direct oxidation and phase transition may occur side by side. These two processes are competing mechanisms that depend upon the activation energy. Although the exact value is still unknown, we propose that the activation energy of oxidation is lower than that of phase transition on an atomically smooth (111) surface. However, the activation energy of phase transition is significantly lower on a rough or stepped surface. Kern and Hafner conducted *ab initio* molecular-dynamics studies of "the graphitization of flat and stepped diamond (111) surfaces.[5] They report that the temperature of "graphitization" is 1000 K lower on stepped (111) than on flat (111).

Another reason for "yes" is that oxidation and phase transition may occur on the same block of diamond but at different crystal facets. Evans and Phaal reported that {100} remains white but {110} becomes black on a big piece of natural diamond (2 to 5 mm

each edge) at 830 ^{o}C in 53 Pa O_2.[9] This observation is again due to the difference of activation energies for these competing processes.

However, phase transition is by no means a step that diamond must go through prior to oxidation. Direct oxidation of diamond from sp^3-bonded carbon to gaseous species CO/CO_2 may certainly occur. This circumstance is discussed in detail in the following Section.

8.3. The Oxidation of Diamond

As stated at the very beginning, the objective of this work is to develop a fundamental understanding of the oxidation behavior of diamond. The author hereby attempts to answer the two questions that have been raised in Chapter 1:

- Where are the active sites on the diamond surfaces?

— On (111), more specifically, on the stepped or distorted (111).

- Is surface reconstruction from sp^3 to sp^2 bond character during oxidation the governing phenomenon?

— Whether oxidation or surface reconstruction occurs is governed by the percentage of surface oxygen coverage on (111).

Two processes could possibly occur during the heat treatment of diamond in oxygen at elevated temperatures: 1) gasification of sp^3-bonded carbon; and 2) sp^3 to sp^2 phase transition (surface reconstruction) first, and then gasification of sp^2-bonded carbon.

Diamond oxidation and phase transition are results of these two competing mechanisms, as a function of crystal texture, temperature, and oxygen partial pressure. There are two issues associated with the phase transition. One is the hybridization state of carbon, either sp^3 or sp^2. Another is whether the carbon material formed is crystalline or amorphous. We hereby propose that surface oxygen coverage, which is determined by the two external conditions, i.e., temperature and partial pressure, is the most influential factor on the surface reaction of diamond. The discussion of oxidation of diamond (111) becomes more straightforward if it is based upon surface oxygen coverage.

8.3.1. Diamond (111) Surface

Among the three low index facets, ie, (111), (110), and (100), the highest oxidation rate is observed on (111). It is where oxygen attacks preferentially. Whether surface reconstruction would occur on (111) depends upon the percentage of surface coverage by chemisorbed oxygen on diamond, which is directly related to oxygen partial pressure and temperature. Surface reconstruction becomes possible only if there is a means to overcome the high activation energy of the reaction, e.g., the thermal energy provided at elevated temperatures.

- With 100 % coverage

Experimentally, oxidation of CVD diamond ET100 in 95 kPa O_2 is undertaken between 420 and 625 ^oC. Oxidation initiates at 515 ^oC in 95 kPa O_2. The surface coverage is somewhere between 60 and 100 % at this temperature. Our simulation suggests that if fully covered by chemisorbed oxygen, (111) surface maintains the sp^3 hybridization state,

and the surface is still 111-(1x1). Auger spectra of the oxygenated surface indicate that the surface oxidized in 95 kPa O_2 possesses the sp^3 bond character.

- With 0% coverage at elevated temperatures

Diamond (111) goes through a phase transition from sp^3 to sp^2 bond character. A transition is observed by quantum mechanical simulation using DFT methods. The kinked (111) layers of diamond flatten and become graphite-like (0001) layers. The interlayer spacing is from 3.40 to 3.80 Å, which actually falls into the range of amorphous carbon instead of crystalline graphite. Experimentally, heat treatment of CVD diamond ET100 is carried out at elevated temperature in very low oxygen partial pressure (1003 to 1478 ^oC in 10^{-9} Pa O_2) for 600 min. A layer of black carbon forms on diamond surfaces. The electronic state of the black layer is identified as sp^2 carbon using Auger spectroscopy, based upon a major difference of the 1st satellite peak of the carbon Auger spectra. The black carbon is amorphous. The amorphous nature of the carbon layer is determined experimentally using electron diffraction, in which the pattern of the carbon layer is a collection of diffusive rings. Our experimental findings also provide solid proof of our computer simulation results.

- The Pandey model and other 2x2 or 2x1 reconstruction models on clean (111)

The Pandey model refers to a surface reconstruction of clean (111) into a chain-like (111)-(2x1).[10] None of these (2x1) or (2x2) reconstruction models are reproduced in our simulation study. At low temperatures, a full reconstruction to sp^2 is prohibited by the high kinetic barrier. These (2x1) or (2x2) reconstruction models are some intermediate

states of reconstruction while energy permits. Nonetheless, quantum mechanical simulation study can by-pass the high kinetic barrier and go directly to the most optimized geometry with respect to the lowest total energy. Experimentally, we did not investigate whether there is any reconstruction on clean diamond surfaces without heat treatment. We suggest that the (2x1) or (2x2) reconstruction models are the possible intermediate states en route to the most stable state:

sp^3 → intermediate state: (111)-(2x1) → the most stable state: sp^2

- With low level partial coverage (11 and 22 %)

Diamond experiences a phase transition to amorphous sp^2-bonded carbon at low partial coverage. Our simulation work reveals that there is a localized perturbation of the sp^2-bond character at which the oxygen is chemisorbed. Kern and Hafner's MD simulation study shows that stepped (111) has a transition temperature 1000 K lower than the flat (111) [5]. This suggests that inducing randomness lowers the activation energy of the phase transition. Hence the phase transition to carbon can occur at lower temperature with the presence of low levels of oxygen on the surfaces. In reality, phase transition and oxidation of diamond occur simultaneously at elevated temperature in low oxygen partial pressure (from 850 up to 1500 ^oC in 0.6 to 15 Pa O_2). It is true in this case that oxidation facilitates phase transition.

- With high level of oxygen coverage (67% coverage)

CVD diamond ET100 was oxidized in 95 kPa O_2 at 550 to 600 ^oC. Based upon Matsumoto, et al., the coverage of diamond surfaces by chemisorbed oxygen is estimated

to be 50 % under these conditions.[11] Our SEM study reveals that nodules sized between 30 and 60 nm form on the tip of crystal facets on oxidized diamond surfaces (Figures 4-15 to 4-17). Although the surface carbon still bears sp^3-bond character, based upon the Auger spectroscopy study, a question is raised as to whether these nodules are amorphous or crystalline. Our simulation study on (111) surface with 60% oxygen-coverage suggests that the surface is amorphous.

8.3.2. Diamond (110) and (100) Surfaces

Oxygen attacks (100) surface and creates (111)-faceted etch pits. This suggests that the oxidation rate on (100) surface is lower than that of (111) surface. Our simulation study shows no significant surface reconstruction on (110) or (100) surface.

8.4. Summary — The Mechanism of Diamond Oxidation

The reaction between oxygen and diamond (111) surface at ambient pressure is summarized as:

- Room temperature and 0 % coverage:
  The (111) surface reconstructs to (2x2) or (2x1) reconstruction. This occurs without any change of the bond character.
- Elevated temperature (~ 700 ^{o}C to 1500 ^{o}C), zero coverage:
  The bond character of diamond (111) surface changes from sp3 to sp2. Thus, diamond goes through a phase transition and forms amorphous, sp2-bonded carbon. If the temperature reaches 1600 ^{o}C or higher, the amorphous carbon graphitizes and becomes crystalline.
- Elevated temperature (~ 700 ^{o}C and higher), low coverage (up to 20%):
  Diamond converts to amorphous, sp2-bonded carbon first. Then the oxidation of carbon proceeds, yielding gaseous products CO and/or CO_2.

- Elevated temperature (~ 500 ^{o}C and higher), high coverage (more than 50%): Diamond converts to amorphous, sp3-bonded carbon first. Then the oxidation proceeds, yielding gaseous products CO and/or CO_2.

Is this simple?

References

1. T. Evans and P.F. James, "A Study of the Transformation of Diamond to Graphite," *Proc. R. Soc. London, Ser. A*, **277** [1369] 260-9 (1964).

2. M. Seal, "Graphitization of Diamond," *Nature*, **185** [4712] 522-3 (1960).

3. M. Seal, "Graphitization and Plastic Deformation of Diamond," *Nature*, **182** [4645] 1264-7 (1958).

4. A. De Vita, G. Galli, A. Canning and R. Car, "Graphitization of Diamond (111) Studied by First Principles Molecular Dynamics," *Appl. Surf. Sci.*, **104/105** 297-303 (1996).

5. G. Kern and J. Hafner, "Ab Initio Molecular-Dynamics Studies of the Graphitization of Flat and Stepped Diamond (111) Surfaces," *Phys. Rev. B: Condens. Matter Mater. Phys.*, **58** [19] 13167-75 (1998).

6. "IUPAC Compendium of Chemical Terminology" (1997) In International Committee of Pure and Applied Chemistry. [World Wide Web]. Accessed on: November 4, 2000. Available at <http://www.iupac.org/publications/compendium/G.html>

7. B.N. Davidson and W.E. Pickett, "Graphite-Layer Formation at a Diamond (111) Surface Step," *Phys. Rev. B: Condens. Matter Mater. Phys.*, **49** [20] 14770-3 (1994).

8. A. Hoffman, K. Bobrov, B. Fisgeer, H. Shechter and M. Folman, "Effects of Deuterium Adsorption-Desorption on the State of Diamond: Surface Degradation and Stabilization of sp^3 Bonded Carbon," *Diamond Relat. Mater.*, **5** [9] 977-83 (1996).

9. T. Evans and C. Phaal, "The Kinetics of the Diamond-Oxygen Reaction," *Proc. Conf. Carbon, 5th*, **1** 147-53 (1962).

10. K.C. Pandey, "New Dimerized-Chain Model for the Reconstruction of the Diamond (111)-(2x1) Surface," *Phys. Rev. B: Condens. Matter Mater. Phys.*, **25** [6] 4338-41 (1982).

11. S. Matsumoto, H. Kanda, Y. Sato and N. Setaka, "Thermal Desorption Spectra of the Oxidized Surfaces of Diamond Powders," *Carbon*, **15** [5] 299-302 (1977).

Appendix I: A List of Thermal Gravimetric Analysis (TGA) Experiments

All the TGA runs are tabulated in the following four tables. Table A1, A2, and A3 include the runs carried out using Setaram TAG24, in 1998, 1999, and 2000, respectively. Each run receives a unique identification number of six digits. For example, 1998-62 refers to the run with ID number 62 carried out in 1998. The first four digits, among them are 1998, 1999, and 2000, indicate the year of the experiment was performed. Table A4 collects the runs carried out at Oak Ridge in February 2000.

Table A1. TGA Runs Series 1998-xx (UHP O_2 flowing at 70 to 95 sccm)

Run ID #	Temperature (^oC)	*Final weight loss (%)	Initial weight (mg)	Comments
62	625/650	93	24.27	
99	625	93	33.86	
1	625	15	30.80	
2	625	50	30.20	
3	625	n/a	36.39	calibration run
4	625	13	17.16	
5	625	< 0.6	17.41	
6	625	0.7	30.44	
7	625	2	19.78	
8	625	9	39.14	
9	625	3.0 and 4.4	32.87	two pieces

* Final weight loss is the percentage of remaining weight to the initial weight. It is not the percentage of burn-off.

Table A2. TGA Runs Series 1999-xx (UHP O_2 flowing at 70 to 95 sccm)

Run ID #	Temp. (^oC)	Comments	Initial weight (mg)
63	420	not oxidized	23.17
64	500	not oxidized	39.67
65	550	oxidized	35.26
66	575	oxidized	36.45
69	575	oxidized	23.87

Table A3. TGA Runs Series 2000-xx (UHP O_2 flowing at 70 to 95 sccm)

Run ID #	Temp (^oC)	pO_2 (Pa)	p_{total} (mbar)	Material and Comments	crucible
58	550	60	3		SiO_2
60	750	0.6-1.6	0.08-0.03	calibration run, no specimen	SiO_2
61	750	0.6	0.03	no observable weight change	SiO_2
62	1000	0.4	0.02		SiO_2
63	1000	14	0.7		SiO_2
64	850	12-18	0.6-0.9		SiO_2
65	600	95 k	*		SiO_2
66	600	95 k	*		SiO_2
67	600	95 k	*	calibration run	SiO_2
68	600	95 k	*	calibration run	SiO_2
69	600	95 k	*	up to 12 % burn-off	SiO_2
70	530	95 k	*	short run	SiO_2
71	530	95 k	*		SiO_2
72	530	95 k	*	oxidized	SiO_2
73	515	95 k	*	lowest oxidation temperature	SiO_2
74	1500	1.2-1.0	0.06-0.05		Pt
75	1400	0.6-1.6	0.03-0.08		Pt
76	1300	0.6	0.03		Pt
77	1500	0.5	0.025		Pt
78	600	95k	*	glassy carbon	SiO_2
79	600	95k	*	glassy carbon	SiO_2
80	600	95k	*	HOPG	SiO_2
81	H-plasma treated ET 100			done in Germany by Sven	n/a

* The total pressure was 95 kPa UHP O_2.

Table A4. List of TGA Runs at Oak Ridge

Run ID #	Temp (^oC)	pO_2 (Pa)	Material and Comments	Crucible
S9-82	1003	6×10^{-10}	600 min holding time	Al_2O_3
S8-83	1478	6×10^{-10}	600 min	Al_2O_3
S11-84	1005	6×10^{-10}	60 min	Al_2O_3
S10-85	1303	6×10^{-10}	600 min	Al_2O_3

Appendix I: A List of Thermal Gravimetric Analysis (TGA) Experiments

All the TGA runs are tabulated in the following four tables. Table A1, A2, and A3 include the runs carried out using Setaram TAG24, in 1998, 1999, and 2000, respectively. Each run receives a unique identification number of six digits. For example, 1998-62 refers to the run with ID number 62 carried out in 1998. The first four digits, among them are 1998, 1999, and 2000, indicate the year of the experiment was performed. Table A4 collects the runs carried out at Oak Ridge in February 2000.

Table A1. TGA Runs Series 1998-xx (UHP O_2 flowing at 70 to 95 sccm)

Run ID #	Temperature (^oC)	*Final weight loss (%)	Initial weight (mg)	Comments
62	625/650	93	24.27	
99	625	93	33.86	
1	625	15	30.80	
2	625	50	30.20	
3	625	n/a	36.39	calibration run
4	625	13	17.16	
5	625	< 0.6	17.41	
6	625	0.7	30.44	
7	625	2	19.78	
8	625	9	39.14	
9	625	3.0 and 4.4	32.87	two pieces

* Final weight loss is the percentage of remaining weight to the initial weight. It is not the percentage of burn-off.

Table A2. TGA Runs Series 1999-xx (UHP O_2 flowing at 70 to 95 sccm)

Run ID #	Temp. (^oC)	Comments	Initial weight (mg)
63	420	not oxidized	23.17
64	500	not oxidized	39.67
65	550	oxidized	35.26
66	575	oxidized	36.45
69	575	oxidized	23.87

Table A3. TGA Runs Series 2000-xx (UHP O_2 flowing at 70 to 95 sccm)

Run ID #	Temp (^oC)	pO_2 (Pa)	p_{total} (mbar)	Material and Comments	crucible
58	550	60	3		SiO_2
60	750	0.6-1.6	0.08-0.03	calibration run, no specimen	SiO_2
61	750	0.6	0.03	no observable weight change	SiO_2
62	1000	0.4	0.02		SiO_2
63	1000	14	0.7		SiO_2
64	850	12-18	0.6-0.9		SiO_2
65	600	95 k	*		SiO_2
66	600	95 k	*		SiO_2
67	600	95 k	*	calibration run	SiO_2
68	600	95 k	*	calibration run	SiO_2
69	600	95 k	*	up to 12 % burn-off	SiO_2
70	530	95 k	*	short run	SiO_2
71	530	95 k	*		SiO_2
72	530	95 k	*	oxidized	SiO_2
73	515	95 k	*	lowest oxidation temperature	SiO_2
74	1500	1.2-1.0	0.06-0.05		Pt
75	1400	0.6-1.6	0.03-0.08		Pt
76	1300	0.6	0.03		Pt
77	1500	0.5	0.025		Pt
78	600	95k	*	glassy carbon	SiO_2
79	600	95k	*	glassy carbon	SiO_2
80	600	95k	*	HOPG	SiO_2
81	H-plasma treated ET 100			done in Germany by Sven	n/a

* The total pressure was 95 kPa UHP O_2.

Table A4. List of TGA Runs at Oak Ridge

Run ID #	Temp (^oC)	pO_2 (Pa)	Material and Comments	Crucible
S9-82	1003	6×10^{-10}	600 min holding time	Al_2O_3
S8-83	1478	6×10^{-10}	600 min	Al_2O_3
S11-84	1005	6×10^{-10}	60 min	Al_2O_3
S10-85	1303	6×10^{-10}	600 min	Al_2O_3